UNIVERSITY OF OKLAHOMA

GRADUATE COLLEGE

STRATEGIES TO REDUCE THE FOREIGN BODY RESPONSE TO CORTICAL NEURAL INTERFACES

A DISSERTATION
SUBMITTED TO THE GRADUATE FACULTY

in partial fulfillment of the requirements for the

Degree of

DOCTOR OF PHILOSOPHY

By

NEIL MARKWARDT
Norman, Oklahoma
2013

STRATEGIES TO REDUCE THE FOREIGN BODY RESPONSE TO CORTICAL NEURAL INTERFACES

A DISSERTATIONAPPROVED FOR THE
DEPARTMENT OF BIOENGINEERING

BY

_____
Dr.David Schmidtke, Chair

_____
Dr.David McCauley

_____
Dr.David Miller

_____
Dr.Edgar O'Rear

_____
Dr.Robert Rennaker

Acknowledgements

This dissertation is the final product of a lengthy process which could never have been completed without substantial help. I would like to thank my advisor Dr. Robert Rennaker for his guidance and support, and Dr. David Schmidtke for his assistance in the assembly of this dissertation. I would also like to thank Dr. John Fagan for his invaluable support of my endeavors, both academic and otherwise. Numerous fellow students of both the University of Oklahoma and the University of Texas at Dallas also contributed significantly to these efforts. In no particular order, I would like to thank Drew Sloan, Doyle Dodd, Jodi Stokol, Taylor Ware, and Dustin Simon for their help on these projects and others. This work would also not have been possible without the US Department of Education Graduate Assistance in Areas of National Need (GAANN) fellowship that supported my first three years of research. Finally, my success in this endeavor is attributable to nothing so much as the continual unwavering support, guidance, and motivation from my parents and my Andrea, for which I am truly grateful.

Table of Contents

List of Tables

List of Figures

Abstract

Cortical neural interfaces offer unique capabilities to researchers and physicians, opening doors to superior understanding and treatment of a host of processes and diseases in the central nervous system. One of modern medicine's greatest challenges stems from the inability of the nervous system to heal following disease or injury, and neural interfaces combined with modern electronics offer significant potential to help patients regain lost function. Current interface technologies fall short of the long term performance that is necessary to be useful in the clinical setting, due in large part to the brain's immune reaction to current implanted neural interface devices. This reaction leads to the death of neurons surrounding the implant, formation of a fibrous glial scar, and eventual loss of neural signals.

This dissertation presents the results of three different studies which evaluated strategies to mitigate the foreign body response and its detrimental effects on implanted neural interfaces. Modifications were made to the implantation scheme, porosity, and substrate material of cortical recording probes, and these modifications were tested to quantify their effects on the foreign body response. The first study examined the relationship between cortical implants and the meninges, and whether the placement of the implants fully below the cortical surface would reduce meningeal contributions to the immune reaction. Sub-meninges implants were found to elicit a significantly reduced glial cell reaction compared to trans-meninges implants, which suggests the presence of a significant meningeal cell contribution to the

immune reaction and motivates the development of fully wireless recording probes which can be implanted entirely below the cortical surface.

The second study evaluated a scheme to take advantage of the above phenomenon in a manner compatible with current interface technology. A series of holes was added to the shank of a planar neural implant near the level of the cortical surface, in order to allow the regrowth of meningeal tissues through the implant structure and discourage migration down the implant shaft. The addition of this feature was found to significantly reduce meningeal tissue levels and improve mean neuron density as well at 4 weeks post implantation.

In the final study, histological evaluation of a recently developed dynamically softening polymer neural interface substrate was performed. Dynamically softening implants were compared to parylene-c implants which possessed a similar initial modulus but lacked softening capability. The addition of dynamic softening capability found to significantly reduce levels of reactive astrocyte encapsulation at 4 weeks post implantation.

When combined, the results of these studies illustrate the importance of meningeal contributions in determining the overall characteristics of the chronic immune response to a cortical electrode and highlight the potential benefits of interventional strategies which target this portion of the immune reaction. The results of the final study suggest that dynamic softening capability is also a desirable design feature for future neural interfaces, and the combination of these techniques in future recording devices should yield significant

improvements in neural signal quality and lifetime, according to the current understanding of the factors affecting neural recording array performance.

1 Introduction and Background

1.1 Neural Interfaces

1.1.1 Definition and brief history

A neural interface is any device which employs electronics to monitor or modify activity within the nervous system. Since the initial development of such technologies in the 1970s, neural interfaces have played a critical role in furthering our understanding of the function of many systems within the CNS, including vision, hearing, movement, and memory. Without the highly detailed, real-time information provided by neural interfacing technologies, many areas of nervous system processing would remain poorly understood. In the past four decades, the development of neural interfacing technologies has followed a path of miniaturization, increasing capability and improving performance, not unlike many other modern technologies. These improvements have expanded the capabilities of researchers and enhanced our understanding of the nervous system, but the development of these technologies has an additional goal: the deployment of neural interfaces in human therapeutic applications. Before this leap from the lab to widespread use can happen, though, significant challenges involving the biocompatibility and service life of current interfacing technologies must be addressed. The focus of this work is investigating solutions to those challenges.

1.1.2 Therapeutic applications

Restoration of nervous system function lost to disease or injury remains a substantial challenge for modern medicine, and this is the ultimate goal of neural interfacing technology development (Cheung, 2007; Lebedev and Nicolelis, 2006; Stieglitz et al., 2009; Welberg, 2012). Perhaps the most common and best known of these injury modalities is spinal cord damage resulting from neck or back injury, which results in partial or total loss of sensation and movement in some or all of the limbs. Such injuries and their associated functional impairments are estimated to affect 200,000 - 300,000 individuals in the United States alone, with 12,000 new cases occurring each year (Qin et al., 2010). Neural interfacing technologies aim to restore function and quality of life to these individuals by acquiring neural signals from the CNS, then processing and relaying them to a variety of potential destinations, ranging from computer cursors to prosthetic limbs(Simeral et al., 2011; Welberg, 2012). Noninvasive, EEG-mediated interfacing modalities have been investigated for their ability to extract neural information for applications such as these, but these systems lack the temporal and spatial resolution necessary for the restoration of many physiological functions (Wolpaw et al., 2002). Such techniques have been successfully used to allow a subject to control a computer cursor, but they require significant training and concentration on the part of the user, and lack the necessary degrees of freedom to control more complex devices like prosthetic limbs (Simeral et al., 2011; Welberg, 2012; Wolpaw et al., 2002). Direct, cortical indwelling recording probes have already

demonstrated this capability in primates by directly recording signals from the neurons which are responsible for limb control (Batista and Andersen, 2001; Hochberg et al., 2006). The activity of these cells directly encodes movement information, and this information can only be acquired with the spatial and temporal resolution required for natural functional restoration via a direct cortical recording implant. Since this type of probe provides the greatest range of potential applications, the focus of this work is the chronic indwelling cortical interface.

While cortical recording probes have only seen limited experimental use in humans, deep brain stimulators have been approved by the Food and Drug Administration and have been in clinical use for more than a decade. Deep brain stimulation (DBS) involves the implantation of stimulating electrodes in specific brain regions associated with movement disorders or other conditions (Krack et al., 2003; Lozano et al., 2012; Romaguera et al., 2012). These devices use electrical pulses to interfere with neural activity in that region. Positioning of the electrodes in the subthalamic nucleus provides relief from the symptoms of Parkinson's disease (Krack et al., 2003), which is the most common application of this technique, but DBS has been applied in the treatment of other neurological conditions as well(Lozano et al., 2012; Romaguera et al., 2012). Although this technique differs significantly from the cortical recording probes which are the focus of this work, it illustrates the therapeutic potential of neural interfacing technology, and provides motivation

for further development thereof, in order to expand these exciting therapeutic capabilities to other brain regions and disease conditions.

Another major area of neural interfacing therapeutic research focuses on the restoration of vision (Normann et al., 1999; Stieglitz, 2009). Various disease conditions or injuries lead to damage of the retina or optic nerve and loss of vision in large numbers of patients, leading researchers to begin development of neural interface based therapeutic strategies. Current work focuses primarily on the development of devices to allow researchers to better understand the visual processing system, as the current level of knowledge concerning visual processing is not sufficient to enable the deployment of a functional cortical vision prosthesis (Normann et al., 1999). The end goal of this work is the development of a stimulating interface which can be implanted in the visual cortex, receiving input from an externally mounted camera and image processing system (Brunton et al., 2012; Normann et al., 1999). In addition to helping elucidate visual processing mechanisms, neural interfaces have been used in research settings to gain large amounts of insight into other brain systems, including auditory processing (Sloan et al., 2009) and the motor system (Batista and Andersen, 2001; Hwang et al., 2012) enhancing basic understanding of brain function and informing future therapeutic strategies in these areas as well. A component of the premotor system known as the parietal reach region has been of particular interest to researchers, as neural activity in this region encodes movement intentions (Hwang and Andersen, 2010; Hwang

et al., 2012). Neural activity acquired from this region may be used in the control of computer cursors, prosthetic limbs, or other devices.

1.1.3 Current technologies

1.1.3.1 Microwire arrays

Penetrating cortical electrodes have taken a few basic forms over the course of their development, and one of the earliest and simplest of these is the microwire array. Some of the earliest neural recordings were conducted using drawn glass micropipettes, also known as cone electrodes. These tended to produce very high signal-to-noise ratios (SNR), but were difficult to make and only permitted a limited number of recording channels (Kennedy, 1989). Microwire arrays are composed of metal wires, usually tungsten or stainless steel, in the range of 10-50 microns in diameter. The wires have an insulating coating, such that neural signals are acquired from the uninsulated tip of the wire, and each wire supports a single recording channel (Nicolelis et al., 2003; Prasad et al., 2012; Winslow and Tresco, 2010). Microwire arrays have the advantage of being inexpensive and easy to manufacture compared to more recently developed silicon-based architectures, which require expensive and sophisticated equipment and techniques borrowed from the semiconductor industry(Rennaker et al., 2005a). Despite their relative simplicity compared to silicon based arrays, microwire electrodes yield similar performance to more complex architectures in terms of recording channel viability and signal-to-noise ratio (Prasad et al., 2012; Ward et al., 2009). Microwire arrays have been used

to record signals from hundreds of neurons in different brain regions simultaneously in primates (Nicolelis et al., 2003), illustrating the adaptability and scalability of the technique. An example microwire array is shown in **Figure 1.1.** Since the basic architecture is limited to a single recording channel per shaft, though, the spatial channel density of microwire arrays is typically lower than that of newer, silicon based architectures, which may have multiple recording sites per shaft (Stieglitz et al., 2009).

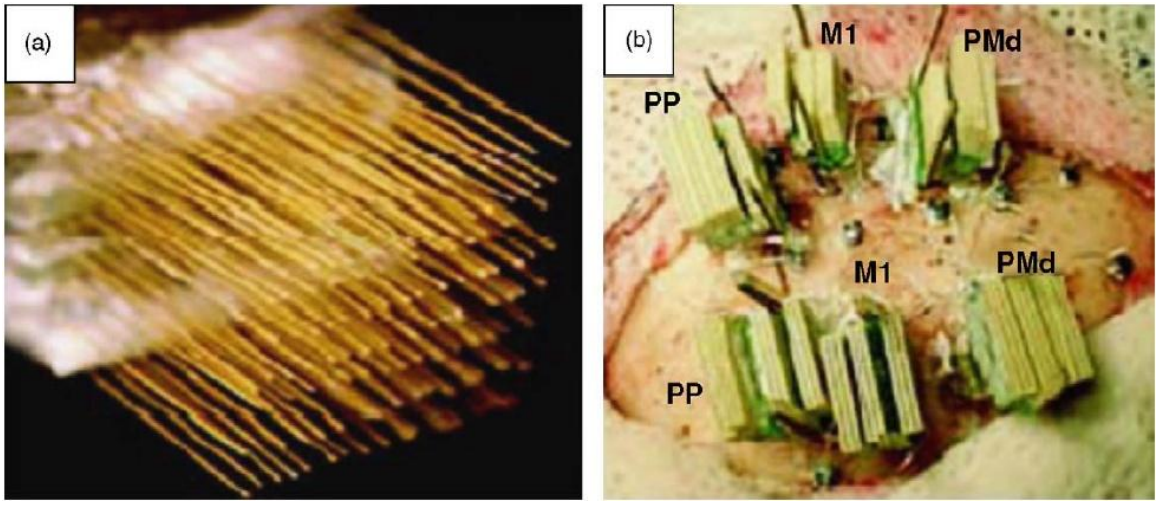

Figure 1.1
(A) Example microwire array
(B) Several such arrays implanted in multiple brain regions in Macacamulatta
From Nicolelis et al. 2003

1.1.3.2 Utah array

The first of the two most commonly employed silicon based neural electrode architectures was developed at the University of Utah and later marketed by Cyberkinetics as the BrainGate system (Stieglitz et al., 2009). It consists of an

array of penetrating spikes around 1mm in length arranged in a grid pattern and affixed to a base plate (**Figure 1.2**) (Normann et al., 1999). Recording sites are located at the spike tips, and the array is designed to be inserted such that the base plate is against the cortical surface and the penetrating spikes are fully inserted in the cortical tissue. The same basic architecture has taken a variety of forms, but the most common is a 10x10 grid of 100 spikes spaced 400µm apart, which is fabricated in a 3D fashion from a single block of substrate (Stieglitz et al., 2009). The Utah array remains the only cortical interface type to have been implanted in humans, beginning with a pilot clinical trial of five patients in 2004 (Simeral et al., 2011). This trial demonstrated the ability to acquire neural signals over several months, as well as the ability of tetraplegic patients to volitionally control a computer cursor using the neural interface system (Hochberg et al., 2006). Continued functionality of the system has been demonstrated as long as 1000 days after implantation in the case of one human subject, with the 100 channel array acquiring signals from an average of 24 individual cells at this point (Simeral et al., 2011), but viable recordings over this extended time period are fairly rare for all current neural electrode types.

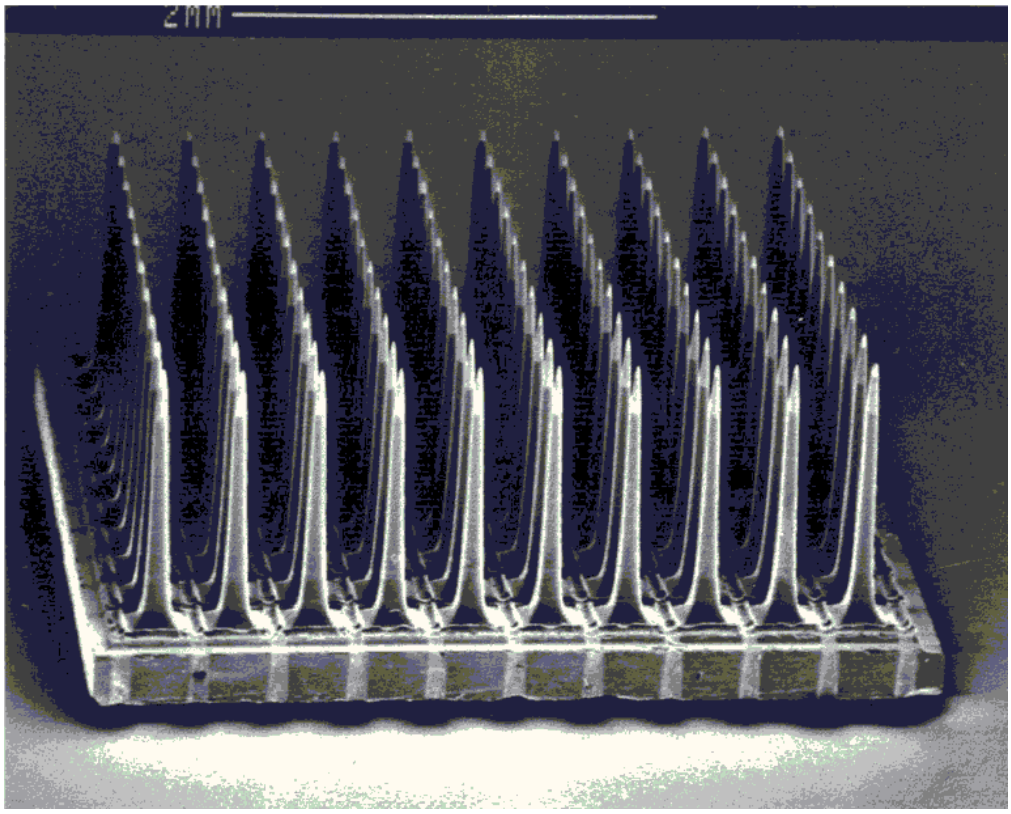

Figure 1.2: The Utah silicon microelectrode array
from Normann et al. 1999

1.1.3.3 Michigan electrodes

The final commonly used neural interface architecture is a planar silicon design developed at the University of Michigan and now marketed by NeuroNexus. Rather than the 3D architecture used in the case of the Utah Array, this design features planar penetrating spikes with a thickness of only 15µm and multiple recording sites distributed along the length of the electrode shaft (Kipke et al., 2003). Individual shafts with up to 16 recording sites per shaft may be mutiplexed together to form a 3 dimensional array with as many as 1024 recording channels and high channel density (Cheung, 2007; Stieglitz et al., 2009). This probe design is unique among the mainstream architectures in

offering multiple recording channels per penetrating spike, allowing the acquisition of a greater amount of neural data relative to the amount of insertion damage caused, in addition to the ability to record from multiple cortical layers simultaneously. The architecture is also highly adaptable, offering an array of penetrating spike shapes and recording site arrangements (Kipke et al., 2008; Kipke et al., 2003), and even offering capabilities for integrated drug loading and microfluidic delivery (Chen et al., 1997; Stieglitz et al., 2009). Example configurations of this architecture are shown in **Figure 1.3.**

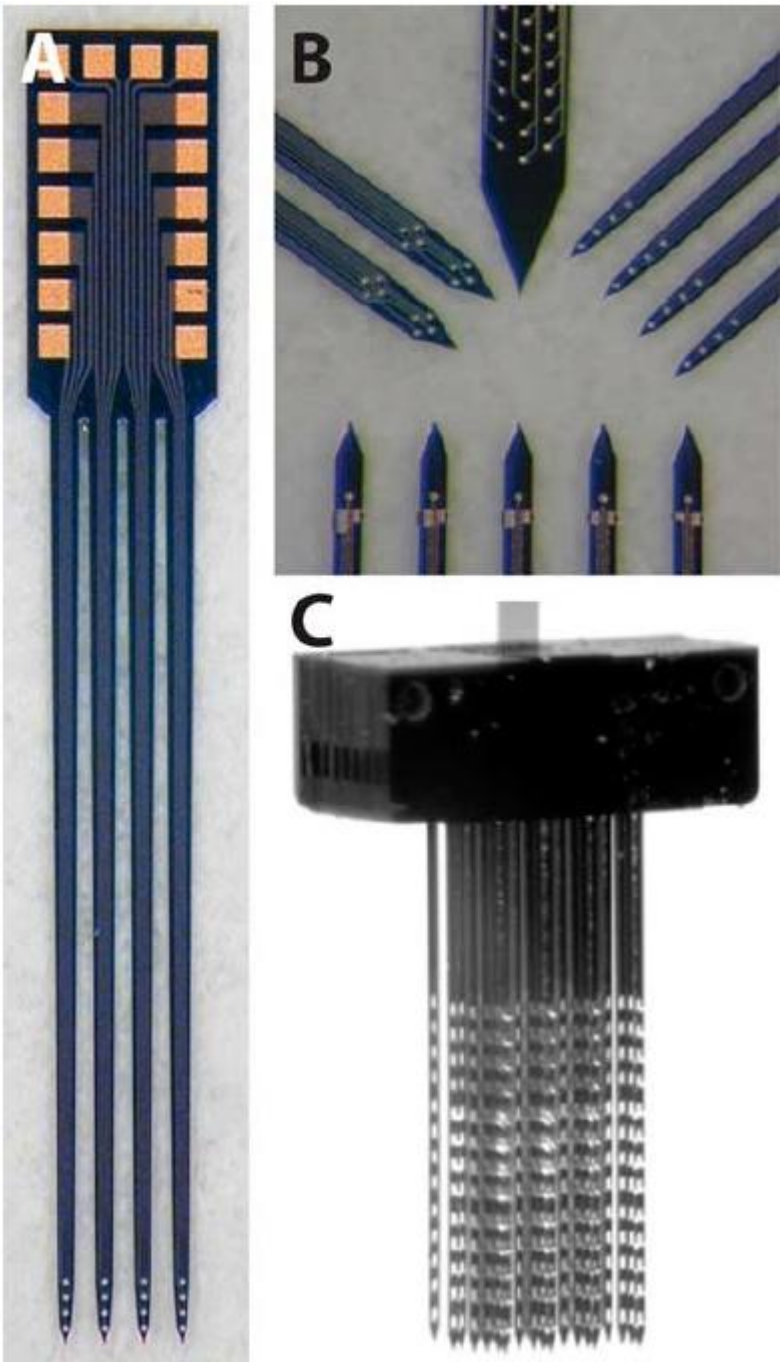

Figure 1.3: Example configurations of the Michigan planar silicon array, with multiple recording sites at the tip of each spike. From Kipke et al. 2008

1.2 The Foreign Body Response

1.2.1 Inflammatory and scarring process overview

The insertion of any type of invasive neural interface in the brain tissue initiates a complex series of events collectively known as the foreign body response. This process involves several types of cells, most of which are unique to the CNS, and results in multiple phenomena which are detrimental to neural interface performance. Chief among these are the encapsulation of the neural implant in an insulating fibrous layer, also known as the glial scar, and the death of neurons in the vicinity of the implant as a result of processes that have not been thoroughly characterized (Biran et al., 2005; Marin and Fernandez, 2010; Polikov et al., 2005; Stieglitz et al., 2009; Szarowski et al., 2003). Glial scarring and neuron dieoff have been implicated as the two primary mechanisms of neural interface recording failure, and the mitigation of these phenomena is the greatest hurdle which must be overcome before neural interfacing technologies may become clinically viable (Polikov et al., 2005; Winslow and Tresco, 2010). A thorough understanding of the foreign body response is of critical importance to this task.

1.2.1.1 Microglia

The central nervous system is unique in the body in that it possesses its own population of immune effector cells that are separate from the immune system of the rest of the body. In the case of a large injury in the CNS with significant

damage to the blood-brain barrier (BBB), circulating macrophages and other cells may play a role in short-term inflammatory processes, but once the BBB is reestablished, immune processes in the CNS are characterized by two main native cell types: microglia and astrocytes (Biran et al., 2005; Fawcett and Asher, 1999; Fujita et al., 1998; Polikov et al., 2005). Both are native glial cells which make up most of the CNS cellular population and perform various structural and chemical support functions for neighboring neurons. Upon the initiation of an injury condition, both glial cell types in the vicinity of the insult change into their reactive phenotypes, which are characterized by significant morphological changes, proliferation, and migration (Fujita et al., 1998; Kreutzberg, 1996; Nakajima and Kohsaka, 2001; Polikov et al., 2005). In the case of microglia, this transformation initiates macrophage-like behavior, in which the cells phagocytose foreign material and cellular debris at the wound site (Fujita et al., 1998). Microglia are most active in the initial inflammatory phase of the foreign body response, and their activity peaks within the first few days following the initial injury or neural interface implantation (Polikov et al., 2005). Reactive microglia have been shown to secrete numerous factors affecting a variety of processes, some of which can directly cause neuronal death (Nakajima and Kohsaka, 2001). Microglial activity surrounding a neural implant tends to decrease from about 1 week post-implantation onward. The remainder of the foreign body response, known as the chronic response, is characterized by reactive astrocytes.

1.2.1.2 Astrocytes

Under normal physiological conditions, astrocytes perform many structural functions in the CNS, such as the formation of the blood-brain barrier and the glia limitans layer which ensheathes the entire CNS (Abnet et al., 1991; Fawcett and Asher, 1999; Kalman, 2003). The transition of astrocytes to their reactive morphology is accompanied by proliferation, migration, hypertrophy, and a large upregulation in the production of glial fibrillary acidic protein (GFAP) filaments (Abnet et al., 1991; Fawcett and Asher, 1999; Kornyei et al., 2000; Polikov et al., 2005). It is via measurement of GFAP levels that reactive astrocytes can be readily distinguished from their nonreactive resting state. The initiation of the inflammatory process causes astrocytes near the wound site to transition to the reactive state and migrate to the surface of the foreign body (Polikov et al., 2005; Turner et al., 1999). In the weeks following the implantation of a neural interface, reactive astrocytes surround the implant and form a fibrous capsule of interdigitating processes commonly referred to as the glial scar (Fawcett and Asher, 1999; Kalman, 2003). This layer impedes the acquisition of neural signals by electrically insulating the recording probe from surrounding neurons, and this process has been implicated as one of the primary mechanisms of recording probe failure (Biran et al., 2005; Polikov et al., 2005; Szarowski et al., 2003; Turner et al., 1999; Winslow et al., 2010). Example images of the glial scarring process are shown in **Figure 1.4.** Minimizing the glial scarring response is critical to ensuring long-term acquisition of neural signals, and thus GFAP expression surrounding a neural implant has become the most frequently

used histological metric for determining the magnitude of the chronic immune response to a neural implant. Measurements of GFAP expression and GFAP+ cellular activity will be used throughout this dissertation as one of multiple techniques to quantify the chronic immune response to various interfacing strategies.

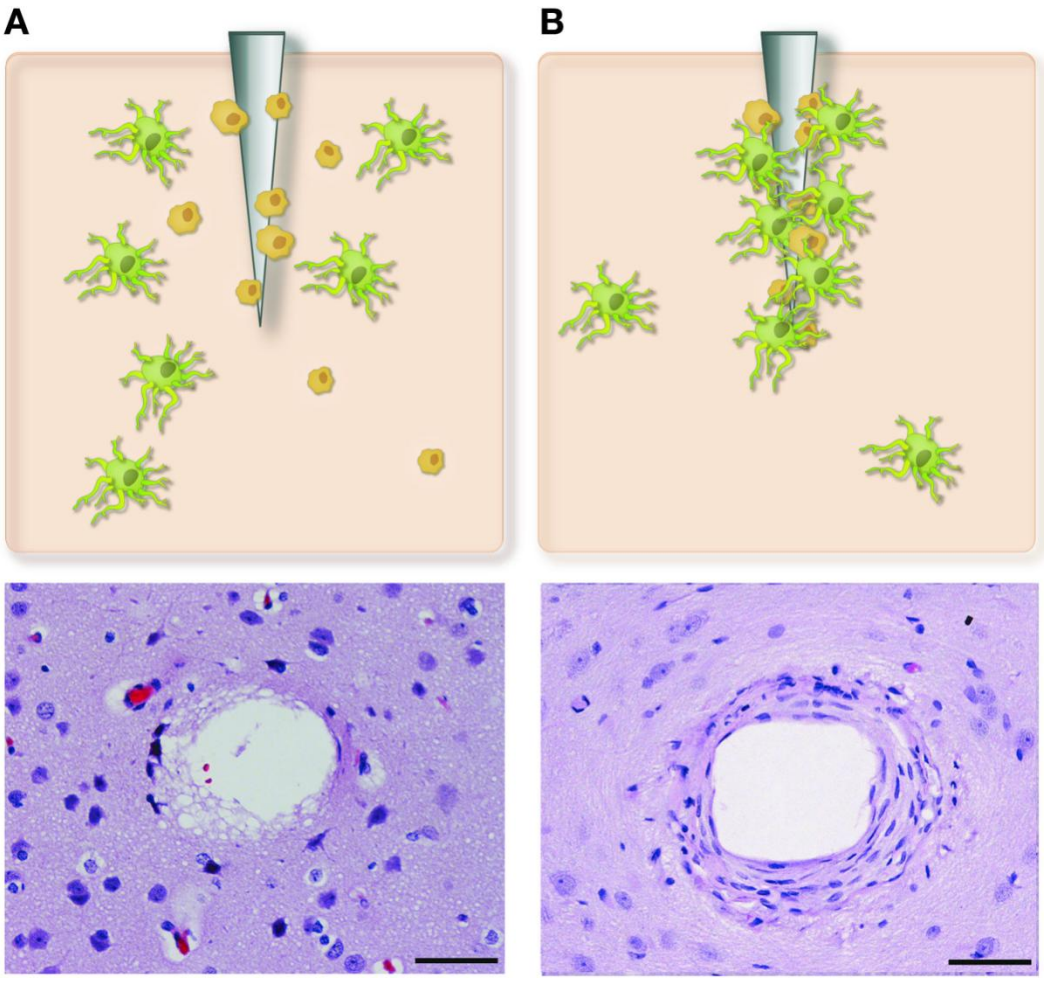

Figure 1.4: Development of glial encapsulation around an intracortical electrode

(A) Acute neural injury caused by electrode insertion. Astrocytes and microglia become activated and migrate to the wound site. Cell nuclei are shown in dark blue.
(B) Chronic response showing formation of dense sheath containing astrocytes and fibroblasts. From Marin and Fernandez 2010.

1.2.1.3 Meningeal cell contributions

In addition to native astrocytes and microglia, previous work has indicated that cells derived from the meninges also contribute to the foreign body response (Cui et al., 2003; Fawcett and Asher, 1999; Kalman, 2003; Maxwell et al., 1990; Ness and David, 1997). The majority of research into the brain's immune response has focused on microglia and astrocytes, but meningeal tissue and meningeally derived cells are known to play some role in the foreign body response to implanted neural interfaces. *In vitro* and *in vivo* studies have shown that interaction of meningeal cells with glial cells triggers the formation of a glia limitans and other fibrous structures which are detrimental to recording electrode performance (Abnet et al., 1991; Carbonell and Boya, 1988). Thus, the relationship of a neural interface to the meninges may prove to be an important aspect of device design. This will be explored further in section 1.2.2.3 below.

1.2.1.4 Effects on neurons

The second major phenomenon of interest produced by the foreign body response, after the generation of the glial scar, is the death of neurons surrounding the implant. Neuron death has been demonstrated to accompany the implantation of several types of neural implants, including planar "Michigan" electrodes (Biran et al., 2005), polymer nanocomposite implants is (Harris et al., 2011a), 3D silicon architectures (Seymour and Kipke, 2007), and metallic

mircowire implants (Thelin et al., 2011; Winslow and Tresco, 2010). It has been demonstrated that this loss of neurons is not only due to the mechanical trauma of insertion, but also due to the persistent inflammatory condition caused by the continued presence of a neural implant (Biran et al., 2005). One study used quantitative immunohistochemistry analysis to compare immune reactions to stab wounds and chronically implanted Michigan electrodes at 2 and 4 weeks post-implantation. Dramatically greater amounts of neuronal cell loss and GFAP expression were found in the case of electrode implants compared to stab wounds (Biran et al., 2005). Sample histology images from this study are shown in **Figure 1.5**, showing the distribution of the various cell types which participate in the immune response. IBA1+ microglia are shown in red, immediately adjacent to the implant, and GFAP+ reactive astrocytes are shown in green. Neuron death surrounding the implant is evident in a reduction in NeuN labeled cell bodies and a reduction in neurofilament (NF160) expression. The maximum radius from which a neural signal may be acquired is thought to be on the order of 100 microns (Biran et al., 2005; Henze et al., 2000), and the death of a large percentage of the neurons within this radius has been observed for multiple interface types (Thelin et al., 2011; Winslow and Tresco, 2010). Independent of the detrimental effects of the glial scarring response, the dieoff of many or all of the neurons within the signal-acquisition radius of a neural implant is clearly a major impediment to proper recording function. Widespread adoption of neural interfacing technologies in the clinical setting will only be practical if this

persistent inflammatory condition and its accompanying scarring response and neuronal dieoff can be significantly reduced or eliminated.

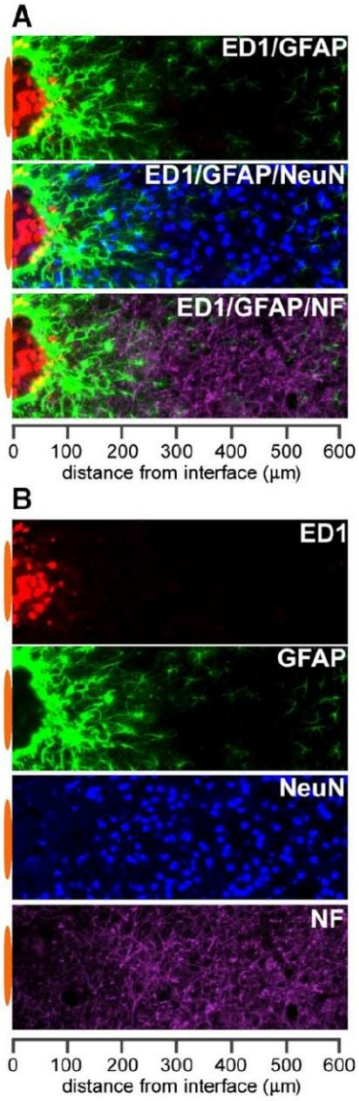

Figure 1.5: Immune cell activity and neuron viability around planar silicon "Michigan" implants. ED1 labels macrophages and microglia, GFAP labels reactive astrocytes, NeuN labels neuron cell bodies and NF labels neuron filaments.

(A) Combined images showing relative locations of markers
(B) Individual markers

From Polikov et al. 2005

1.2.2 Existing mitigation strategies

1.2.2.1 Biochemical functionalization

A diverse array of approaches has been taken in attempting to mitigate the brain's foreign body response and its detrimental effects on neural implant function. One such approach is the addition of bioactive components to the electrode. One study found that dexamethasone, a synthetic glucocorticoid hormone used to treat many inflammatory responses, was helpful in reducing the astrocyte response (Shain et al., 2003) and a subsequent study investigated the addition of a dexamethasone-eluting coating directly to the electrode, which was found to reduce the glial scarring response and improve neuron density near the implant at one and four weeks post-implantation (Zhong and Bellamkonda, 2007). Other bioactive components that have been added to neural implants include nerve growth factor (NGF) (Kennedy, 1989; Rousche et al., 2001) and nanoscale laminin (He et al., 2006). Many of these approaches have shown promising reductions in the foreign body response up to one month post-implantation, but the addition of a pharmacological component to the interface is not an ideal solution for long-term clinical mitigation of the inflammatory response. Release rates and concentrations of drugs are notoriously difficult to control over the long term, and the inflammatory condition may return when the concentration of the drug being released by the implant eventually becomes too low.

1.2.2.2 Coatings and surface treatments

Another focus area of existing work is the addition of non-bioactive coatings or surface features to neural interfaces in order to mitigate the foreign body response. One such coating is parylene-c, which is an FDA Class VI polymer that has been used in medical devices in other areas of the body with good results (Hsu et al., 2009; Rodger et al., 2006; Schmidt et al., 1988). It is applied via a chemical vapor deposition process, which is compatible with commonly used neural interface architectures (Hsu et al., 2009). When applied to planar silicon Michigan probes, though, it was found to have no effect on glial cell activity or neuronal viability at 2, 4 or 12 weeks post-implantation (Winslow et al., 2010). Other efforts have investigated nanoscale surface features as a possible route to influence the behavior of glial cells surrounding the implant (Moxon et al., 2007; Moxon et al., 2004; Turner et al., 1997). It has been shown that nanoscale surface architecture can influence the adhesion behavior of astrocytes *in vitro* (Turner et al., 1997), and nano-porous silicon surfaces were found to attract neurite ingrowth *in vitro* without impeding recording performance, but a detailed histological evaluation was not conducted to determine the effects on the immune response (Moxon et al., 2004). Although the techniques in this area have generally produced relatively subtle effects on the immune response, more work is merited to determine the ideal characteristics for neural interface coatings. Results from these and other studies are summarized in **Table 1.1.**

Study	Implant Type	Coating Type	Result
Winslow 2010	Michigan	Parylene-C	No effect on immune response
He 2006	Michigan	Laminin	Reduced microglia and astrocytes, no effect on neurons
Zhong 2007	Michigan	Dexamethasone in nitrocellulose	Reduced inflammatory response and neuronal loss
Moxon 2004	Ceramic	Nanoporous Silicon	Improved neurite ingrowth *in vitro*
Kennedy 1989	Glass cone	Nerve Growth Factor	NGF produced adverse local tissue reaction

Table 1.1: Neural interface coatings and bioactive components with experimental results

1.2.2.3 Implantation methods

The manner in which a neural implant is inserted has also been shown to exert significant influence over the magnitude of the immune response and subsequent recording performance. In the case of widely-used microwire and silicon arrays, high speed insertion methods have been found to reduce tissue trauma during insertion compared to slower methods, which result in more deformation of the surface (Rennaker et al., 2005b; Rousche and Normann, 1992). The method in which a neural implant is affixed after it has been implanted has also been shown to significantly affect the chronic immune response. Neural implant architectures currently in use either necessitate

fixation of the probe to the skull for support or sit on the cortical surface with relatively little mechanical connection to the skull. By comparing these two implantation schemes, two studies have found that skull fixation increases the magnitude of the chronic immune response compared to similar implants placed free-floating in the cortical tissue (Kim et al., 2004; Thelin et al., 2011). This is likely due to chronic irritation caused by relative motion between the brain and skull in the case of the fixed implants. One of these studies employed porous hollow fiber membrane implants, which are much larger than typical neural implants and composed of a very different material (Kim et al., 2004). The second, though, employed microwire-like implants and demonstrated not only increased immune activity in the case of fixed implants, but also enlargement and elongation of the implant track voids in the rostral-caudal axis (Thelin et al., 2011). Free-floating implants elicited a smaller immune response and exhibited no void elongation. It seems likely that this elongation was due to relative motion between the skull-fixed implant and the brain tissue. Generally speaking, these studies have found that techniques which reduce mechanical stresses on the cortical tissue, either during implantation or the chronic indwelling phase, helped to mitigate the glial scarring response.

1.2.2.4 Flexible interface substrates

In a further effort to mitigate the chronic inflammatory condition surrounding neural implants, much recent work has focused on the mechanical properties of the neural interface itself. Namely, studies using various materials in various tissues have shown that less compliant materials contribute to greater chronic inflammation, due to the "mechanical mismatch" between the implant and the surrounding tissue. Reduction of this chronic inflammatory reaction is thought to result in both improved recording quality and extended functional lifetime of the electrode. Thus, researchers have designed and tested neural interface architectures which utilize much lower-modulus materials than conventional silicon substrates. Such materials include polyimide (Cheung, 2007; Fomani and Mansour, 2011; Mercanzini et al., 2008; Rousche et al., 2001), an adaptive polymer nanocomposite (Harris et al., 2011a), parylene-c(Kim et al., 2013; Takeuchi et al., 2005; Wester et al., 2009) and benzocyclobutene (Lee et al., 2005). In one case, improved neuron proximity to a mechanically adaptive neural implant was demonstrated (Harris et al., 2011a). These techniques still suffer from certain compromises related to the stiffness of the implant substrate and the ability to insert it into the cortical tissue. A minimum buckling strength is required in order to facilitate insertion, and this is usually maintained by either using a substrate that is stiffer than would be desired for mechanical matching with the surrounding tissue or by increasing the size of the implant, and thus increasing insertion trauma. One workaround

to facilitate implantation of a soft probe employs an insertion shuttle, but this also significantly increases insertion trauma (Kozai and Kipke, 2009). Also, although these interface substrates are significantly less stiff than conventional silicon architectures, they are still five to six orders of magnitude stiffer than the surrounding brain tissue (Ware et al., 2012). Certain types of new shape memory polymers, which will be covered in more detail in Chapter 4, offer significantly reduced stiffness compared to current flexible substrates, combined with dynamic softening properties which address the insertion strength compromise (Ware et al., 2012).

1.3 Outline of experiments

The common theme of the experiments described in this dissertation is the investigation of novel neural interfacing techniques and materials in order to better understand the factors influencing the brain's immune reaction to a cortical recording probe and the ways in which those factors may be manipulated in order to mitigate the undesirable aspects of the immune response. Three studies were conducted, the first two of which deal with the relationship between the implant and the meninges, and the influence of the meningeal reaction on the rest of the immune response. The third experiment evaluated a novel dynamically softening shape memory polymer (SMP) implant

substrate and measured the effects of this capability on the chronic immune response.

1.3.1 Sub-meninges and trans-meninges implantation

Previous work regarding the spatial characteristics of the cortical immune response which suggested the presence of a significant meningeally mediated component served as the motivation for the experiment described in Chapter 2, which sought to measure the magnitude of the meningeal contribution to the chronic immune response. Microwire implants placed entirely below the cortical surface (sub-meninges) were compared to similar implants placed in a trans-meninges configuration, but not anchored to the skull. Multiple previous studies have found that implants of various types which are fixed to the skull elicit a greater immune reaction than similar implants which are free-floating in the cortical tissue, likely due to chronic perturbations caused by relative movement of the brain and skull (Biran et al., 2007; Kim et al., 2004; Thelin et al., 2011). Meningeal tissue has been shown to grow down around the shaft of a penetrating electrode, and the previously observed effects may be a result of this phenomenon as well, since the meninges-crossing aspect of the implantation has not been isolated from other factors by these studies (Biran et al., 2007; Kim et al., 2004; Thelin et al., 2011). It is possible that the ingrowth of meningeal tissues and cells down the shaft of the implant contributes significantly to the immune reaction to a trans-meninges probe. The study described in Chapter 2 was conducted in order to determine whether the

placement of a neural implant completely below the meninges resulted in a reduction in the chronic immune response by physically removing the implant from the meningeal space and thus reducing or eliminating the meningeal contribution to the immune response. A substantial reduction in both reactive astrocyte and microglial activity was found for sub-meninges implants, indicating that meningeally derived cells likely play a significant role in the immune response.

1.3.2 Implant porosity

The findings of Chapter 2 highlighted the importance of the meningeal contribution to the immune response, and the experiment described in Chapter 3 sought to evaluate a method to take advantage of this immune response reduction technique with a method that can be applied to current wired interface technologies. Previous work has demonstrated that meningeal tissues can infiltrate the structure of a porous implant (Kim 2004), but no further investigation of this property had been made. Trends of decreasing immune activity with increasing distance down the implant shaft have been found, which is consistent with the hypothesis that meningeal ingrowth contributes to the immune response (Thelin et al., 2011; Woolley et al., 2013). A porous implant structure was fabricated and evaluated to determine whether allowing meningeal tissue to regrow through the implant structure would reduce its growth down the implant shank to the recording zone. Significant reductions in meningeal tissue ingrowth were found for the porous implants, in addition to a

significant improvement in neuron density in the immediate vicinity of the probe compared to non-porous control implants.

1.3.3 Dynamically softening interface substrate

Chapter 4 describes the histological evaluation of a novel dynamically softening neural interface substrate. A shape memory polymer (SMP) was recently developed which is sufficiently stiff to facilitate insertion into the cortical tissue, but then softens significantly in the physiological environment following implantation. Several previous studies have found that lower-modulus implant substrates reduce the chronic immune response, but most designs suffer from compromises to facilitate insertion of soft flexible probes. This study was conducted to determine whether the dynamic softening capability of the SMP substrate offers beneficial reductions in the chronic immune response compared to another commonly used flexible interface substrate which does not soften. Dummy implants consisting of the SMP substrate were implanted along with parylene-c implants of identical dimensions to compare the chronic immune response. Previous work has generally compared flexible implants of constant or variable modulus to very stiff controls, but this experiment fully isolates the effect of the dynamic softening capability by comparing the SMP substrate to parylene-c, which has a very similar modulus to that of the SMP substrate upon implantation, but does not soften. SMP implants were found to reduce levels of reactive astrocyte encapsulation compared to parylene-c controls at 4 weeks.

2 Sub-meninges Implantation

2.1 Introduction

The purpose of extracellular neural interfaces is to allow acquisition of neural signals with a high signal-to-noise ratio over a long period of time, in order to facilitate a wide range of therapeutic and research applications. Devices already in use provide relief from the symptoms of Parkinson's disease (Krack et al., 2003), restore hearing, or control a computer cursor or a robotic arm, in addition to allowing researchers to study neural processing (Stieglitz et al., 2009). Future neural interfacing applications include restoration of function lost due to CNS disease or trauma, including blindness and paralysis, and chronic CNS mediated control of prosthetic devices (Polikov et al., 2005; Stieglitz et al., 2009). Significant advances have been made in the past 30 years towards developing a reliable cortical neural interface, but challenges still remain which prevent such technology from being clinically viable. Chief among these is the biocompatibility of the interface. Insertion of a recording implant into the cortex initiates short- and long-term inflammatory processes which can result in neuron death and eventual encapsulation and failure of the implant (Biran et al., 2005; Kalman, 2003; Turner et al., 1999). Numerous strategies have been employed to attempt to mitigate the brain’s foreign body response, reduce encapsulation and minimize neuronal loss, improving recording performance. These strategies include alterations to the probe’s size and shape, addition of drugs or polymers, and modification of the implantation

procedure (Chen et al., 1997; Cui et al., 2003; He et al., 2006; Hsu et al., 2009; Rousche et al., 2001; Shain et al., 2003; Williams et al., 2005). The addition of a dexamethasone-eluting coating was found to help reduce the astrocytic response (Shain et al., 2003), but a coating of parylene-c, often used in other medical device applications, did not affect the immune response (Winslow et al., 2010). Reduced implant size and elimination of conventional skull fixation have also been shown to reduce the immune response (Biran et al., 2007; Kim et al., 2004; Thelin et al., 2011). Despite the improvements that have been made, the majority of recording lifetimes for many different types of interfaces are still on the order of several months, far short of what is necessary for a clinically viable therapeutic interface (Merrill and Tresco, 2005; Polikov et al., 2005; Rennaker et al., 2005b; Shain et al., 2003). Viable recordings have been acquired for as long as two to three years in some cases, but such extended lifetimes are generally rare (Simeral et al., 2011). One common aspect of current array technology which has not received significant attention is the basic dura-crossing design of conventional wired probes. Essentially all current neural interfaces consist of some kind of penetrating electrode spike or wire which is embedded in the cortical tissue and attached to a structure and wires on the surface of the cortex, which convey the signal out of the skull.

It has been suggested that some of the cells which participate in the immune response are derived from the meningeal space, in addition to the native astrocytes and microglia (Cui et al., 2003; Fawcett and Asher, 1999;

Kalman, 2003; Maxwell et al., 1990; Ness and David, 1997). The development of methods to prevent these cells from migrating down the electrode might improve chronic recording performance. In effect, meningeal cells and glial cells attempt to encapsulate a penetrating electrode in the same glia limitans which encapsulates the rest of the CNS (Fawcett and Asher, 1999). *In vitro* experimentation has shown that the formation of a glia limitans is triggered when astrocytes and meningeal cells come into contact, so it seems likely that reduction of meningeal cell migration into the area surrounding a cortical electrode would alleviate the glial encapsulation response (Abnet et al., 1991). Rapid regrowth of the dura mater has been observed during the use of chronic neural recording chambers in primates, often interfering with recording procedures and illustrating the ability of meningeal tissue to respond quickly to injury (Arieli et al., 2002; Gray et al., 2007). The spatial relationship between the meningeal space and the implant has not yet been examined for its effects on the encapsulation response. A study using porous hollow fiber membrane implants showed relatively modest immune activity despite their large size compared to typical neural interfaces. It is possible that the immune response was minimized because of the porous nature of the implant, allowing meningeal derived cells to grow through the implant versus down the implant (Kim et al., 2004).

This study directly examines the effect of trans-meningeal implantation on the chronic immune response to a neural implant. For ease of availability and ready comparison to current technologies, microwire segments were used

in the current study in two implantation configurations, conventionally (trans-meninges) and sub-meninges, in the rat cortex for a period of four weeks, and brain sections were subjected to quantitative immunohistochemistry analysis.

2.2 Materials and Methods

2.2.1 Subjects

Ten male Long Evans rats were individually housed in a temperature- and humidity-controlled environment and were exposed to a 12:12 h light-to-dark cycle with free access to food and water.

2.2.2 Implants

Implants for this study consisted of individual lengths of 50μm diameter stainless steel microwire with a polyimide coating. This is similar to materials which have been used to construct microwire recording arrays (Nicolelis et al., 2003; Williams et al., 1999). Each animal received three sub-meninges implants and three trans-meninges implants. To ensure consistent implantation depth, insertion of the microwire implants was performed using a mechanical insertion device. The insertion device consisted of a 25gauge needle with a plunger wire inside the needle and the device was mounted to a micromanipulator. To perform an insertion, a microwire segment which has been sonicated in ethanol and rinsed with sterile saline is inserted into the end of the inserter needle with the plunger retracted, then the assembly is lowered, bringing the tip of the

implant into contact with the cortical surface. The inserter is then lowered to allow the implant and needle tip to incise the dura. The plunger is then depressed to push the implant out of the end of the inserter needle into the cortical tissue. Two different plunger lengths are used for the two implantation types – sub-meninges implants are accomplished using a plunger which extends to the end of the needle tip when depressed, forcing the implant ~200μm below the cortical surface. Trans-meninges implants utilize a shorter plunger which leaves the end of the implant ~200μm above the cortical surface. A diagram of the insertion device and the two implant types is shown in **Figure 2.1.**

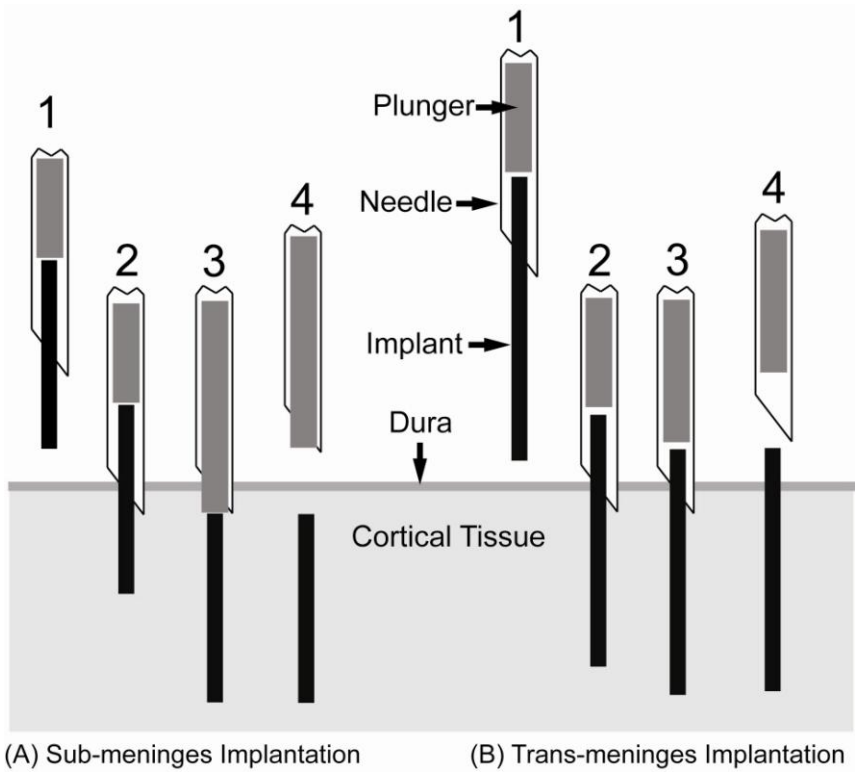

Figure 2.1: Implantation Scheme

Needle loaded with implant is positioned above implant site (1).
Tip of implant and needle are lowered into cortical tissue through the dura (2).
Plunger is depressed, pushing implant into tissue (3).
Needle is retracted, leaving implant in place (4).
Sub-meninges probes are placed approximately 200μm below the cortical surface.

2.2.3 Surgical Procedures

Surgical procedures are similar to those reported previously (Rennaker et al., 2005b). Briefly, rats were anesthetized using ketamine, xylazine and acepromazine (targeted dosage 50, 20, 5 mg/kg respectively). A midline incision was made in the scalp and the connective tissue was dissected from the skull. Two bone screws were implanted into the left side of the skull to

secure the acrylic skull cap. A 3 mm × 5 mm portion of the right parietal bone was removed using micro-rongeurs. Three microwire implants of each treatment were inserted in the manner described above. All subjects received both implant types in order to minimize the effects of animal-to-animal variability. Following implantation, the brain was covered by a layer of silicone elastomer (Kwik-Cast; World Precision Instruments, Inc., FL) and a layer of acrylic was added to seal the craniotomy and secure the structure to the bone screws. The initial incision was closed using absorbable sutures. All procedures were carried out in accordance with protocols approved by the University of Oklahoma Institutional Animal Care and Use Committee.

2.2.4 Immunohistochemistry

At 4 weeks post-implantation, subjects were euthanized and perfused. Subjects were administered 0.7 mL of the same ketamine cocktail used for the surgical procedure, and then transcardially perfused with 100 mL of phosphate buffered saline (PBS) followed by 100mL of 4% paraformaldehyde in PBS. The brain was removed and stored (4°C) for 48 h immersed in a solution of 30% sucrose by volume and 4% paraformaldehyde for postfixation and cryoprotection. Both sub- and trans-meninges implants were still in the brain following removal of the skull. These wires were removed from the brain prior to and during blocking of tissue around the implant site for sectioning. The brain was cut into 40μm thick horizontal sections which were collected free-floating in PBS. Alternating sections were stained with antibodies for GFAP to

label activated astrocytes, and IBA1 to label activated microglia in both phagocytic and nonphagocytic forms (Jones and Tuszynski, 2002; Nakajima and Kohsaka, 2001; Polikov et al., 2005). All sections were also labeled with NF160 anti-neurofilament antibody to visualize neuronal processes surrounding the tracks. Following three washes in PBS, sections were blocked in 3% normal donkey serum for 30 minutes. Sections were then incubated overnight in primary antibody solutions (NF160 and GFAP or IBA-1, 1:250) in a buffer containing 3% normal donkey serum and 0.3% Triton X-100. The following day, sections were rinsed and then incubated in secondary antibodies for 2h and then visualized with AlexaFluor 555 (Invitrogen) and coverslipped using Vectashield with DAPI (Vector Laboratories). All tissue sections in this study were stained at the same time with the same primary and secondary solutions to ensure consistency. Images were taken using an Olympus BH-2 microscope with a 10x objective and an Olympus DP70 digital camera.

2.2.5 Analysis

Images were analyzed using ImageJ software (NIH) to perform automated thresholding and area measurements of the activated regions surrounding electrode tracks for GFAP labeled images. Contralateral control sections were used to determine average background fluorescence levels and set threshold values for each cell type for each animal. Pixel count was converted to square microns of activated area around each track. An example track is shown in **Figure 2.2** with the above-threshold region outlined to

illustrate the area that was measured. Due to the nature of the cells, IBA1 labeled images could not be subjected to the same simple area counting method as GFAP images. Instead, a radial intensity profile function in ImageJ was used to measure the average fluorescence intensity as a function of radius from the implant-tissue interface. These intensity integrals, consisting of the area under the intensity curve, were then separated into 6 bins of 50μm each for statistical analysis. The same radial intensity profile technique was also used to examine GFAP labeled activity. For all analyses except for depth comparisons, a single mean intensity or area value was found for each track across all section depths.

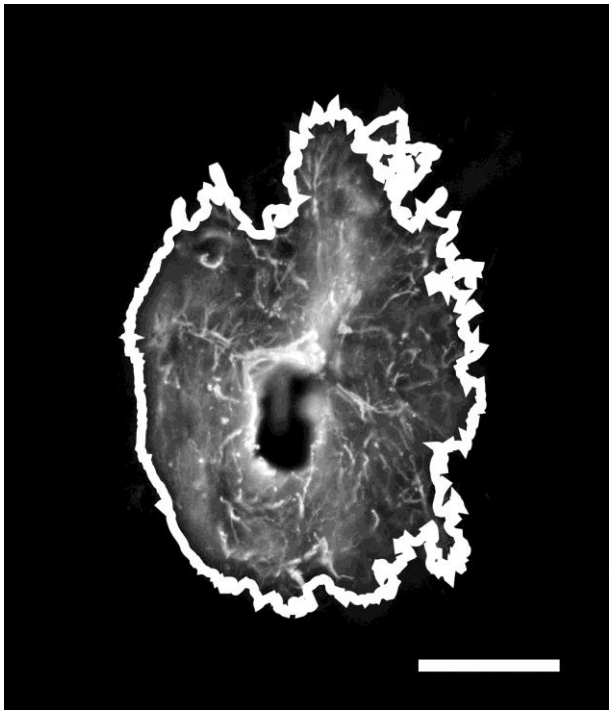

Figure 2.2: Typical GFAP labeled trans-meninges implant track showing area count border generated by ImageJ. Scale bar = 100μm.

2.3 Results

2.3.1 Astrocyte activity

Fluorescent labeling with antibodies for glial fibrillary acidic protein (GFAP) was used to identify reactive astrocytes while IBA-1 antibodies were used to label activated microglia. GFAP labeled images exhibited regions of reactive astrocyte activity surrounding each implant track, forming a densely packed, multilayered capsule which is typical of a neural implant at a 4 week time point. An example track showing all 4 imaging markers is shown in **Figure 2.3.**

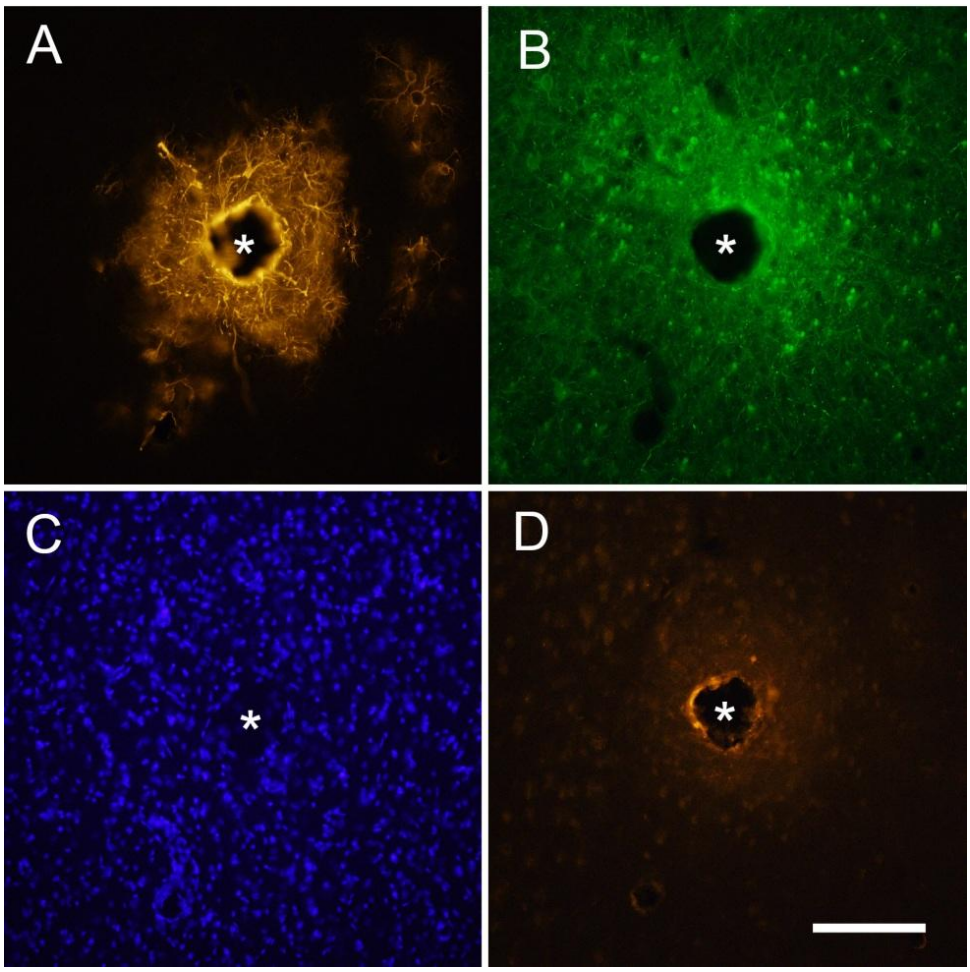

Figure 2.3: Representative images of the same sub-meninges implant track at 4 weeks with four different markers (* denotes implant location)
A) GFAP showing reactive astrocytes;
B) NF160 showing neuronal processes;
C) DAPI showing all cell nuclei;
D) IBA-1 showing activated microglia. Scale bar = 100μm

2.3.1.1 Morphology

Morphology of GFAP+ cells was consistent with that of reactive astrocytes in the CNS. The GFAP+ sheath surrounding each implant track was accompanied by a surrounding area of GFAP+ cells extending tens to a few

hundred microns from the implant center in a generally radially symmetric fashion. The GFAP+ regions surrounding the tracks were clearly delineated from the surrounding background, allowing the use of simple threshold-based software to determine the regions' size.

Figure 2.4 shows two example images from a single tissue section stained for GFAP. The trans-meninges implant (A) and sub-meninges implant (B) are shown side by side for comparison. This representative sample illustrates the dramatic difference in GFAP expression between the two implantation methods.

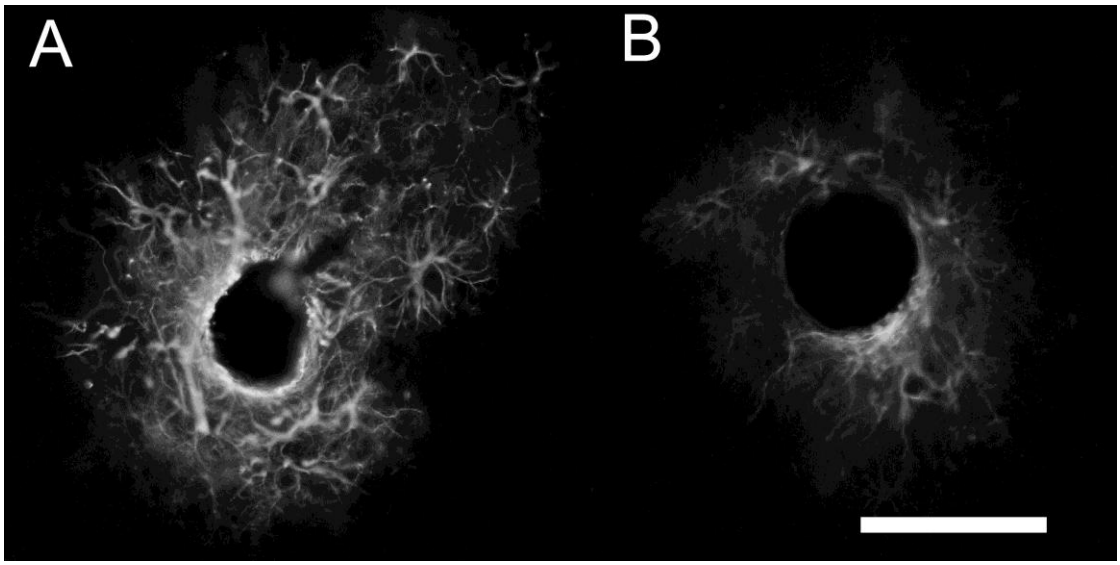

Figure 2.4: Representative sample of GFAP reactivity in a single cortical slice to trans-meninges (A) and sub-meninges (B) implants. Scale bar = 100μm

2.3.1.2 Quantitative GFAP measures

The areas for each section were measured using Image-J. Sub-meninges implants showed 63% less GFAP labeled cellular area on average than trans-meninges implants, as shown in **Figure 2.5** (t-test, n=30, $p<0.001$). A previous study (Thelin et al., 2011) found that implants tethered to the skull tended to form larger cavities that were elongated in the rostral-caudal axis. It is possible that the trans-meninges implants in the current study were mechanically attached to the silicone used to cover the brain following implantation. This is unlikely given that we removed the wires from the brain after the skull was detached. The silicone came off with the skull in most cases.

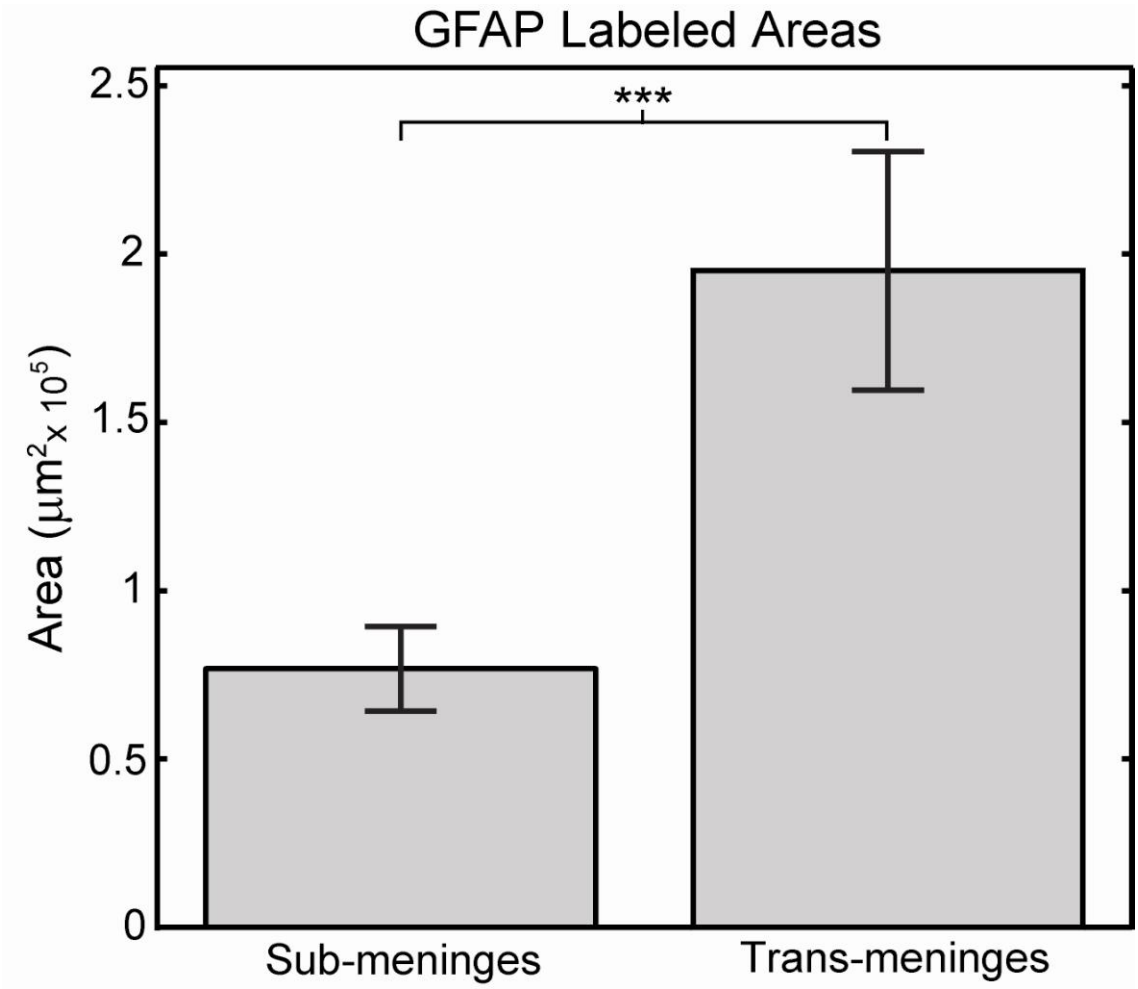

Figure 2.5: GFAP labeled track areas for sub-meninges and trans-meninges implants +/- 95%CI (*p<.001)

If the trans-meninges implants were attached to the silicone, it is likely that an asymmetry in the wound site or GFAP response would be present due to relative motion between the brain and the skull. An examination of the voids at the center of the GFAP labeled areas found no differences in void area between implant types (t-test, p =0.76). Measurement of the voids' edge-to-edge distances in the rostral-caudal and medial-lateral directions revealed no significant elongation of the voids along either axis for either sub-meninges

(p=0.47) or trans-meninges implants (p=0.75), as shown in **Figure 2.6**. This scatter plot reveals a general grouping of the data around the line y=x, which indicates a circular void, and suggests that the trans-meninges implants were not tethered to the skull.

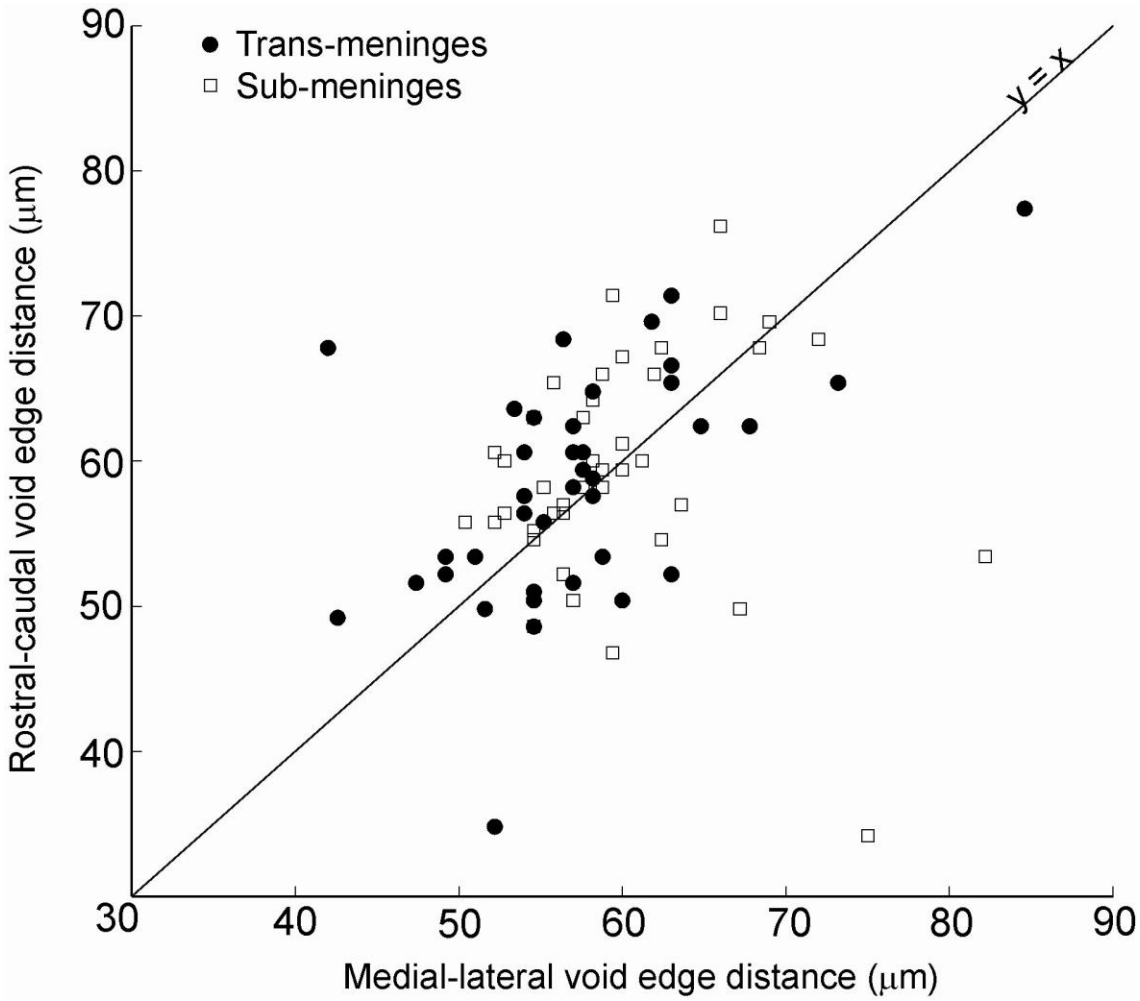

Figure 2.6: Edge-to-edge dimensions of track voids for both implant types showing data from deepest and shallowest sections only. Line (y=x) indicates no void elongation in either direction.

The same images were also subjected to analysis via radial intensity profiling, in order to measure the fluorescence intensity as a function of distance from the implant-tissue interface and examine the spatial distribution of the astrocyte response. It was found that sub-meninges implants taken from the same cortical slice had significantly less GFAP labeled cellular activity out to a radius of 300μm (**Figure 2.7**). The intensity profile analysis illustrates both the reduced intensity and reduced radial extent of reactive astrocyte activity for sub-meninges implants. The general scale of the astrocyte response is consistent with other histological studies using implants of this general size (Biran et al., 2005; Winslow and Tresco, 2010). Due to imaging constraints and the proximity of neighboring tracks and section edges, we could not measure fluorescence intensity consistently any further than 300μm for the entire data set, therefore the measurements at 350μm are from a subset of about 1/2 of all tracks. For this radius bin, though, no difference in integrated intensity was found between the two implant types (t-test, $p = 0.057$). This indicates that GFAP+ reactivity has returned to background levels at 350μm from the implant surface for trans-meninges implants. ANOVA comparison of the radius bins for sub-meninges implants showed no difference between the 250, 300 and 350μm radii, indicating that GFAP+ activity has returned to background levels at a 250μm radius for the sub-meninges implants. Thus, the typical maximum extent of reactive astrocyte activity is reduced by about 100μm by sub-meninges implantation.

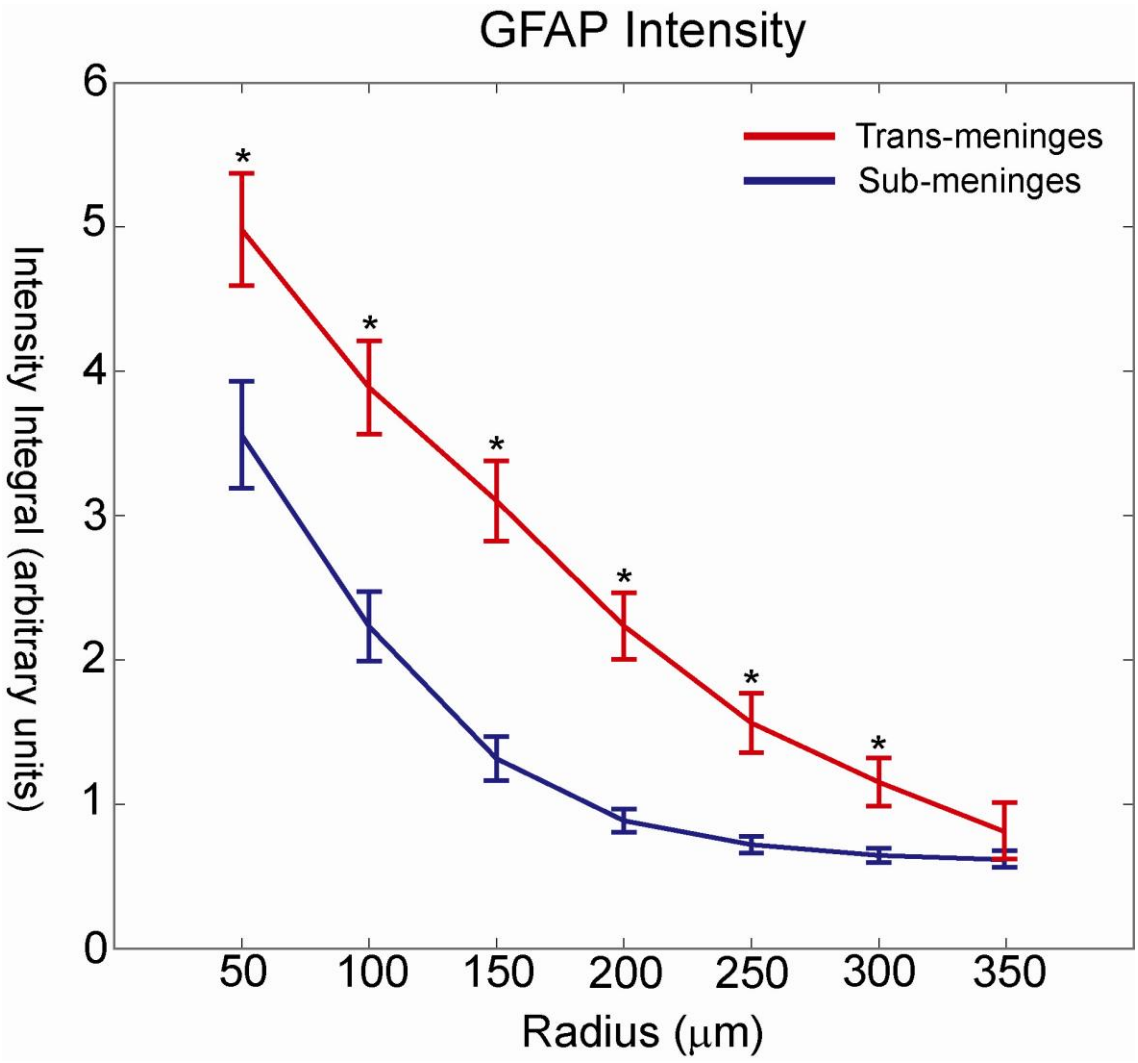

Figure 2.7: GFAP intensity as a function of radius for trans-meninges and sub-meninges implants +/- 95%CI (*p<.001)

2.3.1.3 Astrocyte activity by section depth

In addition to examining mean track areas across all section depths to compare sub-meninges and trans-meninges implants, GFAP area data were grouped and analyzed according to section depth in order to better understand the spatial distribution of the astrocyte response. If the meningeal tissue were

growing down the shaft, it is reasonable to assume that the glial scar would be larger at the more superficial layers. When the data from this study are arranged by depth, no such trend is evident (**Figure 2.8**). Neither type of implant shows statistically significant differences in astrocyte activity between section depths. It is likely that the elevated response near the cortical surface was not captured because we only compared sections in which both sub and trans-meninges implants were present (>200μm below the cortical surface). The topmost layers of the cortex were not collected due to the lack of chronic sub-meninges implant tracks. Additionally, it is possible that any cellular migration from the cortical surface is already complete by the 4 week time point employed in this study.

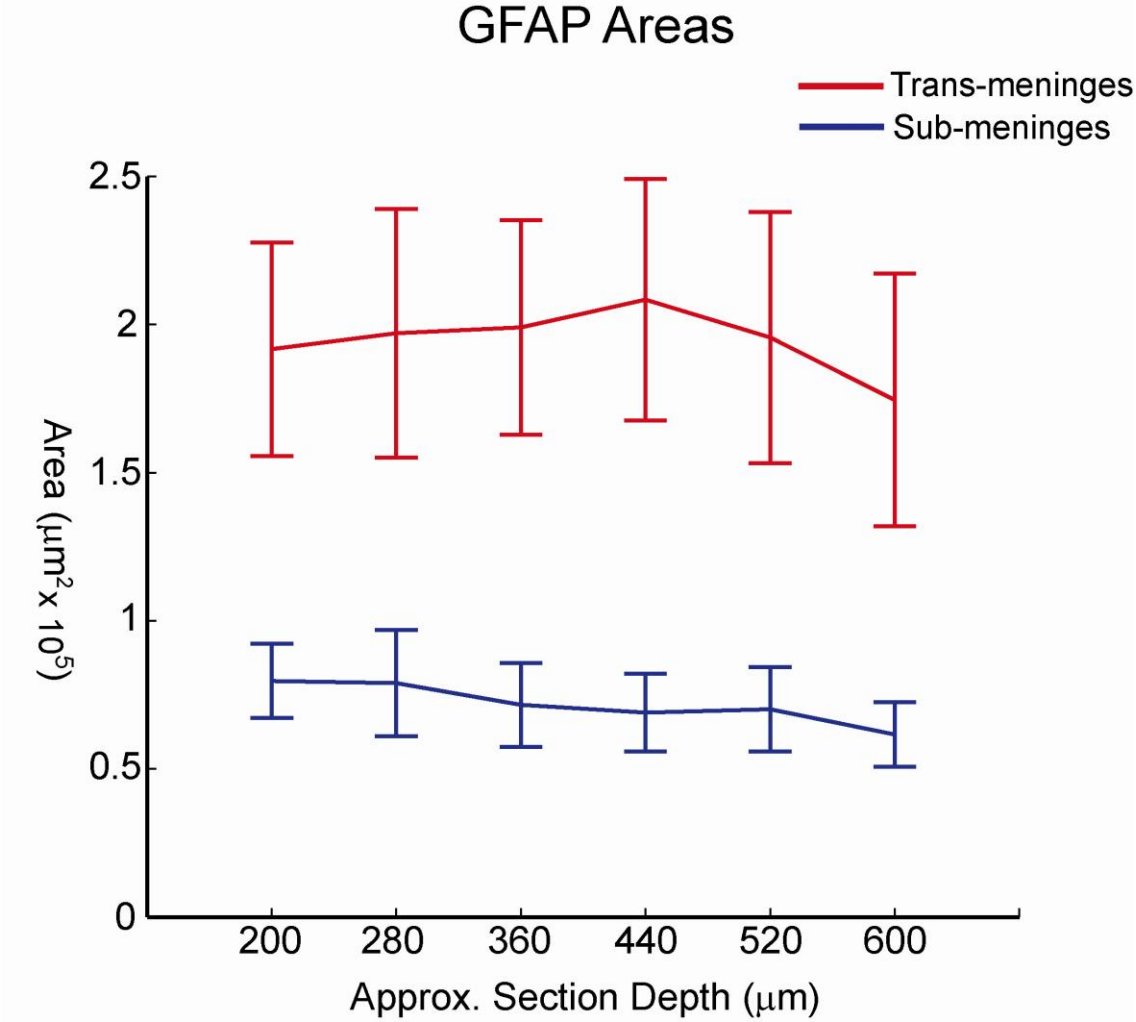

Figure 2.8: Mean GFAP labeled areas grouped by section depth for sub-meninges and trans-meninges implants

2.3.2 Microglia activity

Adjacent sections utilized IBA1 antibodies to label activated microglial cells, and these also showed a region of cellular activity immediately surrounding the implant. Cellular morphology was consistent with that of activated microglial cells. IBA1+ regions were much smaller than GFAP+

regions for the same tracks, which is consistent with other findings that microglial activity peaks in the first week post-injury and astrocyte activity dominates from then on (Biran et al., 2005; Polikov et al., 2005). Due to the sometimes more diffuse nature of the microglial cellular activity and the lack of a well-defined border between labeled cells and unlabeled tissue, intensity profiling was used exclusively for analysis rather than area measurements. IBA1 labeled sections showed statistically significant reductions in fluorescence intensity for the first three radius bins of 0-150μm from the implant surface (t-test, $p<.05$), as shown in **Figure 2.9**. There were no significant differences in IBA1 reactivity for sub-meninges or trans-meninges implants at radii greater than 200μm from the center of the electrode track.

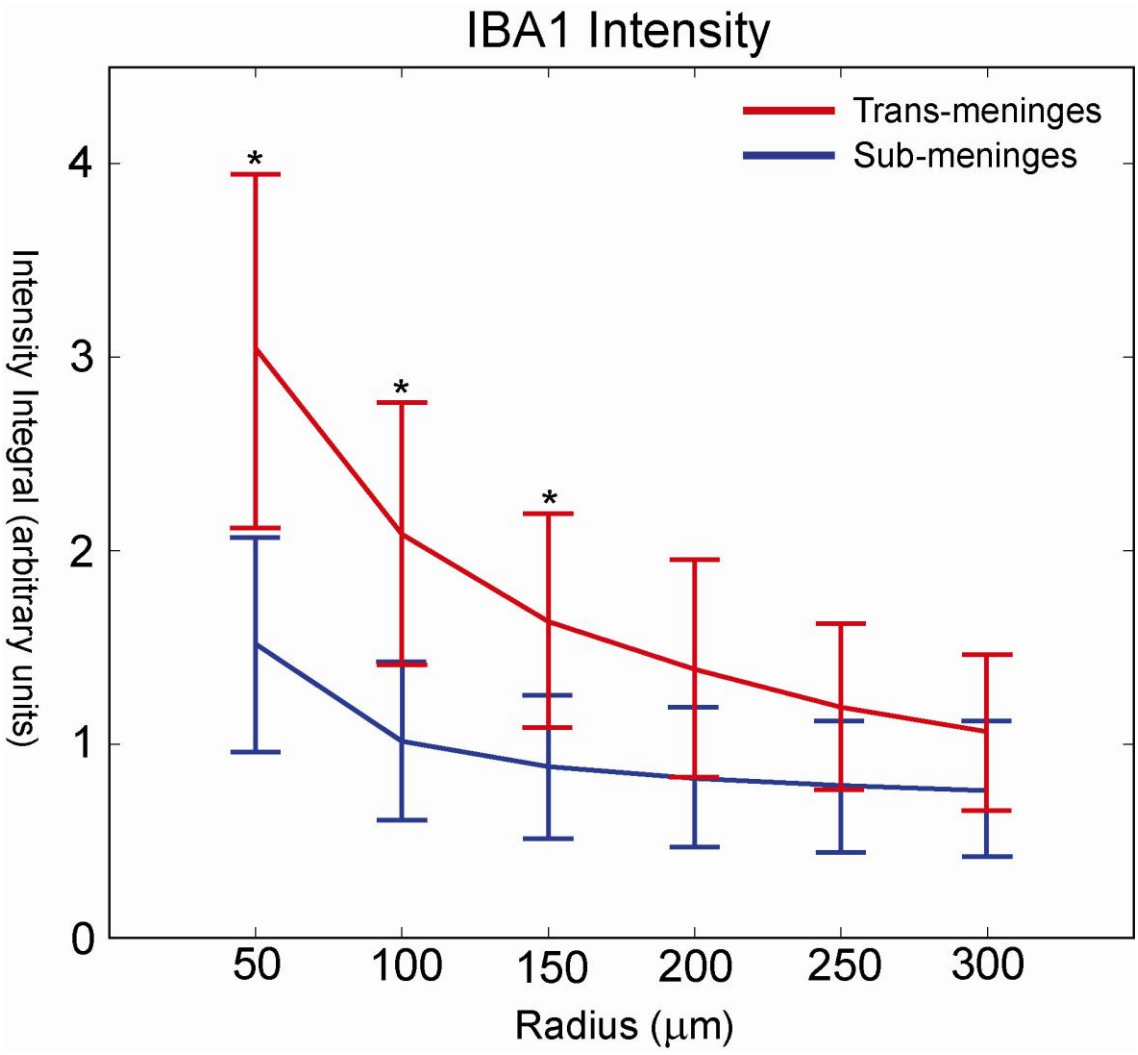

Figure 2.9: IBA1 intensity as a function of radius for sub-meninges and trans-meninges implants +/- 95% CI (*p<0.05)

Both the mean intensity and the radial extent of microglia cellular activity were reduced by sub-meninges implantation. Combined with the reduction in reactive astrocyte activity, this constitutes a large reduction in the size and scope of the foreign body response for sub-meninges implants, which should correspond to an improvement in recording array performance for sub-meningeally implanted recording devices.

As with GFAP sections, no significant trend was found when IBA1 fluorescence intensity values for the significant radius bins were compared according to section depth (data not shown). Given that a greater degree of variability was found in IBA1 labeled activity than with GFAP, a subtle trend in reactivity with depth is more difficult to separate from normal variation.

2.3.3 Neurofilament results

Visualization of neuronal processes using NF160 antibody labeling did not produce sufficiently consistent results for meaningful data to be obtained. Morphology of labeled structures was consistent with neuronal processes, indicating proper function of the antibody, but the degree of labeling exhibited a high degree of variability from track to track and section to section not seen with the other techniques used in this study. Some implant tracks exhibited areas of elevated NF160 immediately surrounding the track, as seen in **Figure 2.3B**. An increase in neuronal density immediately surrounding a track is not consistent with widely observed neuronal dieoff surrounding an implant (Biran et al., 2005; Turner et al., 1999; Winslow and Tresco, 2010), but a similar phenomenon has been observed by other researchers when using the NF160 antibody (Winslow and Tresco, 2010). Future studies will employ NeuN to label neuron cell bodies and better allow quantification of viable neurons around the implant site.

2.4 Discussion

The results of this study suggest that the meninges play a role in determining the extent of the immune response at 4 weeks post-implantation. The data demonstrate that the immune response to a cortical implant is greatly reduced when the entire implant is not in contact with the meninges. The average amount of GFAP-labeled cellular activity, which is the primary metric of the chronic immune response (Kalman, 2003; Polikov et al., 2005; Szarowski et al., 2003; Turner et al., 1999)**,** was nearly threefold greater for trans-meninges implants than sub-meninges implants (**Figure 2.5**). As fibrous encapsulation by reactive astrocytes has been shown to be strongly correlated with neural recording device failure, this reduction should correspond to an improvement in recording device performance and signal lifetime (Polikov et al., 2005).

Radial intensity profile analysis was also used to examine the astrocyte response. This revealed a reduction in both the intensity and the extent of GFAP labeled cells surrounding sub-meninges implant tracks. GFAP intensity was significantly reduced for all 6 radius bins that were measured out to a distance of 300 microns from the implant-tissue interface (**Figure 2.6**). At 350μm, GFAP intensity had returned to the background level. The greatest reductions in integrated fluorescence intensity were seen in the 150μm and 200μm radius bins, indicating a reduction in the overall extent of the astrocyte response in addition to the intensity reduction. This is consistent with the findings of the threshold-based area measurements. The reduction of mean astrocyte activity in this 100 micron radius zone is particularly important for

neural interface function, since this is thought to be the maximum radius from which neural signals may be acquired, and elevated GFAP+ activity has been shown to be negatively correlated with neuron viability (Biran et al., 2005; Henze et al., 2000; Winslow and Tresco, 2010).

A reduction was also seen in areas of IBA1 labeled microglial activity. Microglial cell activity tends to peak around 1 week post-injury (Biran et al., 2005; Kalman, 2003; Polikov et al., 2005) and is reduced from its peak level by the 4 week time point used in this study, but a thin sheath of activated cells still surrounds each implant track, in the same region as the activated astrocytes. As microglia participate primarily in the acute inflammatory phase of the immune response and their activity should have decreased significantly by the 4 week time point used in this study, (Biran et al., 2005; Kreutzberg, 1996; Nakajima and Kohsaka, 2001; Polikov et al., 2005) the observed reduction in microglial activity indicates that sub-meningeal implantation likely has desirable effects on the acute phase of the immune response in addition to the chronic phase, which is characterized mainly by reactive astrocyte activity and the formation of the glial scar (Carbonell and Boya, 1988; Kalman, 2003). The reduction of microglial activity is also likely to have a desirable effect on neuronal viability in the region surrounding the implant, as the presence of these cells has been correlated with neuronal death (Biran et al., 2005). This may be mediated directly by a number of cytotoxic compounds that have been shown to be secreted by microglia which cause neuron death or alteration of function, including monocyte chemotactic protein-1 (MCP-1) and tumor necrosis

factor-alpha (TNF-α), among numerous others (Biran et al., 2005). The presence of IBA1+ cells in the immediate vicinity of the implant may suggest the existence of a persistent inflammatory state, based on findings that such cellular reactions are only found in the case of indwelling implants, and not in the case of stab wounds (Biran et al., 2005). Given the observed decrease in IBA1 immunoreactivity for sub-meninges implants in the current study, it seems likely that a reduction in chronic inflammatory activation makes up some part of the mechanism responsible.

The mechanisms which may account for the observed reduction in the foreign body response due to sub-meningeal implantation are not fully understood, but there are some factors which are thought to contribute to the immune response which may be affected by the implant's location. Meningeally derived fibroblasts have been found to migrate into the wound from the meningeal space and contribute to the inflammatory response (Kalman, 2003; Kim et al., 2004; Maxwell et al., 1990; Ness and David, 1997), and positioning the implant below the cortical surface may reduce this component. In one study, an encapsulating sheath of meningeal fibroblast cells was found surrounding silicon "Michigan" probes implanted in the guinea pig cortex at two weeks (Cui et al., 2003). In effect, these cells participate along with reactive astrocytes in the process of forming a new glia limitans around the implant which migrates down the wound track from the pial surface (Maxwell et al., 1990). Sub-meningeal implantation of the device physically removes it from the pial space, and thus likely inhibits this process.

Placement of the implant below the meninges may reduce chronic micromotion between the implant and the surrounding cortical tissue, which has been implicated in exacerbating the chronic immune response. It has been shown that hollow fiber membrane cortical implants that were free-floating in the cortical tissue had reduced chronic immune activity compared to implants which were anchored to the skull (Kim et al., 2004). It is possible that the reactive cells grew through the membrane and not down the membrane. This suggests that an electrode with a porous substrate at the meninges might reduce the immune response. In the current study, available surgical techniques make it impossible to completely isolate the effects of implant location and chronic micromotion, as the upper ends of the trans-meninges implants are still in contact with the silicone elastomer used to seal the craniotomy. The amount of interface is small, though, and much softer than the fixation materials which have been employed for tethered implants to study this effect (Kim et al., 2004; Thelin et al., 2011). Also, the effects of tethered implantation, namely enlarged, elongated void areas (Thelin et al., 2011), were not present for either implant type in the present study. **Figure 2.6** shows the distribution of track void dimensions along the rostral-caudal and medial-lateral axes, showing no void elongation or enlargement for either type of implant. Thus, it seems safe to conclude that chronic micromotion between the brain and implant did not play a large role in producing the observed difference between the implant types.

2.5 Conclusion

Quantification of glial cell activity surrounding sub-meninges and trans-meninges microwire implants revealed that sub-meninges implantation yields a substantial decrease in the chronic immune response to a microwire implant. Subdural implantation of microwire segments produced an average reduction in astrocyte activity of 63% compared to conventionally implanted controls. Microglial activity was also reduced. This offers insight into the factors that govern the brain's response to a neural implant, and these results also suggest that techniques which isolate implants from the meninges may reduce the encapsulation response and improve chronic recording quality.

3 Implant Shank Porosity

3.1 Introduction

The current understanding of neural recording electrode failure holds that the loss of neural signals is caused in large part by the fibrous encapsulation of the implant by reactive microglia and astrocytes (Polikov et al., 2005), although other mechanisms related to death or displacement of neurons near the implant have also been implicated in the failure of these devices (Biran et al. 2005). Recent work has indicated that meningeally derived cells may play a significant role in the inflammation and encapsulation response as well (Markwardt et al., 2013; Woolley et al., 2013). Contact between astrocytes and meningeal cells has been shown to trigger the formation of a glia limitans *in vitro*, which suggests that the presence of meningeal cells around a cortical electrode would contribute to the fibrous encapsulation response(Abnet et al., 1991). Fluorescent antibody labeling of vimentin around planar silicon implants revealed significantly increased presence of this protein in the cellular mass surrounding the implant (Woolley et al., 2013). Meningeal fibroblasts and reactive astrocytes are known to express vimentin, but reactive astrocytes also strongly express GFAP, which is not expressed by meningeal fibroblasts. Since GFAP was not evident in the observed superficial cell clusters in this study, this strongly suggests the presence of vimentin-expressing meningeally derived fibroblasts (Woolley et al., 2013). The lack of significant IBA-1 labeling in this region also supported this conclusion, indicating the absence of native

microglia. Additionally, a trend of decreasing immune cell activity with increasing depth along the implant shaft was revealed, which is consistent with the idea of a strong meningeal component in the immune response. The study described in Chapter 2 compared loose microwire segments that were placed completely below the cortical surface to conventional meninges-crossing implants, and found that sub-meninges implantation produced a substantial reduction in the immune response at four weeks (Markwardt et al., 2013). These results support the hypothesis that meningeal tissue contributes to the chronic immune response.

Current neural interface technologies rely upon meninges-crossing designs for data transmission, so although our previous study offers insight into the factors governing the immune response, fully sub-meninges recording probes are not currently technically feasible. In order to take advantage of the observed phenomena, other techniques must be employed to mitigate the meningeal contribution to the immune response and fibrous encapsulation in the recording region of penetrating intracortical electrodes. Ingrowth of vimentin+ meningeal tissue into the porous structure of a cortical implant has been demonstrated previously (Kim et al., 2004). This study employed porous hollow fiber membrane implants which showed changes in immune response as a result of differing implantation techniques, but hollow fiber membranes do not represent a viable recording electrode material and are porous the entire length of the structure.

The current experiment investigates the influence of the addition of pores in the region of the planar polymer implant in contact with the meninges on the brain's immune response. It is thought that the addition of pores near the cortical surface may encourage ingrowth of meningeal tissue in a similar manner to that previously demonstrated with hollow fiber membranes, and thereby minimize growth down the implant shaft to the recording region, ultimately minimizing neuronal death or displacement. Planar implants composed of a previously described shape memory polymer substrate were employed for this study (Ware et al., 2012). Experimental implants had a set of 9 pores in the shank region near the cortical surface, and control implants were solid. The 4-shank (150μm x 35μm cross section; spike center-to-center 450μm, 800 μm long) polymer implants in the shape of intracortical multi-electrode arrays were implanted in rat cortex for four weeks, and quantitative histological analysis was performed using markers for reactive astrocytes, neuron cell bodies, IgG to measure blood-brain barrier integrity and vimentin to identify meningeal tissue and proximal reactive astrocytes.

3.2 Methods

3.2.1 Subjects

Six male Long Evans rats which made up the main cohort of the study were individually housed in a temperature- and humidity-controlled environment and were exposed to a 12:12 h light-to-dark cycle with free access to food and

water. IgG and neuron density data were obtained from an additional four rats which were implanted in the same manner as the main cohort.

3.2.2 Implants

Implants for this study consisted of planar polymer electrodes laser cut from 35μm thick sheets. Each implant consisted of four penetrating spikes attached to a common tab, which remained above the cortical surface. Each animal received one nonporous implant and one porous implant with two arrays of laser-cut holes in each penetrating spike, as shown in **Figure 3.1.**Eacharray consists of nine 20μm holes with 20μm edge to edge spacing with each row offset at an angle of 60 degrees. This design facilitates future recording electrodes by leaving sufficient area to pattern electrode traces between holes. The implants were positioned such that each penetrating spike was fully embedded in the cortical tissue and the connecting tab was flush with the cortical surface after implantation. The implant substrate material is a thiol-ene based shape memory polymer which undergoes a hydration-mediated dynamic softening process following implantation, in order to yield an improved mechanical match with the surrounding cortical tissue and reduce long-term inflammation. Fabrication and characterization of this material are described in further detail in Ware 2012 and Chapter 4.Implants were UV sterilized prior to implantation.

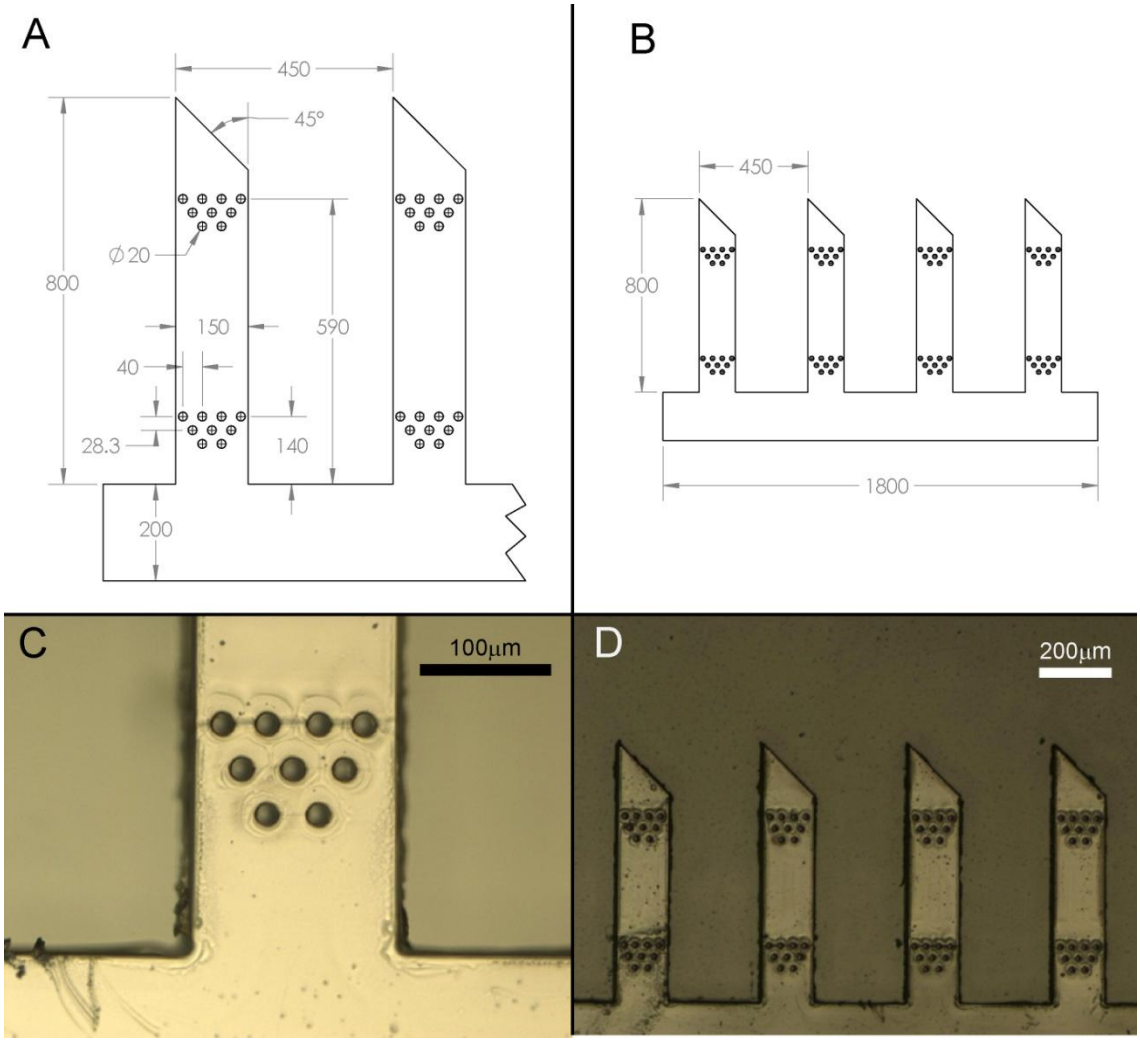

Figure 3.1: Diagrams and images of porous implants. Control implants are dimensionally identical aside from the lack of pores. Thickness of all implants is 35μm.

(A) Detail drawing showing pore arrangement and location. All dimensions in μm.
(B) Drawing showing overall size and shape of porous implant.
(C) Detail photograph showing pores near base of shank
(D) Photograph of entire implant

3.2.3 Surgical Procedures

Surgical procedures are similar to those reported in section 2.2.3. Rats were anesthetized using ketamine, xylazine and acepromazine (targeted dosage 50, 20, 5 mg/kg respectively). A midline incision was made in the scalp and the connective tissue was dissected from the skull. Two bone screws were implanted into the left side of the skull to secure the acrylic skull cap. A 3mm×5mm portion of the right parietal bone was removed using micro-rongeurs, and the dura was removed. One 4-shank implant of each treatment was inserted using micro-forceps. The implants were positioned such that each penetrating spike was fully embedded in the cortical tissue and the connecting tab was flush with the cortical surface after implantation. All subjects received both implant types in order to minimize the effects of animal-to-animal variability, and rostral/caudal arrangement of the two implant types was alternated between animals in order to eliminate potential confounding effects of positioning in the brain tissue. Following implantation, the brain was covered by a layer of silicone elastomer (Kwik-Cast; World Precision Instruments, Inc., FL) which secured the implant handling tabs. A layer of acrylic was then added to seal the craniotomy and secure the structure to the bone screws. The initial incision was closed using absorbable sutures. All procedures were carried out in accordance with protocols approved by the University of Texas at Dallas and University of Oklahoma Institutional Animal Care and Use Committees.

3.2.4 Immunohistochemistry

At 4 weeks post-implantation, subjects were euthanized and perfused. Subjects were administered 0.7mL of the same ketamine cocktail used for the surgical procedure, and then transcardially perfused with 100mL of phosphate buffered saline (PBS) followed by 100mL of 4% paraformaldehyde in PBS. Implants were removed from the brain upon removal of the skull cap following perfusion. The brain was removed and stored for 4h immersed in 4% paraformaldehyde for postfixation. Following postfixation, excess tissue surround the areas of interest was removed and the resulting tissue blocks were placed in 30% sucrose in PBS for cryoprotection for 72h. The brains were cut into 20μm thick horizontal sections which were collected onto slides. All tissue was batch stained to minimize differences due to processing. The main group of tissue sections were labeled with antibodies for GFAP to label reactive astrocytes, NeuN (FOX3) to visualize neuron cell bodies, and vimentin to indicate meningeal fibroblasts and reactive astrocytes (Jones and Tuszynski, 2002; Nakajima and Kohsaka, 2001; Polikov et al., 2005). Antibodies specific to IBA1 labeling reactive microglia are frequently used in studies of this kind (Harris et al., 2011a; Kim et al., 2004; Polikov et al., 2005; Winslow and Tresco, 2010) but preliminary studies using this marker and similar implants found no migroglial activity at four weeks. Microglial activity is known to prevail much earlier in the time course of the immune response and decrease substantially by four weeks post implantation (Kalman, 2003; Polikov et al., 2005). Thus, analysis of the microglial reaction in this experiment was eliminated in favor of

more informative markers. Every third section was placed in a separate batch and labeled with a fluorescent antibody specific to rat IgG, in order to assess blood-brain barrier integrity at the implant site (Hoshino et al., 1996; Potter et al., 2012; Skousen et al., 2011). Antibody concentrations are shown in **Table 3.1.** Sections were also taken from similar locations in the unimplanted left hemisphere for each rat to serve as controls for image analysis. These were processed in the same batch as the experimental sections. Following three 10min washes in PBS, sections were blocked in 3% normal goat serum for 30 minutes. Sections were then incubated overnight in primary antibody solutions in PBS containing 3% normal donkey serum and 0.3% Triton X-100. The following day, sections were incubated in conjugated secondary antibodies for 2h and coverslipped using Vectashield with DAPI (Vector Laboratories). IgG labeled sections were incubated in the conjugated antibody solution overnight, then washed and coverslipped the following day. Images were taken using an Olympus BH-2 microscope with a 10x objective and an Olympus DP70 digital camera.

Primary Antibodies			**Secondary Antibodies**		
Abcam #	Type	Dilution	Abcam #	Type	Dilution
4674	Chicken anti-GFAP	500:1	96951	Anti-chicken 488	100:1
104225	Rabbit anti-FOX3 (NeuN)	500:1	7087	Anti-rabbit TRITC	100:1
8069	Mouse anti-vimentin	250:1	150119	Anti-mouse 647	100:1
7094	Anti-rat IgG TRITC	100:1			

Table 3.1: Antibody types and concentrations

3.2.5 Analysis

Following acquisition, images were subjected to computerized analysis to quantify various aspects of the immune response. The primary techniques used were intensity profiling to determine the magnitude and distribution of GFAP, vimentin and IgG labeled cells and cell counting to measure neuron density.

3.2.5.1 Intensity analysis

An intensity profiling scheme was used to measure pixel brightness values as a function of distance from the edge of the implant track. Radial intensity profiling has been used previously for microwire implants (Markwardt et al., 2013) but this method is not optimal for the oblong tracks produced by the planar implants used in the current study. A profiling method was developed wherein the user selects the two end points of the track along the center of its

longest axis, and the program measures 50 evenly spaced intensity profiles perpendicular to this centerline in each direction. Images are converted to greyscale, then threshold-based analysis is used to select the dark area of the track void, which is excluded from the intensity profile analysis in order to control for variations in void size and shape, as well as better characterizing the device-tissue interface. This analysis scheme utilizing track void exclusion and integrated mean intensity profiling is based upon those used by other researchers in the assessment of neural interface immune reactions (Biran et al., 2005; Harris et al., 2011a; Winslow and Tresco, 2010). The selected track void area is overlaid with a black mask, and the track centerline is then selected manually. Each profile line consists of the first 200μm of pixels with a value >0 (e.g. beyond the void area mask). The resulting 100 profiles are averaged together to yield a mean profile for each track, which is then separated into 25μm bins for analysis. Intensity values shown represent mean pixel values for each 25μm bin. An example track with overlaid intensity profile lines is shown in **Figure 3.2.** To control for animal to animal variations in native expression levels of the markers of interest, intensity measurements were taken from the unimplanted contralateral hemisphere and the mean values for each rat were subtracted from the corresponding mean implant profiles. Background intensity profiles were taken from the same locations in the image frame as the experimental tracks in order to account for spatial nonuniformities in microscope illumination (Biran et al., 2005). Quantification of meningeal tissue at the implant sites was performed by subtracting the GFAP labeled image from the

vimentin labeled image for that section, leaving only areas which are vim+ and GFAP-. Example images illustrating the subtraction analysis process are shown in **Figure 3.3.** For pixels in which the GFAP intensity value is greater than the same pixel in the vimentin image, the value in the resulting subtraction image is zero. Due to the differences in spatial distribution of this tissue, void area masks could not be used, and all distance metrics are relative to the implant centerline rather than the void edge. When analyzing vim+/GFAP+ proximal reactive astrocytes, void masks from GFAP labeled images were overlaid on the vimentin labeled images, and then the intensity profile was taken. Since the GFAP mask excludes all vim+/GFAP- meningeal tissue and any other areas within or near the void not expressing GFAP, this ensures that only intensity values of vim+/GFAP+ tissue are measured. This cell population has been previously distinguished from vim-/GFAP+ “distal” reactive astrocytes (Ridet et al., 1997).

In order to further characterize the spatial distribution of the various immune response components, the collected intensity profiles were also grouped for analysis by section depth. Although tissue sections were collected and numbered in an ordered manner, due to the geometric characteristics of the cortex and occasional loss of some sections, it is not possible to reliably assign a specific depth value to each tissue section. However, it is still possible to group the data into more general depth categories and obtain some idea of the distribution of the cells of interest according to cortical depth. Brains were sectioned until no visible implant tracks were present, allowing the depth of the

electrode tip to be determined by locating the deepest section with a discernible track void. Using this point as a reference and knowing the length of the implants, it is possible to gain an approximation of the depth of the rest of the sections. For analysis, tissue sections were grouped into three depth zones, with the superficial zone beginning at the cortical surface and the deepest zone ending at the deepest section containing a full-width implant track. The number of intervening sections for each implant between these two levels is then evenly divided into the three analysis zones, and intensity profiles within those zones are averaged to gain a mean intensity curve for each track for each zone. Sections located in the tapered area of the electrode tip were excluded from all analyses to avoid confounding effects of reduced implant cross section at that location. This leaves 650μm of implant shank which was analyzed, meaning each depth zone accounts for approximately 1/3 of that length.

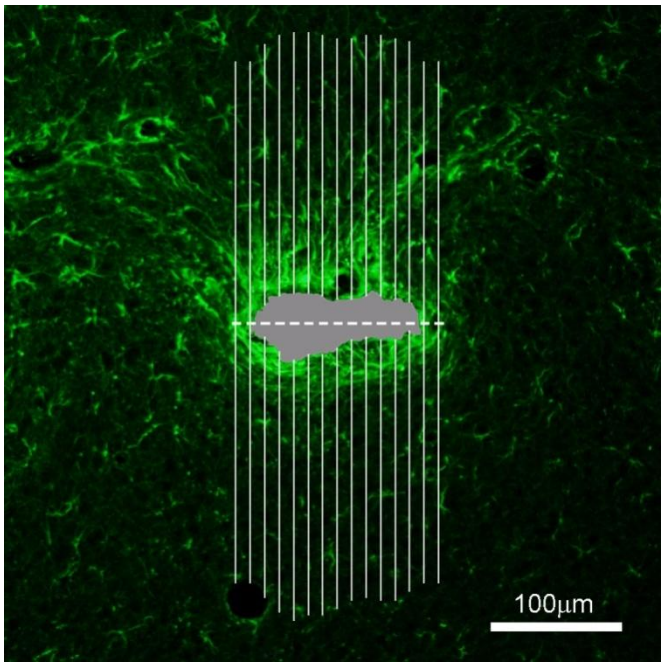

Figure 3.2: Illustration of intensity profile scheme on a typical GFAP-labeled implant track. Gray region indicates track void, which is excluded from intensity analysis. Dashed line shows track centerline and solid lines represent intensity profiles. Number of profiles has been reduced for clarity; actual analysis uses 50 profiles per side.

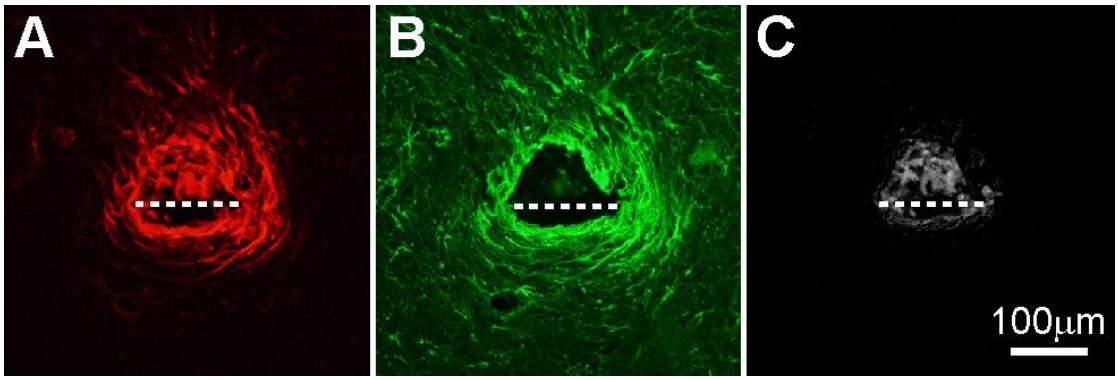

Figure 3.3: Image subtraction process

(A) Vimentin labeled image of representative control implant track. Dashed line indicates implant size and approximate location
(B) GFAP labeled image of the same track
(C) Resulting greyscale image following subtraction of (B) from (A) showing Vim+/GFAP- meningeal tissue

3.2.5.2 Cell counting

ImageJ software (NIH) was used to perform threshold-based automated cell counting to assess neuronal density surrounding the implant tracks. Cell selection criteria were fine tuned for each subject using unimplanted contralateral tissue sections. A range of threshold values were used for each implant track in order to account for variations in brightness, and the largest cell count returned was entered. The area of the track void in the NeuN labeled image was measured via a similar thresholding process and subtracted from the area of the 200μm diameter region of interest to calculate the cell density. This ensures that the resulting cell density value is not influenced by the size of the track void, since the area value used in the cells/area density calculation represents the amount of cortical tissue within the counting radius and excludes the void area. For the implant type comparison, density values from varying depths were averaged to gain a single mean density value for each implant shaft for statistical analysis. Vimentin, GFAP and meningeal tissue data were collected from a total of 42 implant tracks (21 porous and 21 controls) and IgG and neuron density data were collected from a total of 71 tracks (37 porous and 34 controls).

3.3 Results

Distribution and general morphology of the four histological markers used may be seen in **Figure 3.4.** An example porous implant track is shown with labels for GFAP **(A)**, vimentin **(B)**, IgG **(C)**, and NeuN **(D)**.

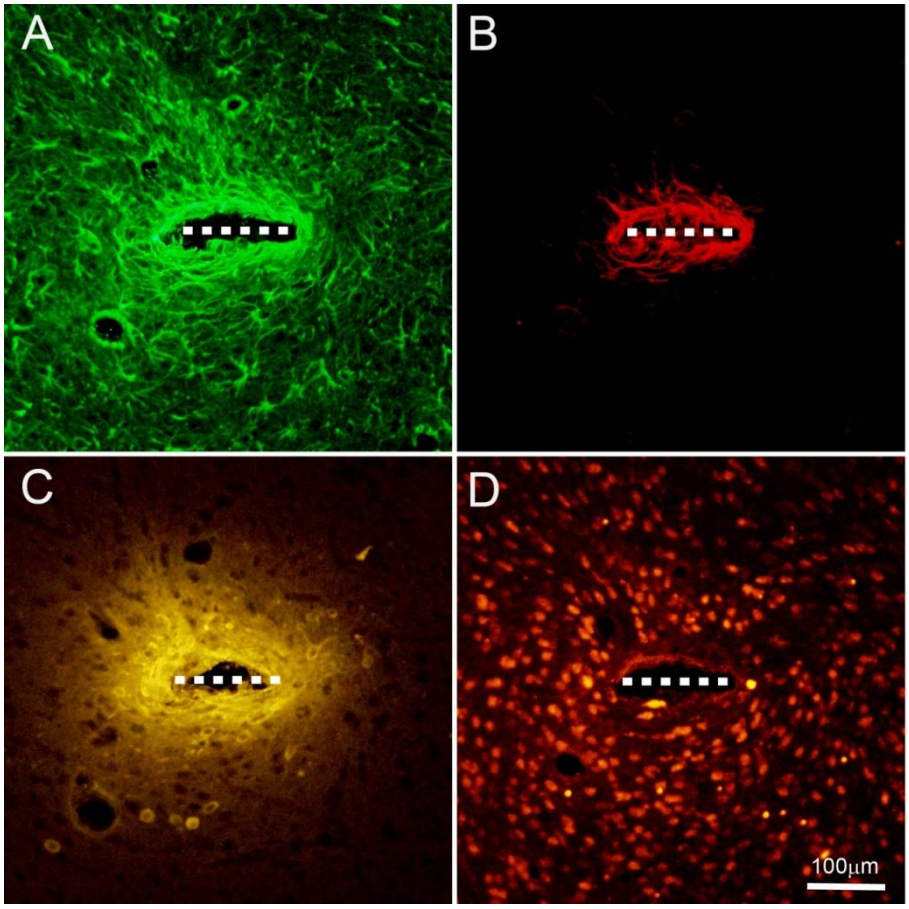

Figure 3.4: Example images of the same implant track for the four markers used in this study, showing relative size and distribution of cellular reactions. Dashed line indicates implant size and approximate location

(A) GFAP showing reactive astrocytes
(B) Vimentin showing meningeal fibroblasts and proximal reactive astrocytes
(C) IgG indicating blood-brain barrier leakage
(D) NeuN showing neuron cell bodies

3.3.1 Meningeal Cells

Vimentin, an extracellular matrix protein produced by meningeal cells but not widely expressed in cortical tissue, was used as a marker to indicate meningeally derived tissue surrounding the implant sites. This tissue was distinguished from vimentin-expressing reactive astrocytes through the subtraction of GFAP expressing regions, since meningeal fibroblasts express vimentin but not GFAP. In cases where meningeal tissue was found, it was located immediately adjacent to the implant, within the envelope of encapsulating reactive astrocytes. Typical images of the two implant types from one subject are shown in **Figure 3.5(A) porous** and **(B) non-porous.** Meningeal fibroblast tissue is shown in red.

3.3.1.1 Quantitative measures

Intensity profile analysis of vim+/GFAP- meningeal tissue around each implant type revealed significantly less meningeal cellular activity surrounding porous implants than control implants. This reduction is statistically significant for the first four of the eight 25μm distance bins that were analyzed, from 0 to 100μm from the implant track centerline (t-tests, n=42, $p<0.05$). Results are shown in **Figure 3.5(C).** The mean intensity curves also illustrate the localized nature of the meningeal cell activity, which disappears almost completely by 75μm in the case of the porous implants. Control implants exhibit mean meningeal reactions that are greater in both intensity and extent than that of the porous implants.

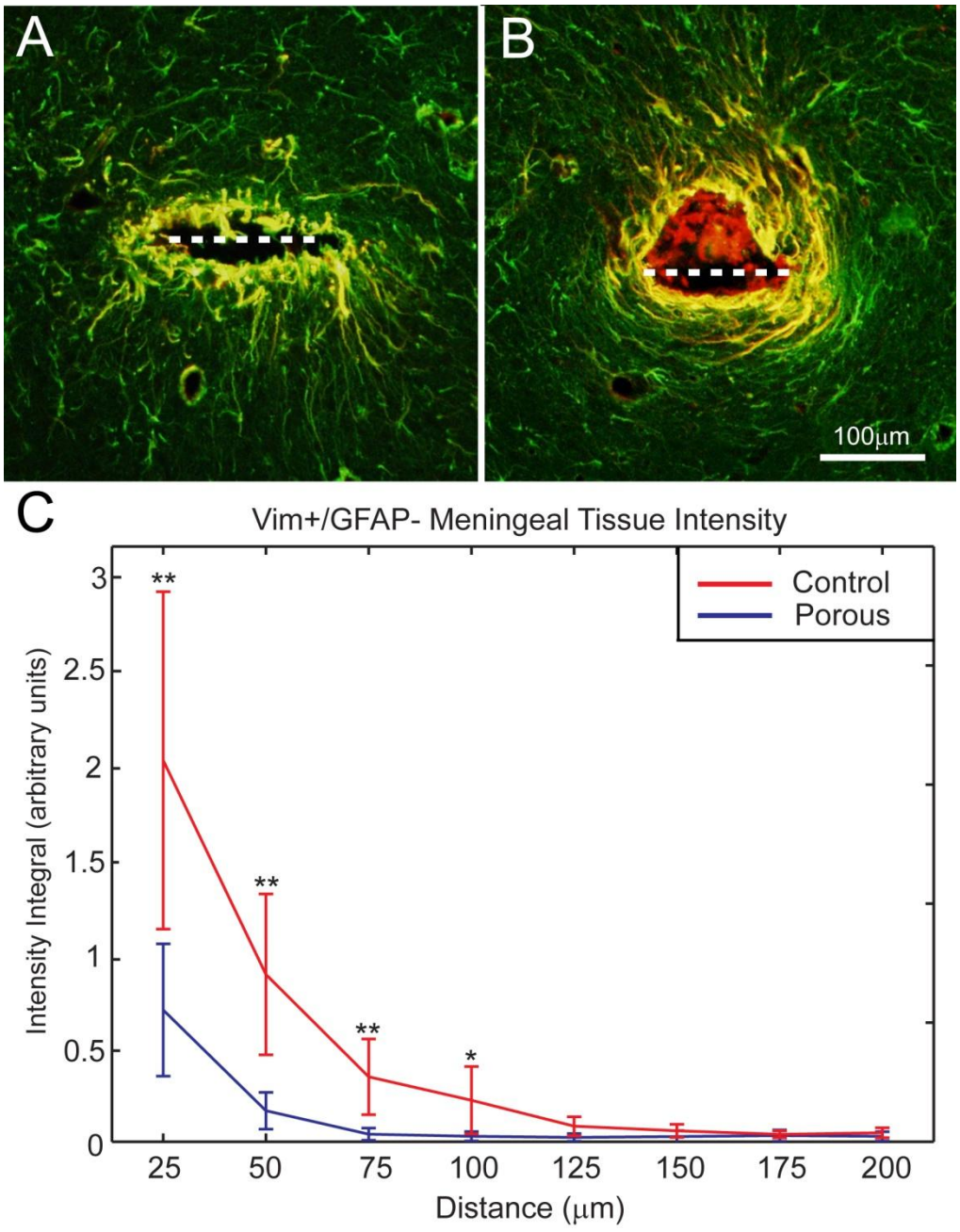

Figure 3.5: Vim+/GFAP- Meningeal tissue results

(A) Typical porous implant track near the cortical surface. Meningeal tissue is shown in red, vim+/GFAP+ proximal reactive astrocytes in yellow, and vim-/GFAP+ reactivity in green
(B) Nonporous control track from the same tissue section
(C) Intensity of Vim+/GFAP- tissue for both implant types as a function of distance from the track centerline. (n=42, *p<0.05, **p<0.01)

3.3.1.2 Meningeal activity by section depth

The same meningeal tissue intensity data shown in **Figure 3.5** were also analyzed according to depth down the electrode tracks in order to examine the effects of implant porosity on the progress of meningeal tissue growth down the electrode shaft. Collected tissue sections were separated into three depth zones, with zone 1 being the most superficial. **Figure 3.6** shows mean intensity values for the first four distance bins of the intensity profiles at each of the three depths for both implant types. A clear trend of decreasing meningeal cell levels in deeper tissue is evident. In the case of the first distance bin, shown in **Figure 3.6(A)**, where the greatest amount of meningeal tissue is found, porous implants provide the greatest reduction in meningeal cell activity in the sections near the implant tip. This is consistent with the hypothesis that implant porosity inhibits the growth of meningeal tissue down the electrode shank. ANOVA comparison between the three depth zones for each radius bin and implant type revealed statistically significant reductions in meningeal tissue levels from shallower to deeper zones in three cases – the zone 3 activity was found to be significantly less than that of zone 1 for the 50μm and 75μm bins in the case of the porous implants, and zone 2 activity was found to be significantly less than zone 1 for the control implants in the 100μm bin (**Figure 3.6D**). No significant trends or differences between the two implant types were found in the outer four distance bins from 125-200μm (data not shown).

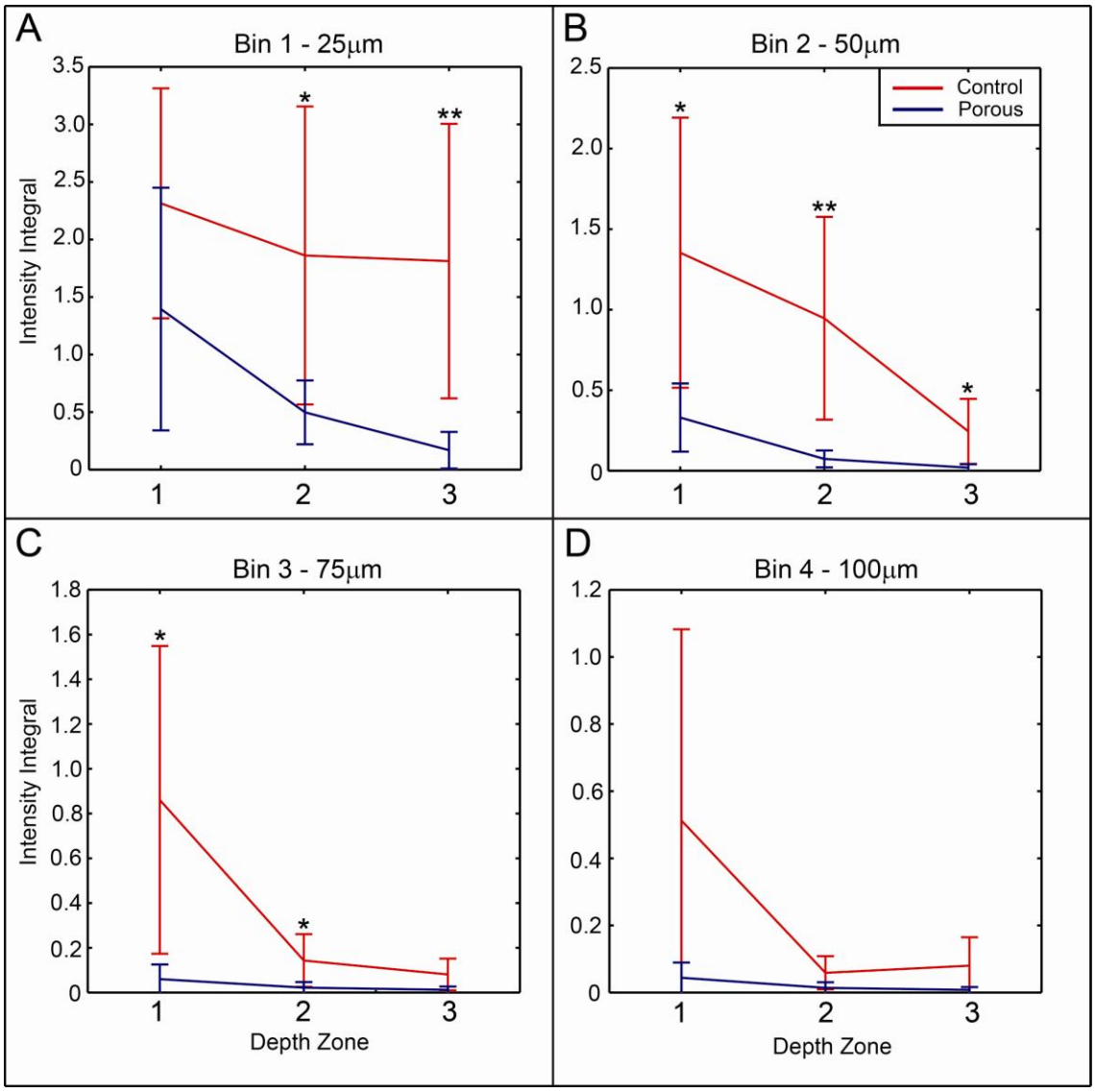

Figure 3.6: Meningeal tissue intensity results for the first four distance bins as a function of tissue depth (t-tests, n=42) (*p<0.05, **p<0.01)

3.3.2 Vim+/GFAP+ reactive astrocyte results

3.3.2.1 Morphology

Dense sheaths of vimentin and GFAP expressing reactive astrocytes were found surrounding both implant types extending tens to at most a few hundred microns into the surrounding tissue. These cells display a stellate morphology which is typical of reactive astrocytes in the CNS. Typical images of implant tracks showing vimentin labeling of proximal reactive astrocytes for porous and control implants from the same subject are shown in **Figure 3.7 (A)** and **(B)** respectively.

3.3.2.2 Quantitative Vim+/GFAP+ results

Intensity profile analysis of vim+/GFAP+ proximal reactive astrocytes revealed no statistically significant differences in the activity of this cell type between the two implant types when averaged across all section depths (t-tests, n=42). Results are shown in **Figure 3.7 (C).**

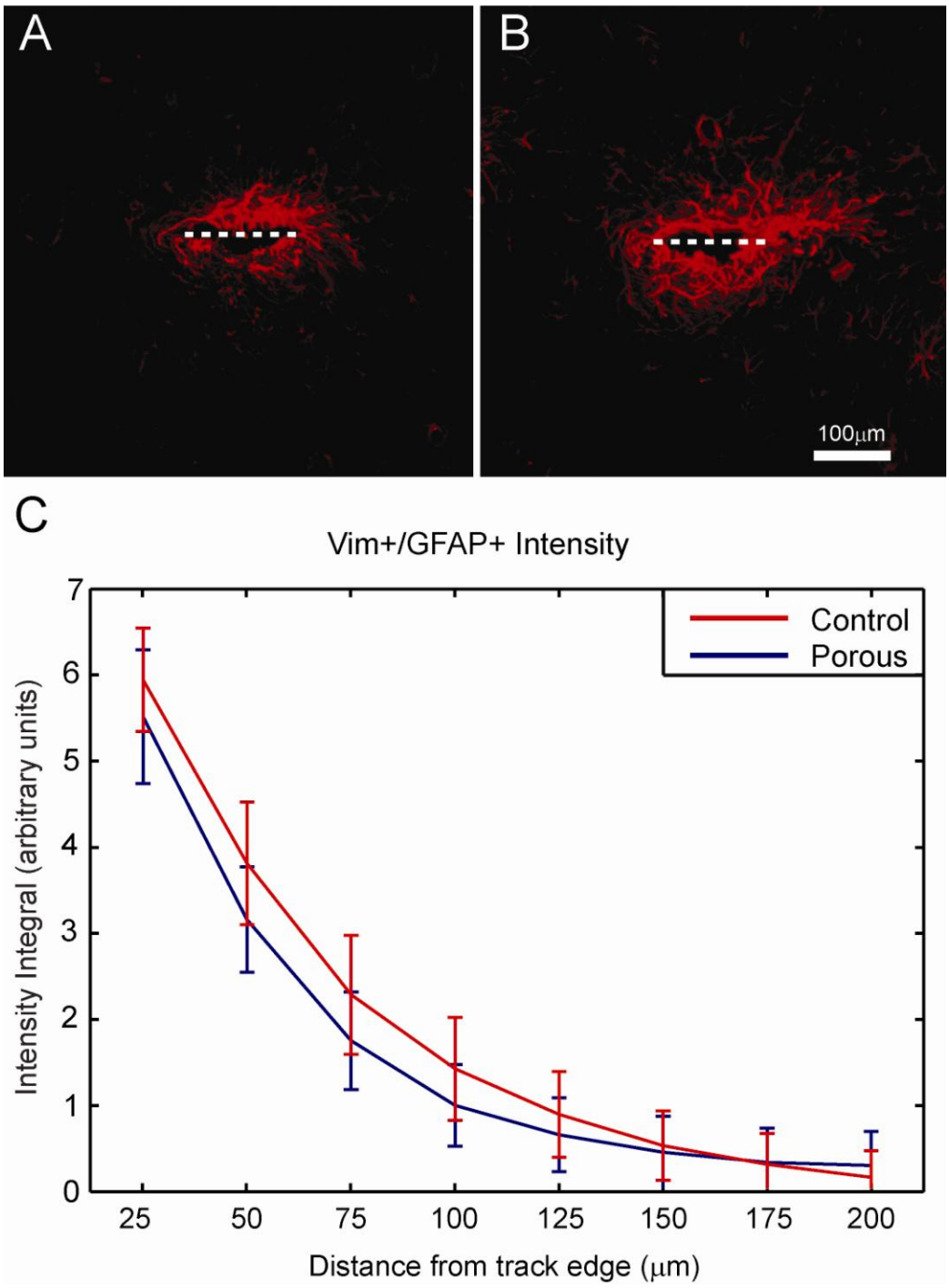

Figure 3.7: Vim+/GFAP+ Reactive astrocyte results

(A) Typical porous implant track showing vimentin expression. Dashed line indicates implant size and location
(B) Control implant track from the same subject
(C) Intensity of vimentin expression by vim+/GFAP+ cells as a function of distance from the implant track edge

3.3.2.3 Vim+/GFAP+ activity by depth

Levels of vimentin expression by proximal reactive astrocytes were also examined according to tissue depth zone, in order to determine whether reductions in meningeal tissue encapsulation at greater depths would correspond to reductions in other aspects of the immune response. Results are shown in **Figure 3.8.** Vimentin levels were found to be significantly greater for control implants than porous implants in the deepest zone for the first radius bin, as seen in **Figure 3.8(A)** (t-test, $n=42$, $p<0.05$). Although a trend of decreasing activity is evident in bin 1 for the porous implants, the pronounced and consistent depth trends that were observed in the meningeal cells are not present in reactive astrocytes. This is to be expected since these Vim+/GFAP+ cells are native to the cortical tissue and do not have to migrate down the electrode shaft from the meningeal space to reach the deeper regions of the implant.

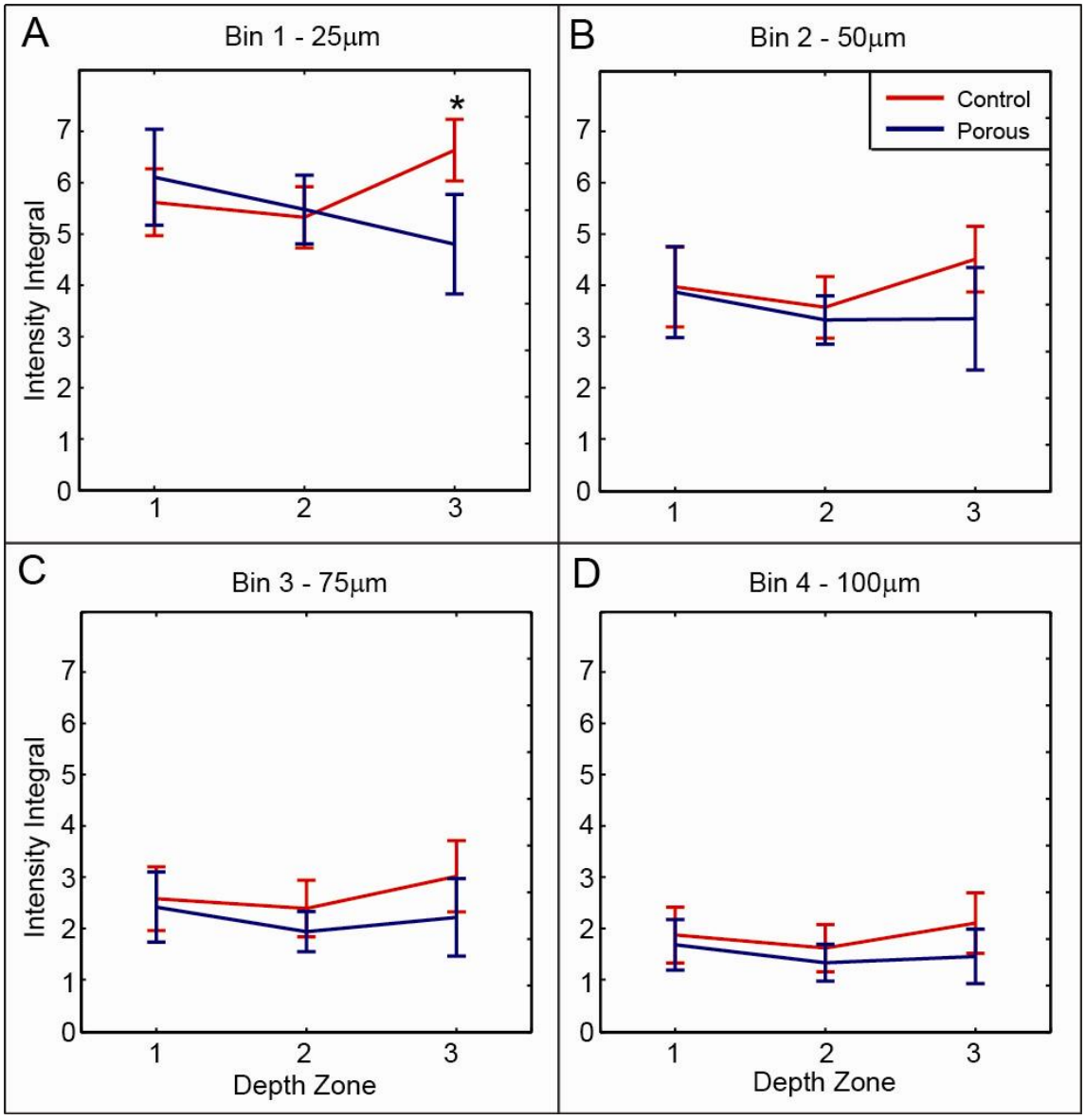

Figure 3.8: Vim+/GFAP+ reactive astrocyte intensity as a function of tissue depth zone for the first four distance bins. (t-test, n=42, *p<0.05)

3.3.3 GFAP results

Fluorescent labeling with antibodies for glial fibrillary acidic protein (GFAP) was used to identify reactive astrocytes surrounding the implants, which make up an important component of the cortical immune response. This metric includes both proximal and distal reactive astrocytes. GFAP labeling revealed regions of reactive astrocyte activity surrounding each implant shank, forming a densely packed, multilayered capsule which is typical of a neural implant at 4 weeks post-implantation.

3.3.3.1 Quantitative GFAP Measures

GFAP labeled images were subjected to the same intensity profiling analysis that was used to assess vimentin results. No significant differences in GFAP expression were found between the two implant types (t-tests, n=42, $p>0.05$). Results are shown in **Figure 3.9.**

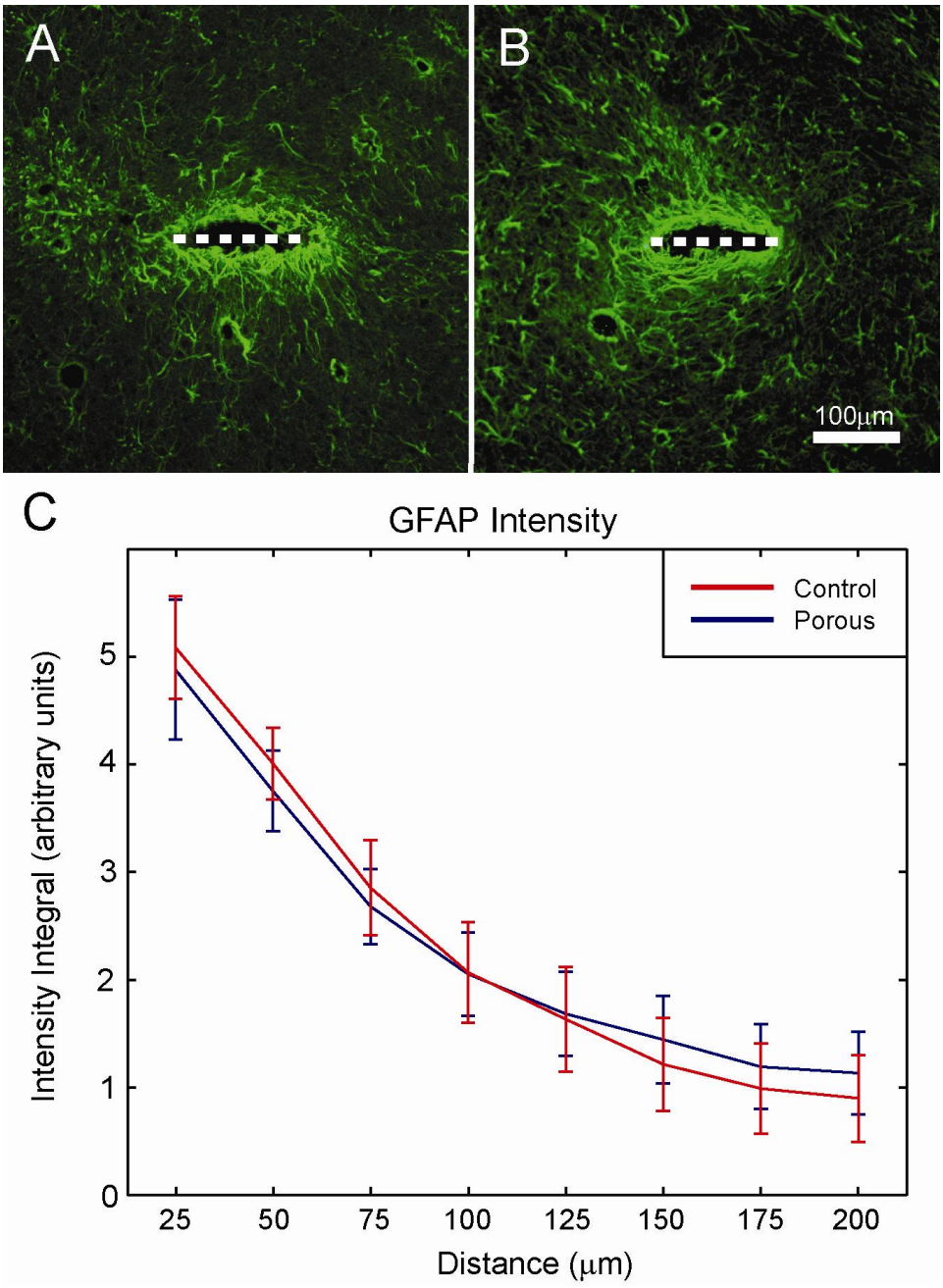

Figure 3.9: GFAP results

(A) Typical porous implant track showing GFAP labeled reactive astrocytes
(B) Control implant track from the same tissue section
(C) GFAP intensity for each implant type as a function of distance from the implant surface

As no significant differences between the two implant types were found in vimentin-expressing astrocyte levels, it is to be expected that the same would be true of the overall GFAP+ response. GFAP data were also examined as a function of section depth, but no significant trends or differences between the implant types were found (data not shown).

3.3.4 Neuron results

Neuron cell body counting via NeuN antibody labeling was performed to determine the effects of implant porosity on neuron density in the surrounding region. Neurons within a 100μm radius of the implant center were counted. The void area surrounding each implant was subtracted from the total area of interest in order to make the resulting neuron density metric independent of void size. No difference in mean void area was found between the two implant types (t-test, n=72, p=0.64). It was found that the mean neuronal density within this region of interest was approximately 20% greater for porous probes than controls. This difference was found to be statistically significant (t-test, n=71, $p < 0.01$). Results are shown in **Figure 3.10.** The reduction of neuronal dieoff in the immediate vicinity of the implant is one of the primary goals of neural interface development, and the observed improvement in neuron viability around the porous implants is likely to correspond to an improvement in recording performance for future functional recording probes.

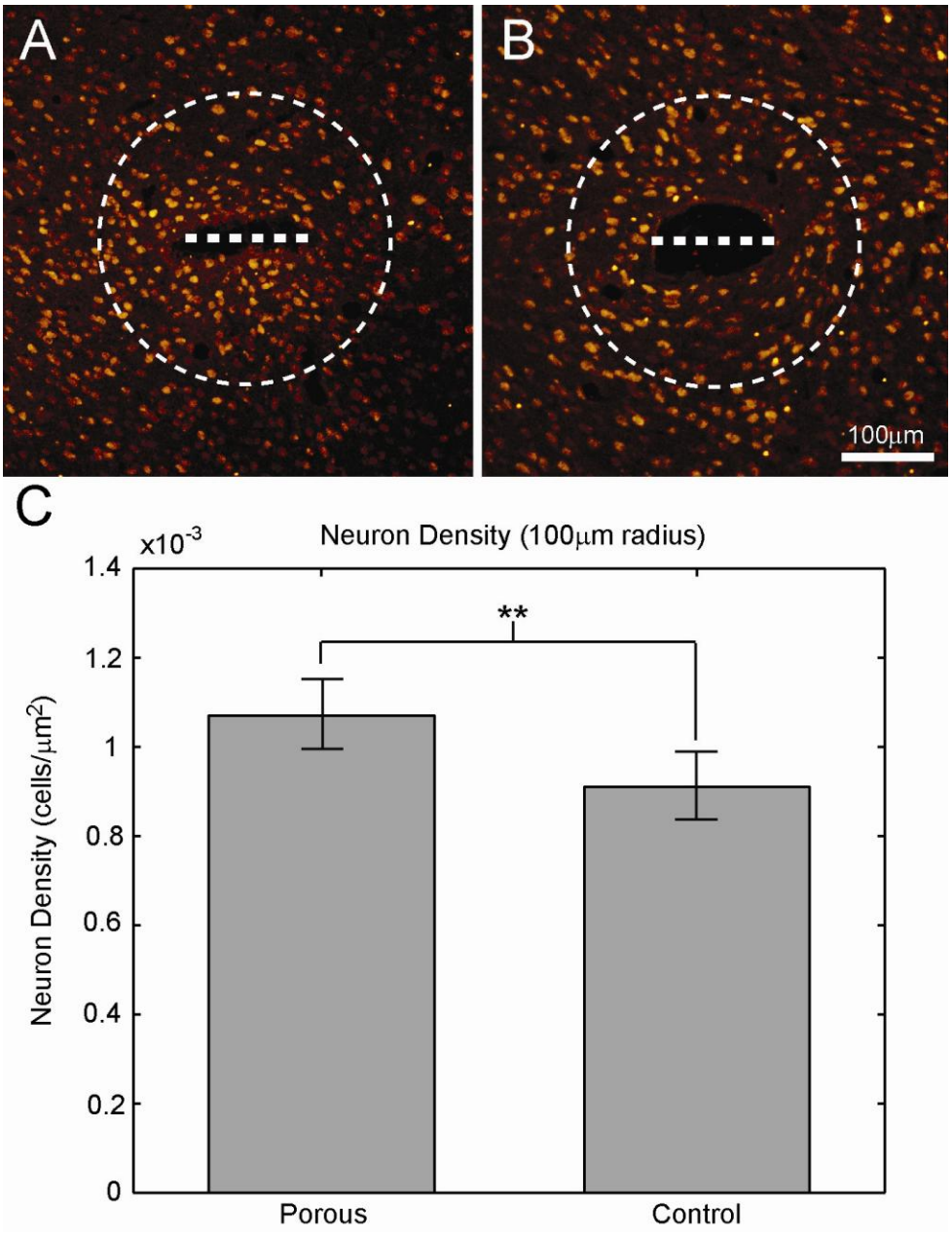

Figure 3.10: Neuron results

(A) Typical porous implant track showing neuron cell bodies (NeuN). Dashed line indicates implant size and location, dashed circle indicates 100μm cell counting radius
(B) Control implant track from the same tissue section
(C) Surrounding neuron density for each implant type (**p<0.01)

3.3.5 IgG results

Fluorescent antibody labeling of IgG was used to assess blood brain barrier integrity by measuring the presence of serum antibody. Every third tissue section was labeled using a conjugated antibody specific to rat IgG. Results were assessed using the same intensity profiling method that was employed for vimentin and GFAP labeled images.

IgG labeled sections exhibited areas of elevated IgG surrounding the electrode tracks, extending tens to a few hundred microns into the surrounding tissue. IgG labeling was not restricted to a particular cell type or cellular morphology, but was instead largely diffuse and locally uniform within the tissue, which is consistent with the diffusion of serum antibodies into the tissue surrounding a neural implant. Example images are shown in **Figure 3.11(A)** and **(B)**.

3.3.5.1 Quantitative IgG results

Intensity profiling analysis of IgG labeling around the two implant types revealed no significant differences between the two implant types (t-test, n=71, $p>0.05$). Results are shown in **Figure 3.11(C)**. As with the astrocyte reaction, the degree of IgG reactivity in cortical tissue is thought to be generally proportional to the level of mechanical stresses and trauma present in the tissue. Since the external dimensions, insertion method, and material of the porous and control implants are identical, this result is in line with expectations. IgG reactivity data were also examined according to section depth zone in the

same manner as above, and no significant trends or differences were found (data not shown).

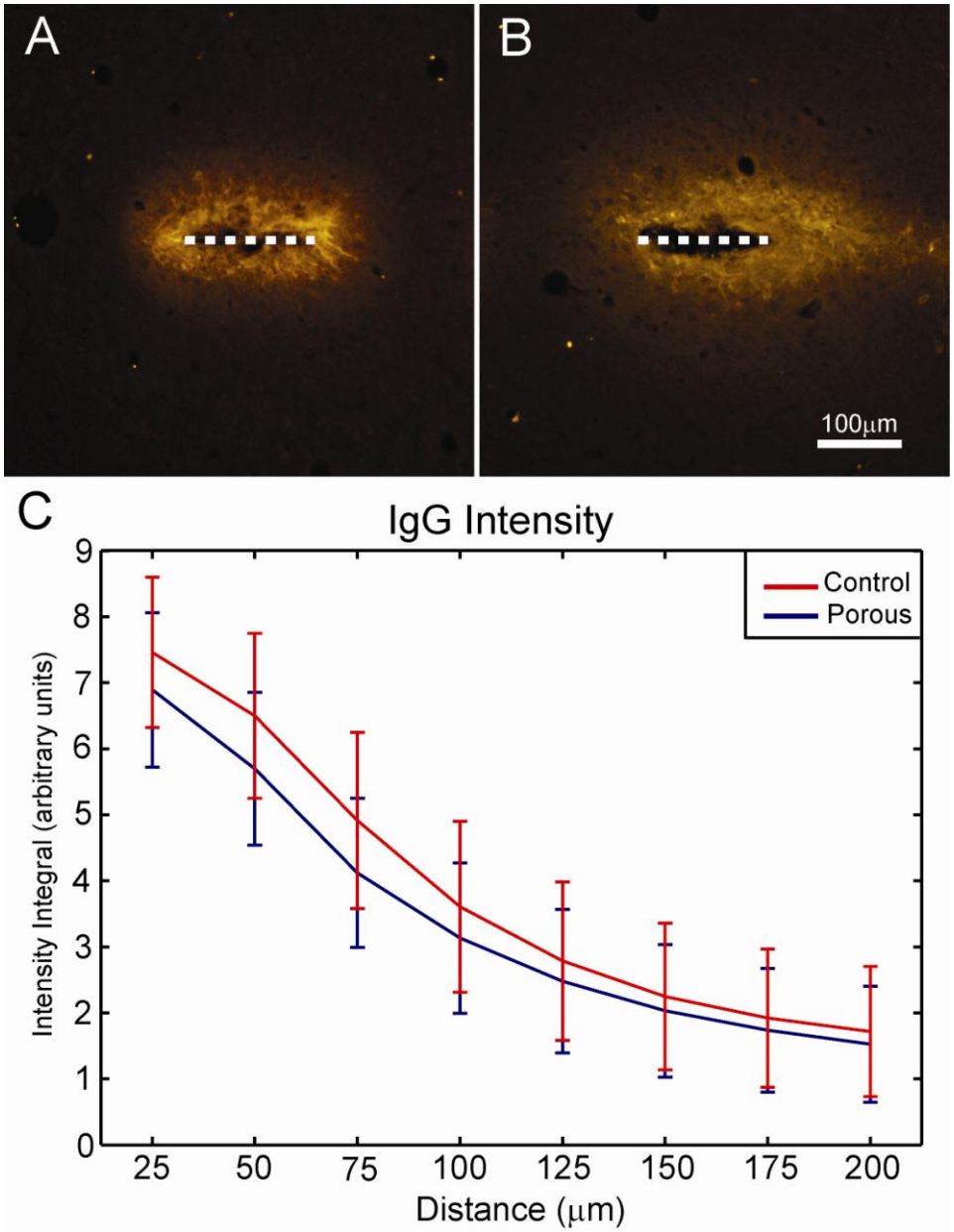

Figure 3.11: IgG results

(A) Typical porous implant track showing IgG reactivity, indicating BBB permeability
(B) Control implant track from the same tissue section
(C) IgG intensity for each implant type as a function of distance from the implant surface

3.4 Discussion

The results of this study demonstrate that the addition of pores to a planar probe near the cortical surface has a significant effect on several aspects of the brain's immune response at 4 weeks post implantation. Significant reductions in vimentin-labeled cellular encapsulation activity and neuron dieoff were found compared to nonporous control implants. Examination of vim+/GFAP- meningeal cell activity according to section depth zone revealed that this tissue is most prevalent nearest the cortical surface, and decreases with increasing depth down the electrode shaft. Measurements of IgG levels and reactive astrocyte activity were made, but no significant differences were found between the implant types.

Encapsulation of penetrating neural electrodes by GFAP-expressing reactive astrocytes constitutes a significant portion of the cortical immune response, and a reduction in reactive astrocyte activity is frequently found in conjunction with reductions in neuron dieoff, such as were seen in the current study (Biran et al., 2005; Polikov et al., 2005; Thelin et al., 2011). A significant reduction in vim+/GFAP+ astrocytes for the porous implants was found for the deepest depth zone in the closest radius bin (**Figure 3.8A**), which could potentially be an indication of an interaction between the meningeal and astrocyte portions of the response. No significant differences were found between the two implants in the mean vim+/GFAP+ or total GFAP+ reactions, though, so any interactive phenomena between the two portions are subtle. Although significant reductions in GFAP and vimentin expressing reactive

astrocytes were not observed, the improvement in local neuron density and reduction in vim+/GFAP- meningeal tissue levels illustrate that the addition of pores to these implants near the cortical surface has a significant effect on the immune response. It seems likely, then, that disparate mechanisms may be responsible for determining the magnitude of the astrocyte- and meningeal cell-mediated portions of the immune reaction. Astrocyte responses have been shown to be affected by changes in implant size, shape, composition, implantation method, and implantation location (Biran et al., 2005; Harris et al., 2011a; Kim et al., 2004; Polikov et al., 2005; Rennaker et al., 2005b; Thelin et al., 2011; Turner et al., 1999). Generally speaking, these factors relate to the degree of mechanical trauma inflicted upon the tissue surrounding the implant. Higher insertion speeds and smaller implants reduce mechanical strains on the tissue, and produce a reduction in GFAP levels (Rennaker et al., 2005b; Rousche and Normann, 1992; Welkenhuysen et al., 2011). Free-floating implants, when compared to those anchored to the skull, reduce chronic micromotion between the implant and the surrounding tissue, reducing chronic mechanical stresses and reducing GFAP expression (Biran et al., 2005; Kim et al., 2004; Thelin et al., 2011). All of these factors were unchanged between the two implant types in this experiment. Although the porous regions may have a small effect on the bulk mechanical stiffness of the implants, none of the factors which have been previously implicated in governing the astrocyte reaction are related to the implant porosity being evaluated in this study. Similarly, no significant differences were found in IgG labeling between the two implant

types, but like GFAP, cortical IgG levels have been shown to be largely related to physical trauma (Hoshino et al., 1996). Since there are no substantial differences in the mechanical behavior of the two implant types used in this study, the lack of significant differences in IgG levels is not surprising. As no differences were observed in the astrocyte-mediated portion of the immune response, but significant differences in meningeal tissue ingrowth were shown, the observed reduction in neuron dieoff appears to be at least partially linked to the activity of meningeally derived, vimentin expressing cells.

Ingrowth of vimentin labeled meningeal cells into a porous cortical implant structure has been shown previously, and served as one of the primary motivations for the current study (Kim et al., 2004). Although the hollow fiber membrane implant employed differs significantly from that used in the current study, the vim+/GFAP- results show that the porous structures in planar SMP implants reduced growth of meningeal tissue around the implant shafts at 4 weeks. Although fibrous encapsulation by GFAP expressing reactive astrocytes receives much attention as a failure mode for penetrating neural interfaces, the results of this study suggest that encapsulation by meningeally derived cells may be another important factor to consider when attempting to improve device performance. Morphologically, the meningeal tissue structures observed in the current study resemble normal meningeal tissue found at the edges of the tissue sections. Although this differs in structure from the glia limitans and fibrous capsule formed by reactive astrocytes, the addition of another fibrous tissue layer between the electrode recording sites and the surrounding neurons

can scarcely improve recording performance. Although functional recording devices were not used in the current study and the specific effects of vimentin+/GFAP- tissue encapsulation on penetrating neural electrode performance remain largely uninvestigated, one expects that the effects of encapsulation by meningeally derived cells on implant performance would be substantially similar to that of astrocytic encapsulation. Namely, a fibrous tissue layer is formed around the electrode, electrically insulating the recording sites from the surrounding neurons and increasing the physical separation between the probe and the cells of interest. Although the meningeal component of the encapsulation response and the detrimental effects thereof could be smaller in magnitude than the astrocytic reaction, it is also significantly less well understood. The results of this experiment demonstrate that at least one physical characteristic of a neural implant can significantly influence this portion of the immune response, and many more potentially beneficial techniques are likely as yet undiscovered. The development of a reliable chronic cortical neural interface will depend upon a thorough understanding not only of the microglial and astrocytic portions of the immune response, but the meningeal components as well, and further work is required in order to fully understand this component of the cortical reaction to a neural implant.

3.5 Conclusion

Quantification of the cortical immune response to porous-shank and nonporous control neural implants revealed that the addition of pores to the implant shank near the level of the cortical surface reduces the migration of vimentin+/GFAP- meningeal cells down the implant shaft at four weeks. Porous implants also improved local neuronal density compared to controls. These results suggest that this novel neural implant design feature may prove to be a beneficial addition to future neural interface designs. These results also indicate that the physical characteristics of a neural electrode can have significant effects on a portion of the encapsulation response which is separate from the glial cell mediated reaction, and other factors influencing this meningeal response to neural implants remain poorly understood. The development of clinically viable cortical neural interfaces necessitates a full understanding of the implant's interaction with all dimensions of the cortical immune response, and more investigation of the meningeal component is warranted.

4 Dynamically Softening Polymer Neural Implant Substrate

4.1 Introduction

4.1.1 Flexible neural interfaces

Recently, a number of groups have investigated neural implants composed of softer, more flexible materials than conventional silicon arrays, in order to reduce the mechanical mismatch between the implant and the surrounding brain tissue and reduce chronic inflammation. *In vivo* and *in vitro* studies have found that higher tissue strain rates and stiffer implant substrates elicit increased astrocyte reactivity (Cullen et al., 2007). These include implants composed of polyimide (Cheung, 2007; Fomani and Mansour, 2011; Mercanzini et al., 2008; Rousche et al., 2001), poly(vinyl acetate) nanocomposites (Harris et al., 2011a), benzocyclobutene (Lee et al., 2005), parylene (Kim et al., 2013; Takeuchi et al., 2005; Wester et al., 2009) and silicone (PMDS) (Kozai and Kipke, 2009; McClain et al., 2011). These implants have shown promise at reducing the chronic immune response but still suffer from serious design compromises. All of these implants must still be made sufficiently stiff to allow insertion into the brain tissue, or use other methods, such as an insertion shuttle (Kozai and Kipke, 2009) or a thick coating of saccharose (Hassler et al., 2011) to aid insertion, which give rise to other issues. For softer materials, the implant must be made thicker and wider in cross section to facilitate insertion, increasing its footprint in the tissue, insertion trauma and chronic inflammation. Even when flexible materials such as polyimide or parylene-c are employed, the

difference between the moduli of the implant and the surrounding tissue is still 5 or 6 orders of magnitude (Rousche et al., 2001; Ware et al., 2012). Harris (2011) describes a polymer nanocomposite neural implant substrate which undergoes a dramatic decrease in tensile storage modulus following introduction to physiological conditions, but this is accompanied by aqueous swelling of 60-75%, leading to additional forces on the surrounding tissue.

4.1.2 Dynamically softening substrate

Shape memory polymers offer the ability to eliminate this compromise by using a single material which changes its mechanical properties following insertion in the cortical tissue. Via careful manipulation of the material's chemistry, the glass transition temperature can be tuned to just above physiological temperature. The addition of hydrophilic polymers to the formulation introduces tunable hydration sensitivity as well. Thus, the implant material is in its stiff state for insertion, and then transitions to the compliant state shortly following insertion due to plasticization by a small amount of fluid uptake. The polymer used in this study has a comparable stiffness to current flexible probes for insertion (Young's modulus of ~3GPa), and then undergoes a dramatic decrease in its stiffness over a period of a few days following implantation to about 10MPa (Ware et al., 2012). Approximate modulus ranges of the SMP system and other neural interface substrates are shown in **Figure 4.1.** Synthesis and characterization of the dynamically softening substrate used in this study is reported in Ware 2012. The experimental implants used in this

experiment consisted of only the SMP substrate without any recording functionality.

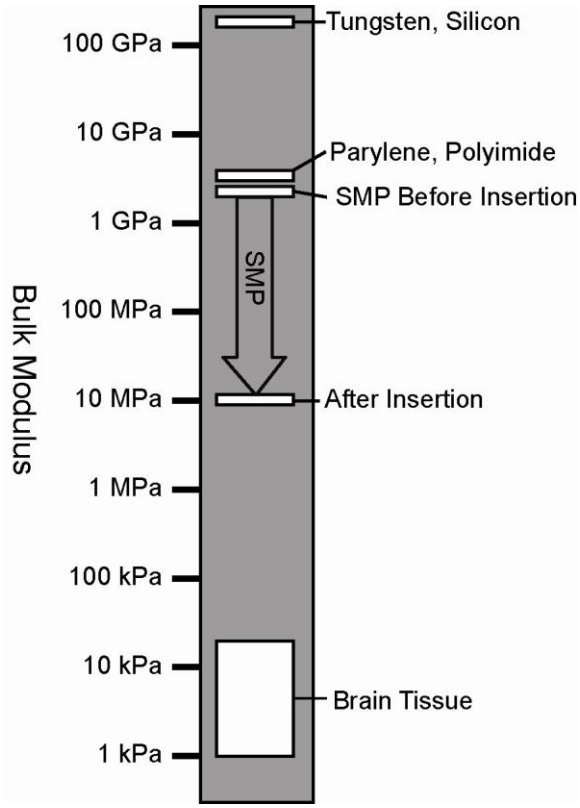

Figure 4.1: Schematic showing modulus ranges of other neural interface materials and the SMP system

The aim of this study is to measure the effect of the dynamic softening property of the SMP system on the brain's immune response. To determine whether this system offers benefits over current neural interface substrates, implants made with our SMP substrate are compared to probes of identical dimensions composed of parylene-c. Parylene-c (poly[dichloro-p-xylylene]) is an FDA Class VI polymer coating used in medical devices in many areas of the

body, and it has been used by several researchers as a coating or flexible substrate for neural interfaces (Hassler et al., 2011; Hassler et al., 2010; Hsu et al., 2009; Schmidt et al., 1988; Takeuchi et al., 2005; Wester et al., 2009). Evaluation of parylene-c coatings on neural implants has found the immune response to be similar to that of uncoated silicon implants (Winslow et al., 2010). Parylene-c provides a good control against which to evaluate the benefits of the SMP substrate's softening capability, as its stiffness prior to implantation is comparable (~3GPa), and parylene-c undergoes no change in modulus over the indwelling period (Hassler et al., 2010). Previous evaluation of the SMP material has shown that its modulus is reduced to ~10MPa after 1 week in physiological conditions and stabilizes thereafter (Ware et al., 2012). Implants used in this study are a planar design consisting of four 150μm wide penetrating spikes 35μm thick joined by a common tab. Six rats were each implanted with one 4-shank SMP implant and one dimensionally identical parylene-c control implant for a period of four weeks. Brains were sectioned and subjected to quantitative immunohistochemistry analysis to quantify the chronic immune response to each implant type and measure the effect of the SMP substrate's dynamic softening capability.

4.2 Methods

4.2.1 Subjects

Six female Sprague-Dawley rats were individually housed in a temperature- and humidity-controlled environment and were exposed to a 12:12 h light-to-dark cycle with free access to food and water.

4.2.2 Implants

Development, synthesis and characterization of the SMP substrate are described in detail in Ware et al. 2012. Briefly, the system consists of 31mol% tricyclodecanedimethanoldiacrylate (TCMDA) and 1,3,5-triallyl-1,3,5-triazine-2,4,6(1H,3H,5H)-trione (TATATO) monomers with 0.1%wt 2,2-dimethoxy-2-phenyl acetophenone (DMPA) and Tris[2-(3-mercaptopropionyloxy)ethyl] isocyanurate (TMICN). Polymerization was performed using 365nm UV. To fabricate the parylene-c control implants, 35μm of parylene-c was deposited in five successive depositions using a Labcoater 2 (SCS Systems). A frequency tripled Nd:YAG laser connected to a μFab workstation (Newport) was used to cut device profiles from the surrounding polymer sheet. The implants used in the current study consisted of only the SMP or parylene-c substrate without any recording functionality. Implant shape and dimensions are shown in **Figure 4.2.** Implant thickness is 35μm. Dynamic mechanical analysis characterization of the SMP material was performed using a Mettler Toledo DMA 861e/SDTA. Samples consisted of 1mm diameter, 3mm thick cylinders placed under shear

deformation at 1Hz following incubation in physiological conditions(Ware et al., 2012).

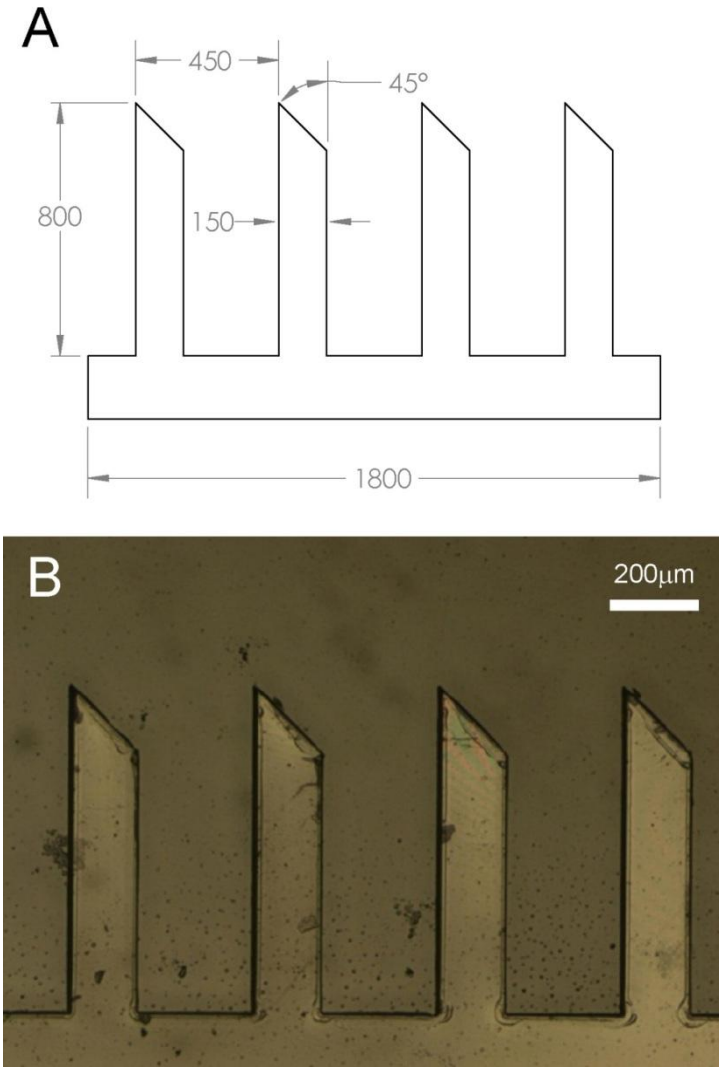

Figure 4.2: Implant dimensions. Implant thickness is 35μm.

(A) Drawing of implant. All dimensions in μm.
(B) Photograph of implant spikes

4.2.3 Surgical Procedures

Rats were anesthetized using ketamine, xylazine and acepromazine (targeted dosage 50, 20, 5 mg/kg respectively). A midline incision was made in the scalp and the connective tissue was dissected from the skull. Two bone screws were implanted in the left parietal bone to secure the acrylic skull cap. A 3mm × 5mm portion of the right parietal bone was removed using micro-rongeurs. A 28-ga needle was used to incise and remove the dura over the implant site before insertion of the probes. One 4-shank implant of each type was inserted using micro-forceps. The implants were positioned such that each penetrating spike was fully embedded in the cortical tissue and the connecting tab was flush with the cortical surface after implantation. All animals received one SMP and one parylene control implant in order to minimize the effects of animal-to-animal variability, and the rostral/caudal arrangement of the two implant types was alternated between animals in order to eliminate potential confounding effects of positioning in the brain tissue. Following implantation, the brain was covered by a layer of silicone elastomer (Kwik-Cast; World Precision Instruments, Inc., FL) and a layer of acrylic was added to seal the craniotomy and secure the structure to the bone screws. The initial incision was then closed using absorbable sutures. All procedures were carried out in accordance with protocols approved by the University of Texas at Dallas and University of Oklahoma Institutional Animal Care and Use Committees.

4.2.4 Immunohistochemistry

At 4 weeks post-implantation, subjects were euthanized and perfused. Subjects were administered 0.7mL of the same ketamine cocktail used for the surgical procedure, and then transcardially perfused with 100mL of phosphate buffered saline (PBS) followed by 100mL of 4% paraformaldehyde in PBS. Implants were removed from the brain upon removal of the skull cap following perfusion. The brain was removed and stored for 4h immersed in 4% paraformaldehyde for postfixation. Following postfixation, excess tissue surround the areas of interest was removed and the resulting tissue blocks were placed in 30% sucrose in PBS for cryoprotection for 72h. The brains were cut into 20μm thick horizontal sections which were collected onto slides. All tissue was stained in a single batch to minimize processing variability. The main group of tissue sections was labeled with antibodies for GFAP to label reactive astrocytes, NeuN (FOX3) to visualize neuron cell bodies, and vimentin to indicate meningeal fibroblasts and reactive astrocytes (Jones and Tuszynski, 2002; Nakajima and Kohsaka, 2001; Polikov et al., 2005). Antibodies specific to IBA1 labeling reactive microglia are frequently used in neural interface immunohistochemistry studies (Harris et al., 2011a; Kim et al., 2004; Polikov et al., 2005; Winslow and Tresco, 2010) but preliminary studies using this marker and similar implants found no migroglial activity at 4 weeks. Microglial activity is known to prevail much earlier in the time course of the immune response and decrease substantially by 4 weeks post implantation (Kalman, 2003; Polikov et al., 2005). Thus, analysis of the microglial reaction in this experiment was

eliminated in favor of more informative markers. Every third section was placed in a separate batch and labeled with a fluorescent antibody specific to rat IgG, in order to assess blood-brain barrier integrity at the implant site (Hoshino et al., 1996; Potter et al., 2012; Skousen et al., 2011). Antibody concentrations are shown in **Table 4.1.** Sections were also taken from similar locations in the unimplanted left hemisphere for each rat to serve as controls for image analysis. These were processed in the same batch as the experimental sections. Following three 10min washes in PBS, sections were blocked in 3% normal goat serum for 30 minutes. Sections were then incubated overnight in primary antibody solutions in PBS containing 3% normal donkey serum and 0.3% Triton X-100. The following day, sections were incubated in conjugated secondary antibodies for 2h and coverslipped using Vectashield with DAPI (Vector Laboratories). IgG labeled sections were incubated in the conjugated antibody solution overnight, then washed and coverslipped the following day. Images were taken using an Olympus BH-2 microscope with a 10x objective and an Olympus DP70 digital camera.

Primary Antibodies			**Secondary Antibodies**		
Abcam #	Type	Dilution	Abcam #	Type	Dilution
4674	Chicken anti-GFAP	500:1	96951	Anti-chicken 488	100:1
104225	Rabbit anti-FOX3 (NeuN)	500:1	7087	Anti-rabbit TRITC	100:1
8069	Mouse anti-vimentin	250:1	150119	Anti-mouse 647	100:1
7094	Anti-rat IgG TRITC	100:1			

Table 4.1: Antibody types and concentrations

4.2.5 Analysis

Following acquisition, images were subjected to computerized analysis to quantify various aspects of the immune response. The primary techniques used were intensity profiling to determine the magnitude and distribution of GFAP, vimentin and IgG labeled cells and cell counting to measure neuron density.

4.2.4.1 Intensity Analysis

An intensity profiling scheme was used to measure pixel brightness values as a function of distance from the edge of the implant track. Radial intensity profiling has been used previously for microwire implants (Markwardt et al., 2013) but this method is not optimal for the oblong tracks produced by the planar implants used in the current study. A profiling method was developed wherein the user selects the two end points of the track along the center of its longest axis, and the program measures 50 evenly spaced intensity profiles

perpendicular to this centerline in each direction. Images are converted to greyscale, then threshold-based analysis is used to select the dark area of the track void, which is excluded from the intensity profile analysis in order to control for variations in void size and shape, as well as better characterizing the device-tissue interface. This analysis scheme utilizing track void exclusion and integrated mean intensity profiling is based upon those used by other researchers in the assessment of neural interface immune reactions (Biran et al., 2005; Harris et al., 2011a; Winslow and Tresco, 2010). The selected track void area is overlaid with a black mask, and the track centerline is then selected manually. Each profile line consists of the first 200μm of pixels with a value >0 (e.g. beyond the void area mask). The resulting 100 profiles are averaged together to yield a mean profile for each track, which is then separated into 25μm bins for analysis. Intensity values shown represent mean pixel values for each 25μm bin. An example track with overlaid intensity profile lines is shown in **Figure 4.3.**

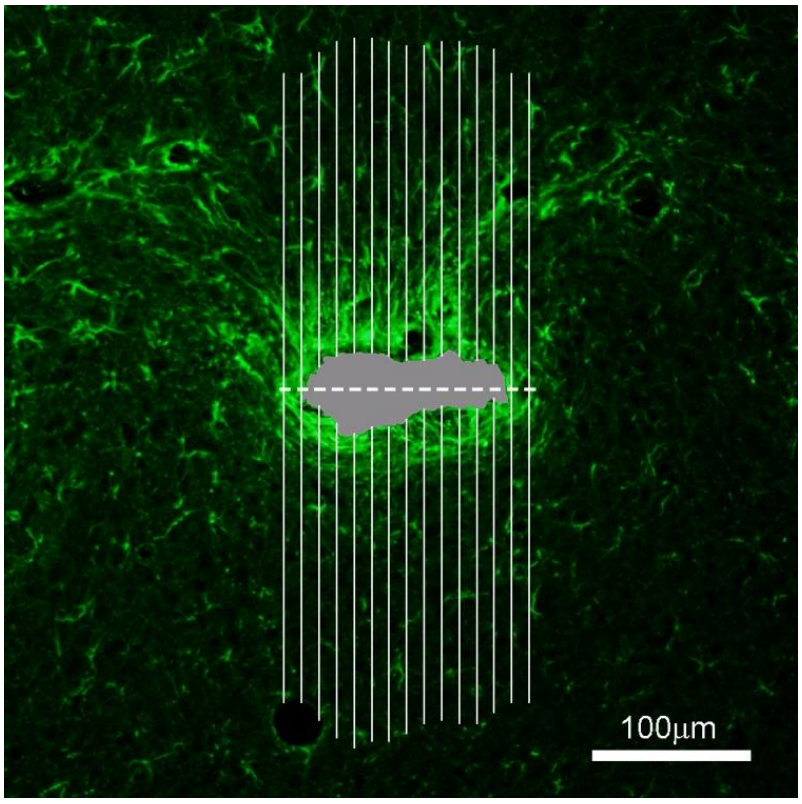

Figure 4.3: Illustration of intensity profile scheme on a typical GFAP-labeled implant track. Gray region indicates track void, which is excluded from intensity analysis. Dashed line shows track centerline and solid lines represent intensity profiles. Number of profiles has been reduced for clarity; actual analysis uses 50 profiles per side.

To control for animal to animal variations in native expression levels of the markers of interest, intensity measurements were taken from the unimplanted contralateral hemisphere and the mean values for each rat were subtracted from the corresponding mean implant profiles. Background intensity profiles were taken from the same locations in the image frame as the experimental tracks in order to account for spatial nonuniformities in microscope illumination (Biran et al., 2005; Kim et al., 2004). Quantification of vim+/GFAP- meningeal tissue at the implant sites was performed by subtracting the GFAP labeled image from the vimentin labeled image for that section, leaving only areas which are vim+ and GFAP-. Example images illustrating the subtraction analysis process are shown in **Figure 4.4.** For pixels in which the GFAP intensity value is greater than the same pixel in the vimentin image, the value in the resulting subtraction image is zero. Due to the differences in spatial distribution of this tissue, void area masks could not be used, and all distance metrics are relative to the implant centerline rather than the void edge. When analyzing vim+/GFAP+ proximal reactive astrocytes, void masks from GFAP labeled images were overlaid on the vimentin labeled images, and then the intensity profile was taken. Since the GFAP mask excludes all vim+/GFAP- meningeal tissue and any other areas within or near the void not expressing GFAP, this ensures that only intensity values of vim+/GFAP+ tissue are measured. This vim+/GFAP+ proximal reactive astrocyte cell population has been previously distinguished from vim-/GFAP+ “distal” reactive astrocytes (Ridet et al., 1997).

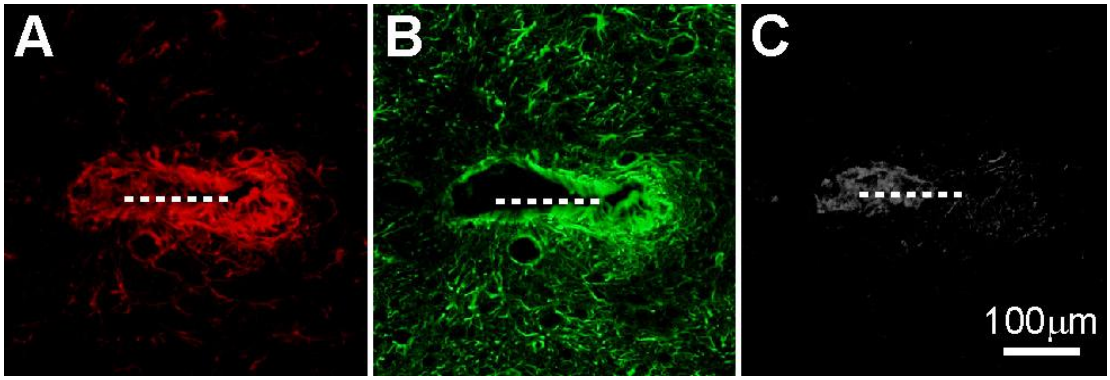

Figure 4.4: Image subtraction process. Dashed line indicates implant size and approximate location

(A) Vimentin labeled image of representative control implant track.
(B) GFAP labeled image of the same track
(C) Resulting greyscale image following subtraction of (B) from (A) showing Vim+/GFAP- meningeal tissue

4.2.4.2 Cell counting

ImageJ software (NIH) was used to perform threshold-based automated cell counting to assess neuronal density surrounding the implant tracks. Cell selection criteria were fine tuned for each subject using unimplanted contralateral tissue sections. A range of threshold values were used for each implant track in order to account for variations in brightness, and the largest cell count returned was entered. The area of the track void in the NeuN labeled image was measured via a similar thresholding process and subtracted from the area of the 200μm diameter region of interest to calculate the cell density. This ensures that the resulting cell density value is not influenced by the size of the track void, since the area value used in the cells/area density calculation represents the amount of cortical tissue within the counting radius and excludes

the void area. For the implant type comparison, density values from varying depths were averaged to gain a single mean density value for each implant shaft for statistical analysis. Analyzable data were collected from a total of 41 implant tracks (22 SMP and 19 parylene).

4.3 Results

Morphology and general distribution of the four histological markers used in this study may be seen in **Figure 4.5.** An example control implant track is shown with labels for GFAP (**A**), vimentin (**B**), NeuN (**C**) and IgG (**D**).

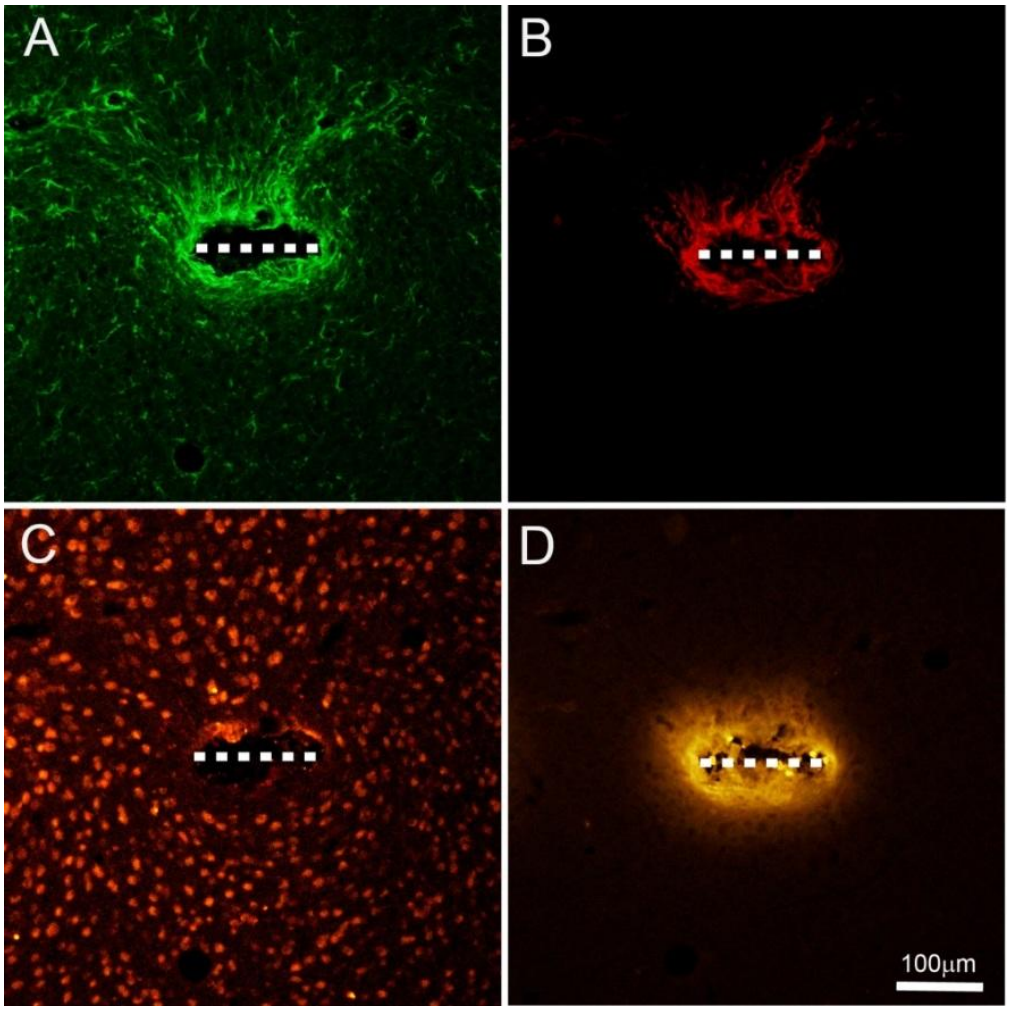

Figure 4.5: Example images. Dashed line indicates implant width and approximate location.

(A) Example control implant track showing GFAP labeling of reactive astrocytes.

(B) Vimentin labeling of the same track showing meningeal tissue and proximal reactive astrocytes

(C) NeuN labeling showing neuron cell bodies

(D) IgG reactivity of the same track in an adjacent tissue section

4.3.1 GFAP

GFAP expressing reactive astrocytes play a central role in the brain's immune reaction, and the reduction of this portion of the immune response is one of the primary goals of current neural interface development. Areas of GFAP+ cells were found surrounding all implant tracks, typically forming a dense capsule immediately surrounding the implant. Individual GFAP+ cells were found extending tens to a few hundred microns into the surrounding tissue. These cells display a stellate morphology which is typical of reactive astrocytes in the CNS. Example GFAP labeled images are shown in **Figure 4.6(A)** and **(B)**.

4.3.1.1 Quantitative GFAP measures

Intensity profile analysis found significantly reduced levels of mean GFAP+ intensity for the SMP implants for the first two distance bins from 0-50μm from the track void edge compared to controls (t-tests, n=41, $p<0.05$). Differences in GFAP expression between the two implant types from 75μm outwards were not significant. Results are shown in **Figure 4.6(C).**

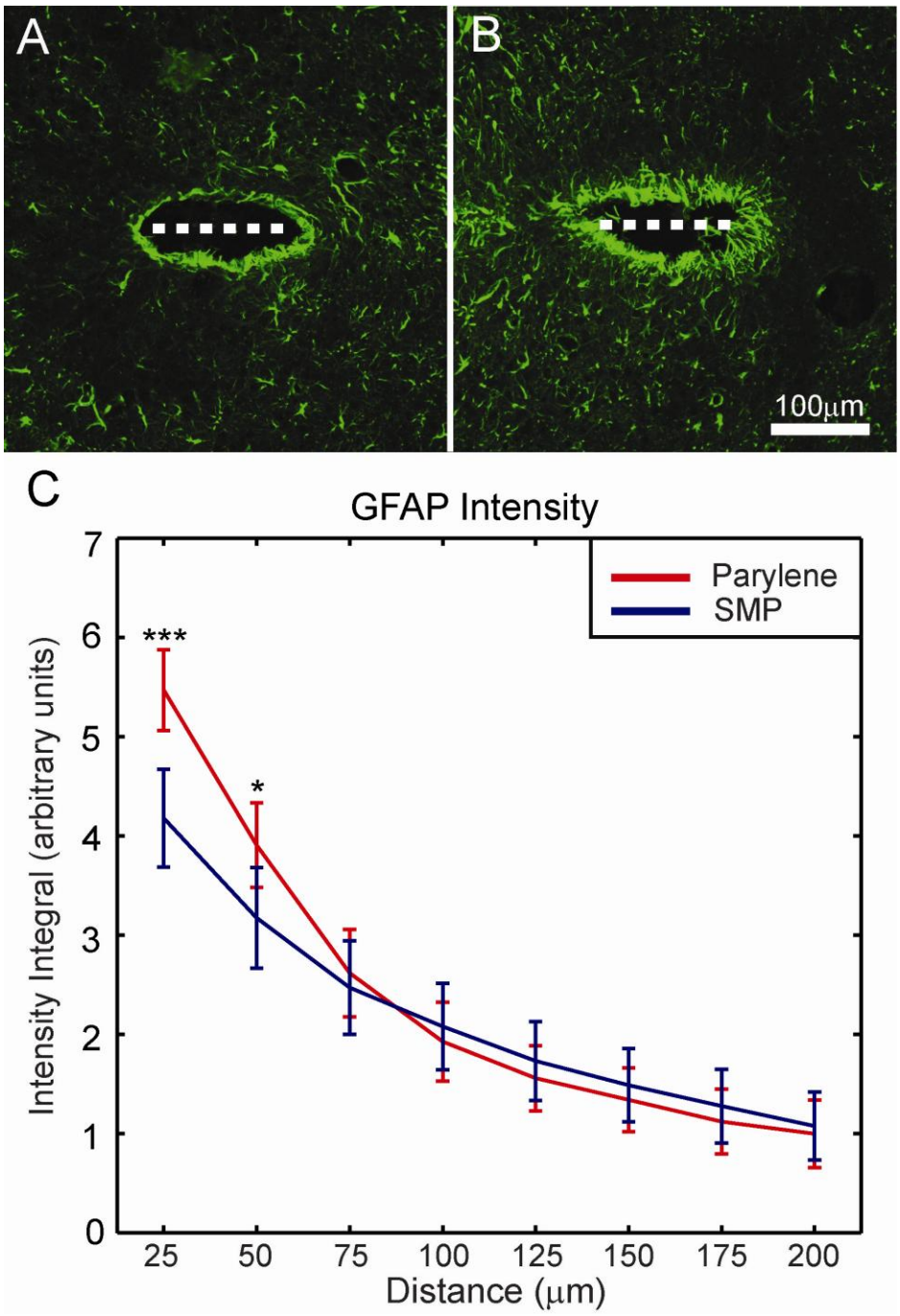

Figure 4.6: GFAP results

(A) Typical SMP implant track showing GFAP labeled reactive astrocytes
(B) Control implant track from the same tissue section
(C) GFAP intensity for each implant type as a function of distance from the track margin +/-95%CI (***p<.001, *p<.05)

4.3.2 Vim+/GFAP+ Results

A subpopulation of reactive astrocytes in the CNS expresses vimentin in addition to GFAP. These have been termed proximal reactive astrocytes, since they tend to be restricted to the more immediate vicinity of the implant. Meningeal tissue, which expresses vimentin but not GFAP, is excluded from this portion of the analysis. Vim+/GFAP+ reactive astrocytes were found immediately surrounding implant tracks, frequently forming a dense capsule of interdigitating cellular processes. Typical vimentin labeled images of SMP and parylene-c implants are shown in **Figure 4.7(A)** and **(B)** respectively.

4.3.2.1 Quantitative Vim+/GFAP+ Results

As is the case with GFAP labeled astrocytes, analysis of vimentin expression showed significantly reduced intensity in the first 50μm for SMP implants compared to controls (t-tests, n=41, $p<0.05$). Differences in intensity from 75-200μm were not significant. Results are shown in **Figure 4.7(C).** Comparison of the GFAP intensity curve shown in **Figure 4.6(C)** with the vimentin intensity curve illustrates the more localized nature of the vimentin expressing astrocyte reaction, which falls off in intensity at greater distance more quickly than the mean GFAP intensity curves.

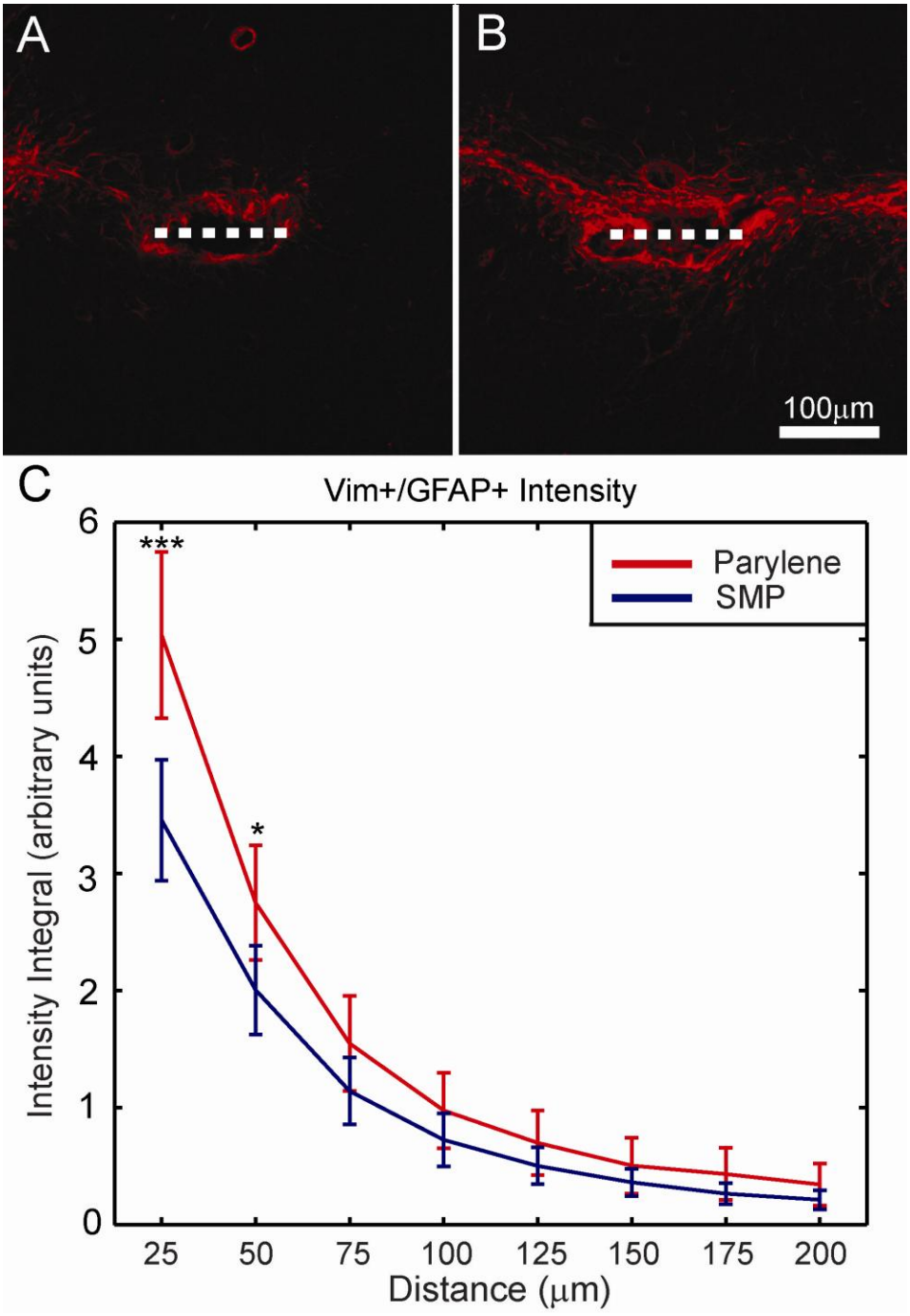

Figure 4.7: Vim+/GFAP+ results

(A) Typical SMP implant track showing vim+/GFAP+ proximal reactive astrocytes
(B) Control implant track from the same tissue section
(C) Vimentin intensity for each implant type as a function of distance from the track margin +/-95%CI (***p<.001, *p<.05).

4.3.3 Vim+/GFAP- Meningeal Tissue Results

Meningeally derived fibroblasts have been shown to migrate into the cortex down the length of penetrating neural implants and participate in the immune response alongside native cell populations. These cells are identified by the subtraction of the GFAP+ labeled image from the vimentin+ labeled image of the same section, leaving areas which express vimentin but not GFAP. These areas, when present, tend to form the innermost layer adjacent to the implant. Example images are shown in **Figure 4.8(A)** and **(B)**.

4.3.3.1 Quantitative meningeal tissue results

Intensity profile analysis of Vim+/GFAP- regions revealed no significant differences in meningeal tissue levels between the two implant types (t-tests, n=41, $p>0.05$). Results are shown in **Figure 4.8(C).** Due to the morphology and distribution of the meningeal tissue and the frequent lack of a clearly defined void, distance bin measurements for this marker are relative to the track centerline rather than the void edge as with all other metrics.

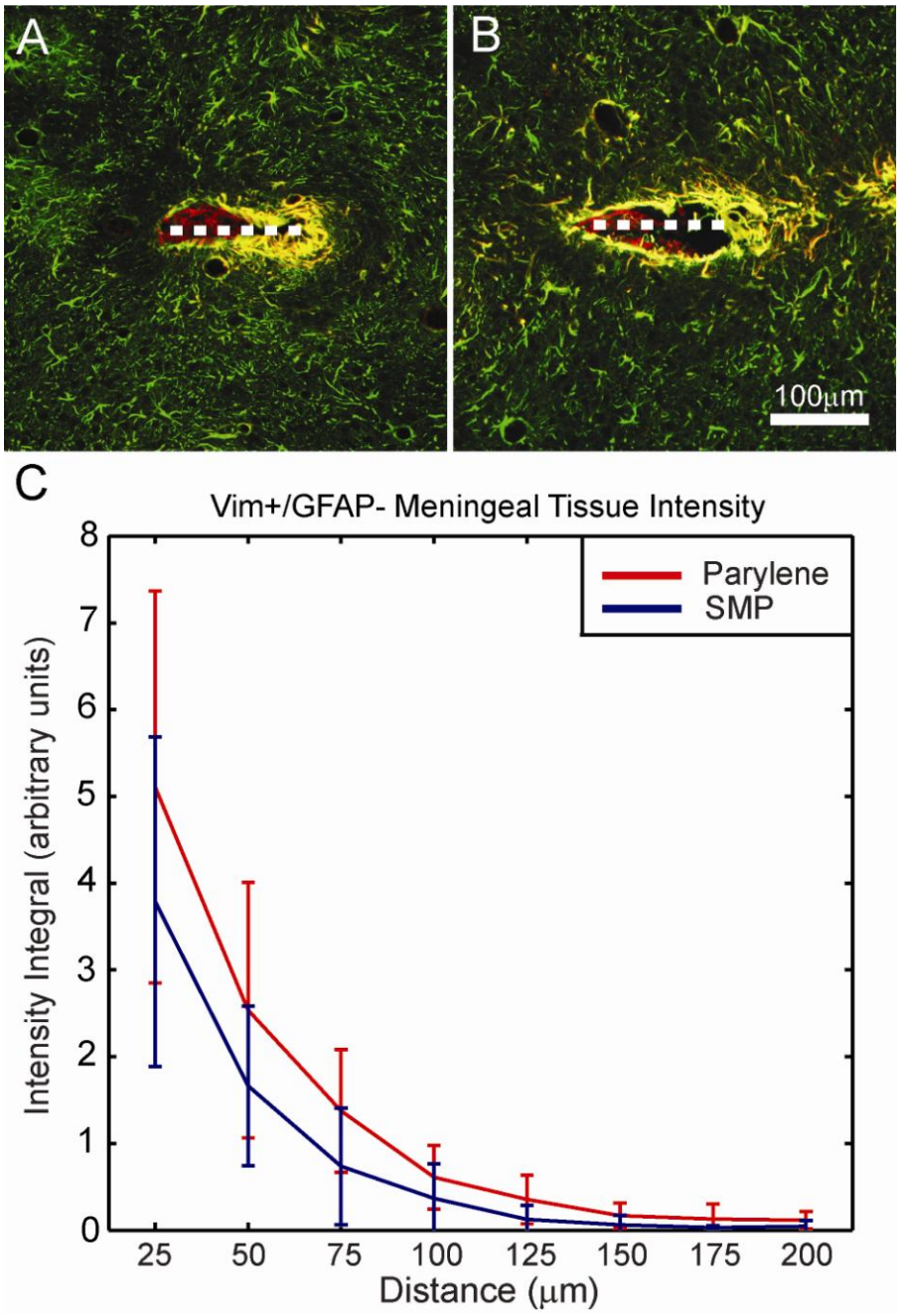

Figure 4.8: Vim+/GFAP- Meningeal tissue results

(A) Representative SMP implant track showing Vim+/GFAP- meningeal tissue in red, Vim+/GFAP+ proximal reactive astrocytes in yellow, and Vim-/GFAP+ astrocytes in green. Dashed line denotes implant location.

(B) Control implant track from the same subject

(C) Vim+/GFAP- meningeal tissue intensity for both implant types as a function of distance from the track centerline +/-95%CI

4.3.4 IgG

A subset of tissue sections was analyzed via fluorescent labeling of IgG, a common serum antibody type. Elevated levels of IgG in cortical tissue, which is normally devoid of serum immunoglobulins, are indicative of blood brain barrier compromise due to mechanical trauma (Hoshino et al., 1996; Potter et al., 2012). IgG labeled sections showed regions of elevated IgG surrounding the implant tracks. IgG labeling was not restricted to a particular cell type, but instead formed diffuse bright regions around each track extending into the surrounding tissue. Example images are shown in **Figure 4.9(A)** and **(B).**

4.3.4.1 Quantitative IgG results

Intensity profile analysis of IgG labeling revealed no significant differences between the two implant types (t-tests, n=41, $p>0.05$). Results are shown in **Figure 4.9(C).**

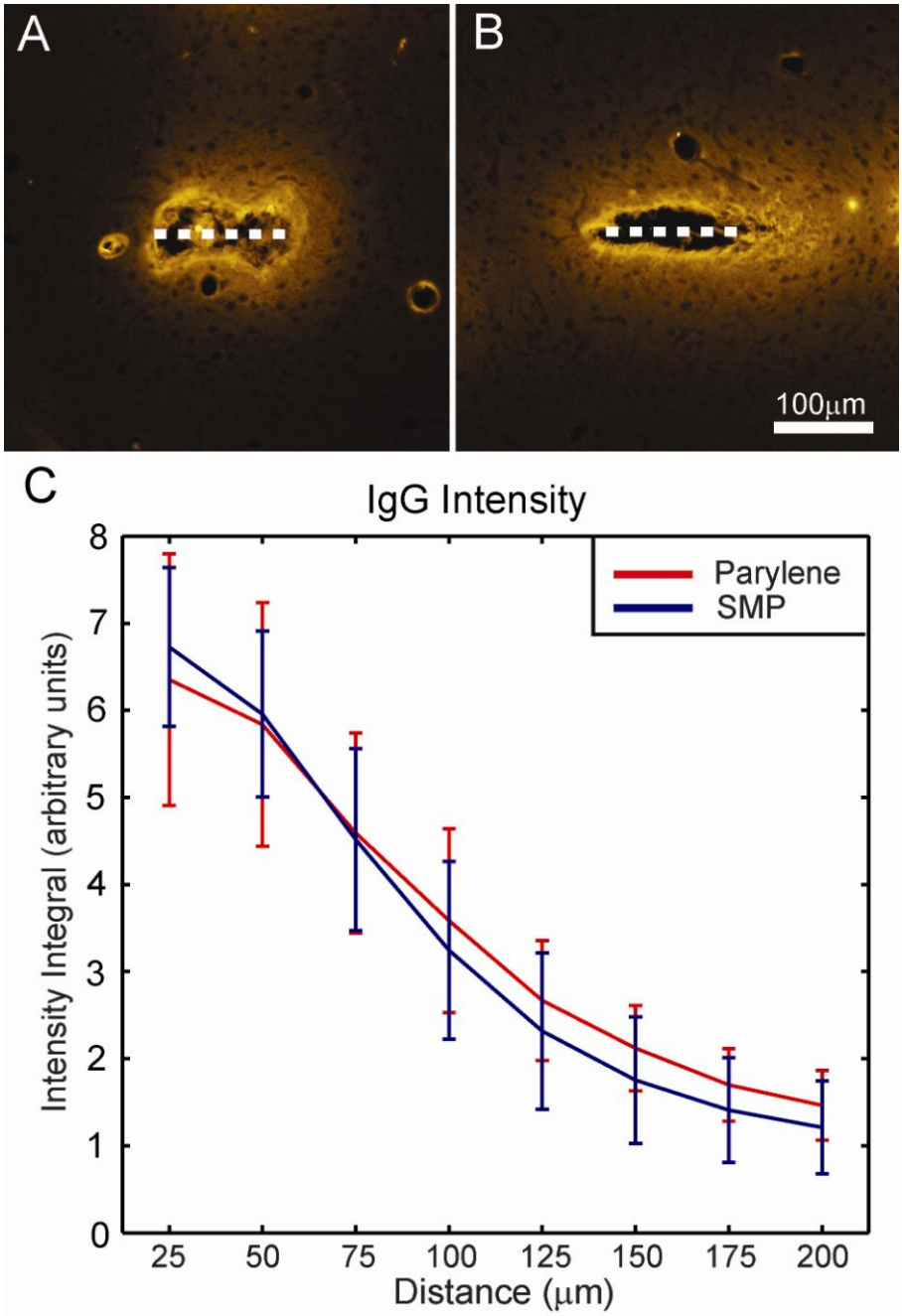

Figure 4.9: IgG results

(A) Typical SMP implant track showing IgG reactivity. Dashed line denotes implant location.

(B) Control implant track from the same subject

(C) IgG intensity as a function of distance from the implant track margin +/- 95%CI

4.3.5 Neuron results

Automated cell counting of NeuN labeled cell bodies was used to quantify levels of neuron dieoff surrounding the implants within a 100μm radius. No significant difference in mean neuron density was found between the two implant types. Results are shown in **Figure 4.10.** Mean void areas were also found to be similar between the two implant types (t-test, n=41, p=0.36).

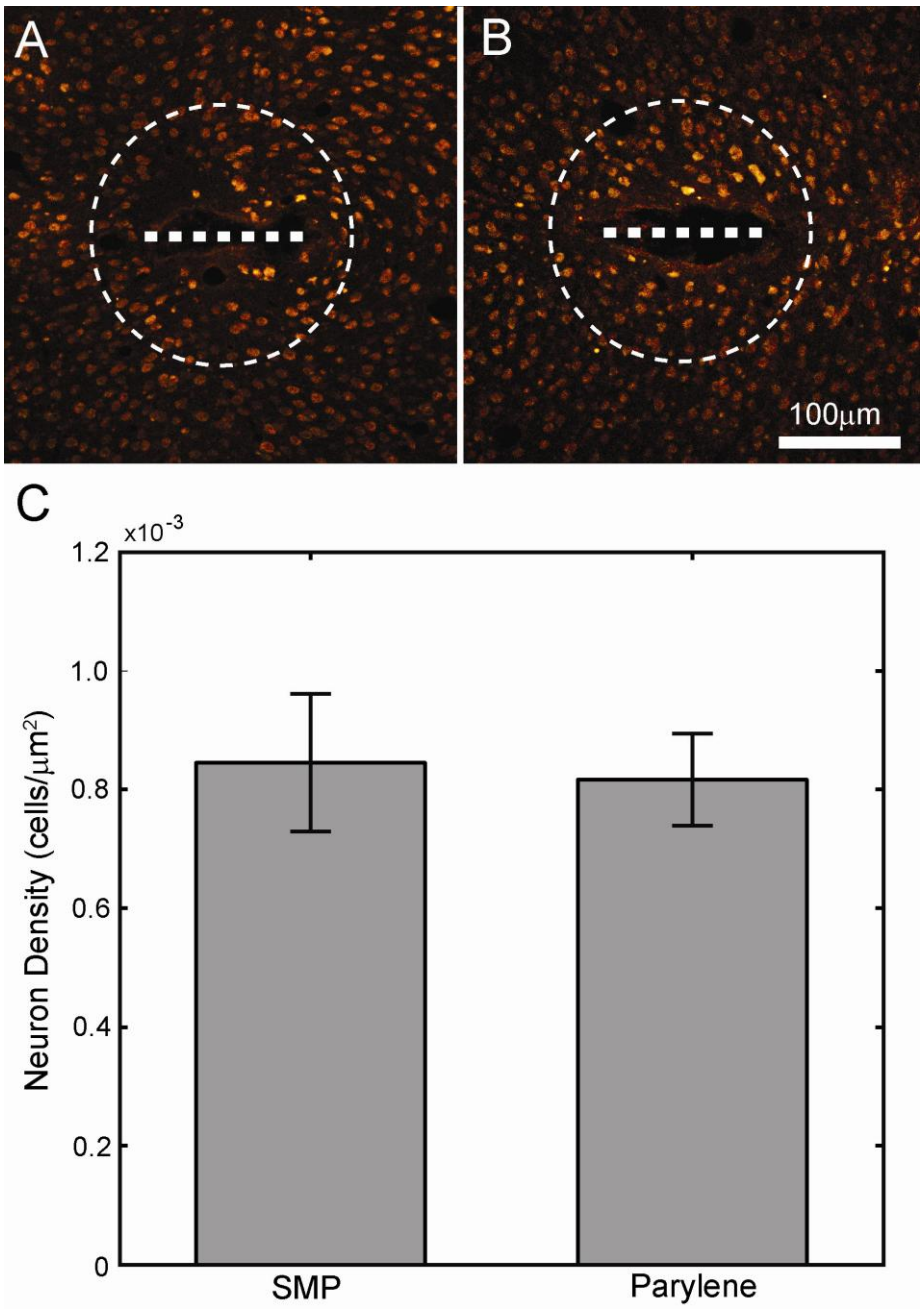

Figure 4.10: Neuron results

(A) Typical SMP implant track showing NeuN labeling of neuron cell bodies. Dashed line indicates implant location, circle shows 100μm cell counting radius

(B) Control implant track from the same subject

(C) Mean neuron densities for both implant types +/-95%CI.

4.4 Discussion

The development of a reliable future chronic neural interface requires a substantial increase in both the reliability and longevity of neural signals over those obtained with current devices. One of the primary strategies for improving recording performance is reduction of the brain's foreign body response to the implant, and the type of material used for the implant's substrate has received much attention as a potential way to mitigate the undesirable aspects of the immune reaction. Flexible implants which provide a closer mechanical match to the surrounding brain tissue and thus reduce chronic irritation have shown promise at reducing the glial scarring response, and the SMP system has mechanical properties and capabilities which should make it a prime candidate for neural interface substrates.

Previous work has gathered significant evidence for the hypothesis that the reactive astrocyte response to a neural interface is related to trauma and mechanical stresses in the tissue surrounding the implant (Biran et al., 2005; Harris et al., 2011a; Harris et al., 2011b; Hassler et al., 2011; Kim et al., 2004; Rennaker et al., 2005b; Rousche et al., 2001; Stice et al., 2007; Thelin et al., 2011). These stresses can be related to the method of implant insertion, type of implant fixation, or the mechanical properties of the implant itself. The results of this study lend further support to this hypothesis. Dynamically softening shape memory polymer neural implants, when compared to dimensionally identical parylene-c implants, were found to elicit a reduced reactive astrocyte reaction at 4 weeks. Previous studies have shown that reactive astrocyte activity may be

reduced via a reduction in implant stiffness and thus a reduction in chronic mechanical stresses in the surrounding tissue, and the results of the current study corroborate those findings (Cheung, 2007; Harris et al., 2011a; Mercanzini et al., 2008). Encapsulation of neural electrodes by reactive astrocytes is thought to be one of the main recording device failure modes, and the glial reaction has been associated with numerous phenomena that are detrimental to neural tissue viability and recording device performance. Although functional recording devices were not employed in the current study, the observed reduction in reactive astrocyte activity as a result of the implant's dynamic softening capability is likely to correspond to an improvement in recording performance, according to the current understanding of reactive gliosis and neural electrode function.

Recent work has begun to focus more on the role of meningeally derived tissues in the immune response. Meningeally derived fibroblasts have been shown to migrate down the shaft of a penetrating neural implant and contribute to the immune reaction (Kim et al., 2004; Woolley et al., 2013). These cells may be differentiated from native glial populations by the fact that they express vimentin but not GFAP. Image subtraction was used to identify meningeal tissue surrounding the implants in the current study, and no significant differences in the amount of this tissue were found between the two implant types. A thorough account of the factors which influence the meningeal portion of the immune response to a neural electrode has yet to be assembled, but the results of this study suggest that the meningeal response is independent of the

modulus of the implant. Other work, including the results outlined in Chapter 3, has shown that the degree of infiltration of meningeal cells is in part dependent upon the spatial relationship between the implant and the meningeal space, as well as implant porosity, and since SMP and control implants in the current study were identical in terms of size, shape, and positioning in the cortex, a significant difference in meningeal tissue levels between the two implant types is not expected.

Examination of IgG levels surrounding also revealed no significant differences between the two implant types. Although significant levels of IgG in cortical tissue are known to be a result of mechanical trauma and resulting blood-brain barrier damage, IgG measurement to evaluate neural interfaces is a relatively novel technique (Cortez et al., 1989; Hoshino et al., 1996). Thus, it cannot be easily determined whether the bulk of the IgG reaction that was observed is a result of initial insertion trauma or chronic mechanical stresses without further investigation at multiple timepoints following implantation. It seems likely that a significant portion of the observed IgG signal would be due to insertion trauma, since the stresses on the tissue during probe insertion are much higher than the chronic stresses generated by small perturbations of the implant. Since the probe dimensions and insertion method did not vary between the two implant types, the mechanical stresses undergone by the tissue during implant insertion should not vary significantly between the implant types. Any differences in IgG release into the tissue which are a result of chronic stress

reduction from dynamic implant softening may well be masked by the large IgG signal produced during implantation.

Examination of neuron density in the 100μm maximum recording radius around the implants revealed no significant differences between the two implant types. One study found that a nanocomposite based softening implant improved neuron viability (Harris et al., 2011a), but the softening implants were compared to tungsten microwires rather than the parylene-c controls used in the current study, giving a difference in modulus two orders of magnitude greater than that used in the current study (400GPa and 12MPa for tungsten and nanocomposite versus 3GPa and 10MPa for parylene-c and softened SMP, respectively). Thus it is possible that the modulus difference between the SMP and control implants in the current study was not large enough to elicit a significant difference in neuron dieoff between the two implant types.

Although the current study did not find improvements in neuron density, the SMP system neatly addresses one of the primary shortcomings of very compliant implants in that it is sufficiently stiff to facilitate insertion without any additional material or devices. Additionally, it offers potentially improved performance due to the reduction of the glial scarring response when compared to parylene-c, which itself has a vastly lower modulus than the silicon or metallic substrates which make up the majority of current neural interface technologies. By using parylene-c as a control to evaluate the dynamically softening SMP material, this experiment provides an isolation of the effects of dynamic

softening capability which is superior to previous studies, and finds that this capability provides a beneficial reduction in the immune response.

4.5 Conclusion

Histological evaluation of dynamically softening polymer neural implants revealed significant reductions in reactive astrocyte activity compared to non-softening parylene-c control implants. These results demonstrate that the dynamically softening shape memory polymer implant substrate which was evaluated provides a desirable reduction in reactive astrocyte encapsulation by reducing chronic mechanical stresses in the surrounding tissue. Encapsulation by reactive astrocytes is thought to be one of the primary failure modes of neural interfaces, and the reduction of the astrocyte response should correspond to an improvement in recording electrode performance. The observed reduction in the astrocytic reaction suggests that the SMP system is a good candidate for use in future neural interfaces. Further work is needed to evaluate the performance of functional recording electrodes on this substrate and determine whether the observed reduction in reactive gliosis translates to improvements in recording signal quality and lifetime. The combination of the SMP substrate system with other mitigation strategies is another promising direction of future work; techniques such as chemical functionalization of the implant surface or manipulation of the tissue adhesion properties may prove to be beneficial additions. Further reductions of the softened modulus of the SMP system will also be pursued, in order to maximize the benefits of its dynamic softening capability.

5 General Conclusions

5.1 Review of Main Findings

The overarching aims of this set of studies were to gain a better understanding of the immune response itself and to evaluate novel methods to reduce the magnitude of the brain's immune response to implanted neural interfaces, in order to inform future neural interface designs and improve their performance. Important insights were gained into the spatial distribution of immune cell activity in the cortex and the influence of multiple implant design characteristics on various aspects of the immune response.

Preliminary studies not described in this dissertation found evidence of a pattern of decreasing immune activity with increasing depth in the cortex, and these findings provided motivation for the study described in Chapter 2, which compared the chronic immune response to conventionally implanted microwires, which were in chronic contact with the meninges, and that of similar implants placed sub-meninges. Sub-meninges implants were found to elicit substantially less immune activity than trans-meninges plants, as measured by levels of both microglia and reactive astrocytes. These findings lend further support to the idea of a significant meningeal contribution to the chronic immune response, and motivate the development of wireless interface designs which may be placed completely below the meninges.

These results provided motivation for the experiment described in Chapter 3, which further investigated the interaction of the implant with the

meningeal tissue. Porous-shank planar implants were found to significantly reduce meningeal tissue growth down the implant shaft compared to non-porous implants by allowing the meningeal tissue to grow into the structure of the implant at or near the level of the cortical surface. Porous implants were also found to improve neuron density in the recording zone around the implant shaft, which is of vital importance to neural electrode recording performance. This novel implant design feature demonstrates that the meningeal portion of the immune response may be reduced by relatively simple means, which is promising and informative for the design of future neural interfaces.

The study described in Chapter 4 examined a new type of dynamically softening neural interface substrate and evaluated its immune system performance compared to similar implants which lacked dynamic softening capability. The drop in modulus was found to significantly reduce the amount of reactive astrocyte encapsulation around the SMP implants by creating a better mechanical match with the surrounding cortical tissue and thus reducing chronic mechanical stresses and irritation. Reduction of reactive astrocyte encapsulation is one of the main goals of neural interface development, and these findings suggest that use of the SMP substrate in future neural interface applications should result in an improvement in recording performance over existing technologies. The use of parylene-c control implants in this experiment allowed the isolation of the effects of dynamic softening capability to a greater degree than has been previously achieved, since previous work has only

compared dynamically softening implant substrates to implant materials which are significantly stiffer than the softening implant in its unsoftened state.

The combined results of these studies provide new insight into the factors governing the chronic immune response to a cortical electrode and suggest design features to help improve the recording performance of future neural interfaces. The findings of the experiments described in Chapters 2 and 3 highlight the importance of meningeal contributions to the chronic immune response and demonstrate interventional strategies which have the potential to improve the performance of future recording devices. Previous work has not generally treated the meningeal and astrocytic portions of the immune reaction as separate, but Chapters 3 and 4, when considered together, suggest that these are at least somewhat independent phenomena. The addition of near-surface pores to the implant altered the meningeal response, but not the astrocyte response. The addition of dynamic softening capability reduced the astrocyte response, which corroborates other findings relating the astrocyte reaction to mechanical stresses in the tissue, but did not affect the meningeal response. Previous work showing the tendency of meningeal cells to initiate glia limitans formation when in contact with astrocytes suggests that the negative effects of meningeal cells on recording performance may be greater than previously thought, since histological methods focusing on the characteristics of the fibrous capsule around the implant track, rather than simply the abundance of reactive astrocytes, are not currently available. The findings presented in this dissertation suggest that a greater understanding of the causes and effects of

meningeal cell infiltration around a cortical neural interface will be important in the development of future devices and the improvement of recording electrode performance.

5.2 Future Directions

The focus of this body of work was to gain a better understanding of the factors which influence the brain's immune response to a neural implant via histological examination and quantification of the cells involved in the immune response. The reduction of these histological metrics of immune activity is, of course, not the ultimate goal, but simply a means to the end of improving the recording performance of neural interfaces. The ultimate measure of the techniques described in this dissertation will be their application to functional recording devices and examination of signal quality and lifetime. The most promising finding in terms the magnitude of its effect on the immune response was described in Chapter 2, where placement of the neural implant completely below the meninges provided a substantial reduction in reactive astrocyte and microglia activity. This finding motivates the development of a wireless recording probe which could be placed completely below the meninges, and should yield improved recording performance over current technologies. The findings of Chapter 4 also inform the design of such an interface, suggesting that the use of the SMP system for the implant substrate could provide a further improvement in recording capability. The findings described in Chapter 3 are

promising, but the ultimate test of porous-shank structures will be in their application in a functional recording electrode. This work has shown that the meningeal component of the cortical immune response is an important consideration of neural interface design, and further investigation of the meningeal response and its functional effects on neural electrodes is warranted. Future work could also include the combination of techniques investigated herein with other successful mitigation strategies, such as the addition of surface treatments to SMP implants to control tissue adhesion or protein adsorption. Also, histological techniques which permit the examination of implants *in situ* within a thick coronal tissue section have been recently developed (Woolley et al., 2013) which would be particularly well suited to a closer examination of depth-related responses and the interaction of porous-shank implants with the meningeal tissue. The use of this device capture histology technique would allow the migration of meningeal tissues to be examined in much more detail, and enable the optimization of the porous-shank design in order to minimize meningeal tissue encapsulation of the implant and improve recording performance.

Neural interfacing is still a young field, and many challenges remain to be overcome before the ultimate goals of these technologies can be realized. When dealing with a system of such truly stupendous complexity as the central nervous system, these challenges are to be expected, but even in the time period over which these experiments were conducted, many significant advances have been made in neural interface design. This rapid pace of

advancement paints a bright and very exciting future for this field, and it is hoped that the work described herein proves to be a significant contribution towards the ultimate goal of clinical viability.

References

Abnet K, Fawcett JW, Dunnett S. Interactions between meningeal cells and astrocytes in vivo and in vitro. Dev. Brain Res., 1991; 59: 187-96.

Arieli A, Grinvald A, Slovin H. Dural substitute for long-term imaging of cortical activity in behaving monkeys and its clinical implications. J. Neurosci. Meth., 2002; 114: 119-33.

Batista A, Andersen R. The parietal reach region codes the next planned movement in a sequential reach task. J Neurophysiol, 2001; 85: 539-44.

Biran R, Martin DC, Tresco PA. The brain tissue response to implanted silicon microelectrode arrays is increased when the device is tethered to the skull. Biomed Materials Res A, 2007; 82A: 169-78.

Biran R, Martin DC, Tresco PA. Neuronal cell loss accompanies the brain tissue response to chronically implanted silicon microelectrode arrays Exp. Neurology 2005; 195: 115-26.

Brunton E, Lowery AJ, Rajan R. A comparison of microelectrodes for a visual cortical prosthesis using finite element analysis. Frontiers in Neuroengineering, 2012; 5.

Carbonell AL, Boya J. Ultrastructural study on meningeal regeneration and meningo-glial relationships after cerebral stab wound in the adult rat. Brain Res., 1988: 337-44.

Chen J, Wise KD, Hetke JF, Bledsoe SC. A multichannel neural probe for selective chemical delivery at the cellular level. IEEE Trans. on Biomed. Eng., 1997; 44: 760-9.

Cheung K. Implantable microscale neural interfaces. Biomed Microdevices, 2007; 9: 923-8.

Cortez SC, McIntosh TK, Noble LJ. Experimental fluid percussion brain injury: vascular disruption and neuronal and glial alterations. Brain Res., 1989; 482: 271-82.

Cui X, Wiler J, Dzaman M, Altschuler R, Martin DC. In vivo studies of polypyrrole/peptide coated neural probes. Biomaterials, 2003; 24: 777-87.

Cullen DK, Stabenfeldt SE, Simon CM, Tate CC, LaPlaca MC. In vitro neural injury model for optimization of tissue-engineered constructs. J. Neurosci. Res., 2007; 85: 3642-51.

Fawcett JW, Asher RA. The glial scar and central nervous system repair. Brain Res. Bul. , 1999; 49: 377-91.

Fomani AA, Mansour RR. Fabrication and characterization of the flexible neural microprobes with improved structural design. Sensors and Actuators A, 2011; 168: 233-41.

Fujita T, Yoshimine T, Maruno M, Hayakawa T. Cellular dynamics of macrophages and microglial cells in reaction to stab wounds in rat cerebral cortex. Acta Neurochir, 1998; 140: 275-9.

Gray CM, Goodell B, Lear A. Multichannel micromanipulator and chamber system for recording multineuronal activity in alert, non-human primates. J. Neurophysiol., 2007; 98: 527-36.

Harris JP, Capadona JR, Miller RH, Healy BC, Shanmuganathan K, Rowan SJ, Weder C, Tyler DJ. Mechanically adaptive intracortical implants improve the proximity of neuronal cell bodies. J. Neural Eng., 2011a; 8: 1-13.

Harris JP, Hess AE, Rowan SJ, Weder C, Zorman CA, Tyler DJ, Capadona JR. In vivo deployment of mechanically adaptive nanocomposites for intracortical microelectrodes. Neural Engineering, 2011b; 8: 13-26.

Hassler C, Guy J, Nietzschmann M, Staiger JF, Stieglitz T. Chronic intracortical implantation of saccharose-coated flexible shaft electrodes into the cortex of rats. IEEE Trans. Biomed. Eng., 2011; 22: 55-69.

Hassler C, Metzen RP, Ruther P, Stieglitz T. Characterization of parylene c as an encapsulation material for implanted neural prostheses. Biomed Materials, 2010; 93B: 266-73.

He W, McConnell GC, Bellamkonda RV. Nanoscale laminin coating modulates cortical scarring response around implanted silicon microelectrode arrays. J. Neural Eng., 2006; 3: 316-26.

Henze DA, Borhegyi Z, Csicsvari J, Mamiya A, Harris KD, Buzsaki G. Intracellular features predicted by extracellular recordings in the hipppocampus in vivo. J. Neurophysiol., 2000; 84: 390-400.

Hochberg LR, Serruya MD, Friehs GM, Mukand JA, Saleh M, Caplan AH, Branner A, Chen D, Penn RD, Donoghue JP. Neuronal ensemble control

of prosthetic devices by a human with tetraplegia. Nature, 2006; 442: 164-71.

Hoshino S, Kobayashi S, Nakazawa S. Prolonged and extensive IgG immunoreactivity after severe fluid-percussion injury in rat brain. Brain Res., 1996; 711: 73-83.

Hsu J, Rieth L, Normann RA, Tathireddy P, Solzbacher F. Encapsulation of an integrated neural interface device with parylene c. IEEe Trans. Biomed. Eng., 2009; 56: 23-9.

Hwang EJ, Andersen RA. Cognitively driven brain machine control using neural signals in the parietal reach region. Engineering in Medicine and Biology Society (EMBC), 2010 Annual International Conference of the IEEE. IEEE, 2010: 3329-32.

Hwang EJ, Hauschild M, Wilke M, Andersen RA. Inactivation of the parietal reach region causes optic ataxia, impairing reaches but not saccades. Neuron, 2012; 76: 1021-9.

Jones LL, Tuszynski MH. Spinal cord injury elicits expression of keratan sulfate proteoglycans by macrophages, reactive microglia, and oligodendrocyte precursors. J. Neurosci. , 2002; 22: 4611-24.

Kalman M. Glial reaction and reactive glia. Adv. in Molec. and Cell Biol. , 2003; 31: 787-835.

Kennedy PR. The cone electrode: a long-term electrode that records from neurites grown onto its recording surface. J. Neurosci. Meth., 1989; 20: 181-93.

Kim BJ, Kuo JTW, Hara SA, Lee CD, Yu L, Gutierrez CA, Hoang TQ, Pikov V, Meng E. 3D parylene sheath neural probe for chronic recordings. J Neural Eng, 2013; 10: 1-16.

Kim Y-T, Hitchcock RW, Bridge MJ, Tresco PA. Chronic response of adult rat brain tissue to implants anchored to the skull. Biomaterials, 2004; 25: 2229-37.

Kipke DR, Shain W, Buzsaki G, Fetz E, Henderson JM, Hetke JF, Schalk G. Advanced neurotechnologies for chronic neural interfaces: new horizons and clinical opportunities. Neuroscience, 2008; 28: 11830-8.

Kipke DR, Vetter RJ, Williams JC, Hetke JF. Silicon-substrate intracortical microelectrode arrays for long-term recording of neuronal spike activity in cerebral cortex. IEEE Trans. Neural Sys. Rehab. Eng., 2003; 11: 151-60.

Kornyei Z, Czirok A, Vicsek T, Madarasz E. Proliferative and migratory responses of astrocytes to in vitro injury. J Neurosci Res, 2000; 61: 421-9.

Kozai TY, Kipke DR. Insertion shuttle with carboxyl terminated self-assembled monolayer coatings for implanting flexible polymer neural probes in the brain. J. Neurosci. Meth., 2009; 184: 199-205.

Krack P, Chabardes S, Koudsie A, Benazzouz A, Benabid A. Five-year follow-up of bilateral stimulation of the subthalamic nucleus in advanced parkinson's disease. N. Engl. J. Med., 2003; 349: 1925-34.

Kreutzberg GW. Microglia: a sensor for pathological events in the CNS. Trends Neurosci. , 1996; 19: 312-8.

Lebedev M, Nicolelis MAL. Brain-machine interfaces: past, present and future. Trends Neurosci., 2006; 29: 536-46.

Lee K, Massia SP, He J. Biocompatible benzocyclobutene-based intracortical neural implant with surface modification. J. Micromech. Microeng., 2005; 15: 2149-55.

Lozano AM, Giacobbe P, Hamani C, Rizvi SJ, Kennedy SH, Kolivakis TT, Debonnel G, Sadikot AF, Lam RW, Howard AK. A multicenter pilot study of subcallosal cingulate area deep brain stimulation for treatment-resistant depression: Clinical article. Journal of neurosurgery, 2012; 116: 315-22.

Marin C, Fernandez E. Biocompatibility of intracortical microelectrodes: current status and future prospects. Front. in Neuroeng., 2010; 3: 1-6.

Markwardt NT, Stokol J, Rennaker RL. Sub-meninges implantation reduces immune response to neural implants. Neuroscience Methods, 2013; 214: 119-25.

Maxwell WL, Follows R, Ashhurst DE, Berry M. The respopnse of the cerebreal hemisphere of the rat to injury 1. The mature rat. Phil. Trans. R. Soc. Lond., 1990; 328: 479-500.

McClain MA, Clements IP, Schafer RH, Bellamkonda RV, LaPlaca MC, Allen MG. Highly-compliant, microcable neuroelectrodes fabricated from thin-film gold and PDMS. Biomed Microdevices, 2011; 13: 361-73.

Mercanzini A, Cheung KC, Buhl DL, Boers M, Maillard A, Colin P, Bensadoun JC, Bertsch A, Renaud P. Demonstration of cortical recording using

novel flexible polymer neural probes. Sensors and Actuators A, 2008; 143: 90-6.

Merrill DR, Tresco PA. Impedance characterization of microarray recording electrodes in vitro. IEEE Trans. on Biomed. Eng., 2005; 52: 1960-65.

Moxon KA, Hallman S, Aslani A, Kalkhoran NM, Lelkes PI. Bioactive properties of nanostructured porous silicon for enhancing electrode to neuron interfaces. J Biomater Sci Polymer Edn, 2007; 18: 1263-81.

Moxon KA, Kalkhoran NM, Markert M, Sambito MA, McKenzie JL, Webster JT. Nanostructured surface modification of ceramic-based microelectrodes to enhance biocompatibility for a direct brain-machine interface. IEEe Trans. Biomed. Eng., 2004; 51: 881-9.

Nakajima K, Kohsaka S. Microglia: activation and their significance in the central nervous system. J. Biochem. , 2001; 130: 169-75.

Ness R, David S. Leptomeningeal cells modulate the neurite growth promoting properties of astrocytes in vitro. Glia, 1997; 19: 47-57.

Nicolelis MAL, Dimitrov D, Carmena JM, Crist R, Lehew G, Kralik JD, Wise SP. Chronic, multisite, multielectrode recordings in macaque monkeys. Proc. Nat. Acad. Sci., 2003; 100: 11041-6.

Normann RA, Maynard EM, Rousche PJ, Warren DJ. A neural interface for a cortical vision prosthesis. Vision Res, 1999; 39: 2577-87.

Polikov VS, Tresco PA, Reichert WM. Response of brain tissue to chronically implanted neural electrodes. J. Neurosci. Meth. , 2005; 148: 1-18.

Potter KA, Buck AC, Self WK, Capadona JR. Stab injury and device implantation within the brain results in inversely multiphasic neuroinflammatory and neurodegenerative responses. Neural Engineering, 2012; 9: 1-14.

Prasad A, Xue Q-S, Sankar V, Nishida T, Shaw G, Streit WJ, Sanchez JC. Comprehensive characterization and failure modes of tungsten microwire arrays in chronic neural implants. Journal of neural engineering, 2012; 9: 056015.

Qin W, Bauman W, Cardozo C. Bone and muscle loss after spinal cord injury: organ interactions. Ann. N.Y. Acad. Sci, 2010; 1211: 66-84.

Rennaker RL, Ruyle AM, Street S, Sloan AM. An economical multi-channel cortical electrode array for extended periods of recording during behavior. J Neurosci Meth, 2005a; 142: 97-105.

Rennaker RL, Street S, Ruyle AM, Sloan AM. A comparison of chonic multi-channel cortical implantation techniques: manual versus mechanical insertion. J. Neurosci. Meth. , 2005b; 142: 169-76.

Ridet JL, Malhotra SK, Privat A, Gage FH. Reactive astrocytes: cellular and molecular cues to biological function. Trends Neurosci., 1997; 20: 570-7.

Rodger DC, Meng E, Weiland JD, Humayun MS, Tai Y-C. Flexible parylene packaged intraocular coil for retinal prostheses. Nano/Micro Eng and Mol Sys, 2006: 743-6.

Romaguera JR, Do Monte FHM, Quirk GJ. Deep brain stimulation of the ventral straitum enhances extinction of conditioned fear. Proc. Nat. Acad. Sci., 2012; 109: 8764-9.

Rousche PJ, Normann RA. A method for pneumatically inserting an array of penetrating electrodes into cortical tissue. Annals of Biomed Eng, 1992; 20: 413-22.

Rousche PJ, Pellinen DS, Pivin DP, Williams JC, Vetter RJ, Kipke DR. Flexible polyimide-based intracortical electrode arrays with bioactive capability. IEEE Trans. on Biomed. Eng., 2001; 48: 361-71.

Schmidt EM, McIntosh JS, Bak MJ. Long-term implants of parylene-c coated microelectrodes. Medical and Biological Engineering and Computing, 1988: 96-107.

Seymour JP, Kipke DR. Neural probe design for reduced tissue encapsulation in CNS. Biomaterials, 2007; 28: 3594-607.

Shain W, Spataro L, Dilgen J, Haverstick K, Retterer S, Isaacson M, Saltzman M, Turner JN. Controlling cellular reactive responses around neural prosthetic devices using peripheral and local intervention strategies. IEEE Trans. Neural Sys. Rehab. Eng. , 2003; 11: 186-8.

Simeral JD, Kim S-P, Black MJ, Donoghue JP, Hochberg LR. Neural control of cursor trajectory and click by a human with tetraplegia 1000 days after implant of an intracortical microelectrode array. J. Neural Eng., 2011; 8: 1-24.

Skousen JL, Merriam ME, Srivannavit O, Perlin G, Wise KD, Tresco PA. Reducing surface area while maintaining implant penetrating profile lowers the brain foreign body response to chronically implanted planar silicon microelectrode arrays. Prog. Brain Res., 2011; 194: 167-80.

Sloan AM, Dodd OT, Rennaker RL. Frequency discrimination in rats measured with tone-step stimuli and discrete pure tones. Hearing Research, 2009; 251: 60-9.

Stice P, Gilletti A, Panitch A, Muthuswamy J. Thin microelectrodes reduce GFAP expression in the implant site in rodent somatosensory cortex. Neural Engineering, 2007; 4: 42-53.

Stieglitz T. Development of a micromachined epiretinal vision prosthesis. Journal of neural engineering, 2009; 6: 065005.

Stieglitz T, Rubehn B, Henle C, Kisban S, Herwik S, Ruther P, Schuettler M. Brain-computer interfaces: an overview of the hardware to record neural signals from the cortex. Prog. Brain Res., 2009; 175: 297-315.

Szarowski DH, Andersen MD, Retterer S, Spence AJ, Isaacson M, Craighead HG, Turner JN, Shain W. Brain responses to micro-machined silicon devices. Brain Res., 2003; 983: 23-35.

Takeuchi S, Ziegler D, Yoshida Y, Mambuchi K, Suzuki T. Parylene flexible neural probes integrated with microfluidic channels. Lab on a Chip, 2005; 5: 519-23.

Thelin J, Jorntell H, Psouni E, Garwicz M, Schouenborg J, Danielsen N, Linsmeier CE. Implant size and fixation mode strongly influence tissue reactions in the CNS. Pub. Lib. Sci. One, 2011; 6: e16267.

Turner JN, Shain W, Szarowski DH, Andersen MD, Martins S, Isaacson M, Craighead HG. Cerebral astrocyte response to micromachined silicon implants. Exp. Neurology, 1999; 156: 33-49.

Turner S, Kam L, Isaacson M, Craighead HG, Shain W, Turner JN. Cell attachment on silicon nanostructures. J. Vac. Sci. Technol. B, 1997; 15: 2848-54.

Ward MP, Rajdev P, Ellison C, Irazoqui PP. Toward a comparison of microelectrodes for acute and chronic recordings. Brain Res., 2009; 1282: 182-200.

Ware T, Simon D, Arreaga-Salas DE, Reeder J, Rennaker RL, Keefer EW, Voit W. Fabrication of responsive, softening neural interfaces. Adv. Funct. Mater. , 2012.

Welberg L. Brain-machine interfaces: Restoring movement in a paralysed hand. Nature Rev Neurosci, 2012; 13: 360-1.

Welkenhuysen M, Andrei A, Ameye L, Eberle W, Nuttin B. Effect of insertion speed on tissue response and insertion mechanics of a chronically implanted silicon-based neural probe. IEEE Trans. Biomed. Eng., 2011; 58: 3250-9.

Wester BA, Lee RH, LaPlaca MC. Development and characterization of in vivo flexible electrodes compatible with large tissue displacements. J Neural Eng, 2009; 6.

Williams JC, Holecko MM, Massia SP, Rousche PJ, Kipke DR. Multi-site incorporation of bioactive matricies into MEMS-based neural probes. J. Neural Eng. , 2005; 2: L23-L8.

Williams JC, Rennaker RL, Kipke DR. Long-term neural recording characteristics of wire microelectrode arrays implanted in cerebral cortex. Brain Res. Prot., 1999; 4: 303-13.

Winslow BD, Christensen MB, Yang WK, Solzbacher F, Tresco PA. A comparison of the tissue response to chronically implanted parylene-c-coated and uncoated planar silicon microelectrode arrays in rat cortex. Biomaterials, 2010; 31: 9163-72.

Winslow BD, Tresco PA. Quantitative analysis of the tissue response to chronically implanted microwire electrodes in rat cortex. Biomaterials, 2010; 31: 1558-67.

Wolpaw J, Birbaumer N, McFarland D, Pfurtscheller G, Vaughan T. Brain-computer interfaces for communication and control. Clinical Neurophysiology, 2002; 113: 767-91.

Woolley AJ, Desai HA, Otto KJ. Chronic intracortical microelectrode arrays induce non-uniform, depth-related tissue responses. Neural Engineering, 2013; 10.

Zhong Y, Bellamkonda RV. Dexamethasone coated neural probes elicit attenuated inflammatory response and neuronal loss compared to uncoated neural probes. Brain Res., 2007: 15-27.